Design and Simulation of a Towed Underwater Vehicle

Amy Linklater

Thesis submitted to the Faculty of the
Virginia Polytechnic Institute and State University
in partial fulfillment of the requirements for the degree of

Master of Science
in
Aerospace Engineering

Dr. Craig A. Woolsey, Chair
Dr. Leigh McCue, Member
Dr. Wayne Neu, Member

June 3, 2005
Blacksburg, Virginia

Keywords: Towfish, Underwater Vehicle, Towed Vehicle, Dynamic Modeling

Design and Simulation of a Towed Underwater Vehicle

Amy Linklater

Abstract

Oceanographers are currently investigating small-scale ocean turbulence to understand how to better model the ocean. To measure ocean turbulence, one must measure fluid velocity with great precision. The three components of velocity can be used to compute the turbulent kinetic energy dissipation rate. Fluid velocity can be measured using a five-beam acoustic Doppler current profiler (VADCP). The VADCP needs to maintain a tilt-free attitude so the turbulent kinetic energy dissipation rate can be accurately computed to observe small-scale ocean turbulence in a vertical column. To provide attitude stability, the sensor may be towed behind a research vessel, with a depressor fixed somewhere along the length of the towing cable. This type of setup is known as a two-part towing arrangement.

This thesis examines the dynamics, stability and control of the two-part tow. A Simulink simulation that models the towfish dynamics was implemented. Through this Simulink simulation a parametric study was conducted to see the effects of sea state, towing speed, center of gravity position, and a PID controller on the towfish dynamics. A detailed static analysis of the towing cable's effects on the towfish enhanced this dynamic model. The thesis also describes vehicle design and fabrication, including procedures for trimming and ballasting the towfish.

Acknowledgements

I would like to say thanks first of all to my advisor Craig Woolsey for the many opportunities he has given me throughout this process to learn and apply different methods to various control problems. I would also like to thank all the members of my lab group: Chris Nickell, Konda Reddy, Mike Morrow, Nate Lambeth, and Jesse Whitfield for always giving me an extra hand when I needed it. Finally I would like to give thanks to all of my friends and family for helping me and always being there for me.

Contents

Nomenclature

A_c	Cross-sectional area of the cable
A_1	Jacobian of the nonlinear towfish equations with respect to the states
AR	Aspect ratio of the fins
b	Span of the fins
$\bar{b}$	Damping coefficient
B	Buoyancy force from the towfish in the z direction due to the inertial frame axis
B_1	Jacobian of the nonlinear towfish equations with respect to the inputs
c	Chord length of the fins
$\bar{c}$	Mean aerodynamic chord length of the fins
c_r	Root chord of the fins
c_t	Tip chord of the fins
cb	Center of buoyancy
cg	Center of gravity
C_{db}	Drag coefficient due to the towfish body
C_{df}	Drag coefficient of the fins
C_{Dc}	Drag coefficient based off the frontal area of the cable
C_{D0}	Drag coefficient at zero angle of attack for a smooth body
C_{D0b}	Drag coefficient at zero angle of attack for the towfish body due to roughness
C_f	Skin friction coefficient from the towfish body
$C_{L\alpha b}$	Lift curve slope of the body
$C_{L\alpha f}$	Lift curve slope of the fins
$(C_{L\alpha f})_{theory}$	Theoretical lift curve slope of the fins
C_{lb}	Lift coefficient due to the towfish body
C_{lf}	Lift coefficient of the fins
C_{lp}	Damping moment coefficient due to roll

$C_{m\alpha b}$	Pitching moment coefficient of the towfish body
C_{mq}	Damping moment coefficient due to pitch
C_{nr}	Damping moment coefficient due to yaw
C_{spl}	Force coefficient of the left stern plane in the water current frame
C_{spr}	Force coefficient of the right stern plane in the water current frame
C_{vf}	Force coefficient of the vertical fins in the water current frame
d_b	Diameter of the towfish body
d_c	Diameter of the cable
d_1	Fin deflection of the right fin
$\dot{d}_1$	Change in fin deflection of the right fin with respect to time
d_2	Fin deflection of the left fin
$\dot{d}_2$	Change in fin deflection of the left fin with respect to time
$\mathbf{D}$	Coupling from different cg and cb locations due to translational and rotational motion and added mass terms
D_b	Drag on the body of the towfish
D_f	Drag on the horizontal fins of the towfish
D_ε	Drag on a differential element of the cable
e	Eccentricity of the towfish body
E	Young's modulus
$\mathbf{f_{ext}}$	External forces acting on the towfish in the inertial frame
F_{axial}	The x component of $\mathbf{F_{ext}}$ in the body frame
$\mathbf{F_{body}}$	Hydrodynamic force that acts on the hull of the towfish represented in the body frame
$\mathbf{F_{buoyancy}}$	Buoyancy force due to the towfish in the body frame
$\mathbf{F_{ext}}$	External force that acts on the towfish
$F_{lateral}$	The y component of $\mathbf{F_{ext}}$ in the body frame
F_{normal}	The z component of $\mathbf{F_{ext}}$ in the body frame
$\mathbf{F_{fin}}$	Hydrodynamic force acting on the fins represented in the body frame
$\mathbf{F_{td}}$	Force from the tether caused by towing the vehicle in the cable frame

$\mathbf{F_{tow}}$	Force from the tether caused by towing the vehicle represented in the body frame
$\mathbf{F_{weight}}$	Force due to the weight of the towfish in the body frame
h	Depth below the towfish
h_i	Depth in which the depressor is below the towfish nose for a specific towing speed
H_{RP}	Random pendulum amplitude
H_s	Significant wave height
$\mathbf{J}$	Rotational inertia and added inertia matrix
$\mathbf{J_{Ab}}$	Rotational added inertia matrix from the towfish body
$\mathbf{J_{Af}}$	Rotational added inertia matrix from the fins
J_x	Moment of inertia of the towfish about the body x axis
J_{xy}	The product of inertia about the x-y axes
J_{xz}	The product of inertia about the x-z axes
J_y	Moment of inertia of the towfish about the body y axis
J_{yz}	The product of inertia about the y-z axes
J_z	Moment of inertia of the towfish about the body z axis
$\mathbf{J_0}$	Rotational rigid body inertia matrix
$\bar{k}$	Spring constant that varies with towing speed
k_{cr}	Critical gain
k_d	Derivative gain
k_i	Integral gain
k_p	Proportional gain
$k_{\theta p}$	Pitch channel proportional gain
$k_{\phi p}$	Roll channel proportional gain
K	A constant that defines the drag polar curve
$K_{\dot{p}f}$	Fin added inertia in roll
$K_{\dot{p}f}^{2D}$	Two-dimensional fin added inertia in roll
K_1	Empirical factor of the towfish
l_b	Length of the towfish body
l_f	Length from the origin of the body frame to the fin's geometric

	center
l_i	The diagonal distance between the towfish nose and the depressor for a designated towing speed
l_t	Length from the hydrodynamic center of the fins to the cb of the towfish body
L	Length of the pigtail
L_b	Lift of the towfish body
L_f	Lift of the horizontal fins of the towfish
L_p	Damping moment due to roll
m	Mass of the towfish
$\mathbf{M}$	Mass and added mass matrix
$\bar{\mathbf{M}}$	Generalized inertia matrix
$\mathbf{M_{body}}$	Hydrodynamic moment on the hull of the towfish represented in the body frame
$\mathbf{M_{damping}}$	Damping moment on the towfish represented in the body frame
$\mathbf{M_{ext}}$	External moment that acts on the towfish
M_{pitch}	The y component of $\mathbf{M_{ext}}$ in the body frame
M_q	Damping moment due to pitch
$M_{\dot{q}b}$	Body added inertia in pitch due to pitch acceleration
$M_{\dot{q}f}$	Fin added inertia in pitch due to pitch acceleration
M_{roll}	The x component of $\mathbf{M_{ext}}$ in the body frame
$\mathbf{M_{fin}}$	Hydrodynamic moment caused by the fins represented in the body frame
$\mathbf{M_{tow}}$	Moment from the pigtail caused by towing the vehicle represented in the body frame
$\mathbf{M_{weight}}$	Moment due to the center of gravity offset represented in the body frame
$M_{\dot{w}f}$	Fin added inertia in pitch due to acceleration along the z_b axis
M_{yaw}	The z component of $\mathbf{M_{ext}}$ in the body frame
N_r	Damping moment due to yaw
$N_{\dot{r}b}$	Body added inertia in yaw due to yaw acceleration

$N_{\dot{r}f}$	Fin added inertia in yaw due to yaw acceleration
$N_{\dot{v}f}$	Fin added inertia in yaw due to acceleration along the y_b axis
p	Roll rate of the towfish in the body frame
$\mathbf{P}$	Linear momentum of the towfish at the body frame center
$\dot{\mathbf{P}}$	Derivative of the linear momentum of the towfish at the body frame center with respect to time
P_{cr}	Critical period
$\mathbf{P_I}$	Linear momentum of the towfish in the inertial frame
$\dot{\mathbf{P}}_\mathbf{I}$	Derivative of the linear momentum of the towfish in the inertial frame with respect to time
q	Pitch rate of the towfish in the body frame
$\bar{q}$	Dynamic pressure
r	Yaw rate of the towfish in the body frame
$\mathbf{r_{cb}}$	Distance from center of the body axis to the center of buoyancy
$\mathbf{r_{cg}}$	Distance from center of the body axis to the center of gravity
$\mathbf{R}$	Vector that represents the distance from the center of buoyancy to the center of the inertial frame
$\mathbf{R_{BC}}$	Rotation matrix that changes a vector in the water current frame to the body frame
$\mathbf{R_{BS}}$	Rotation matrix that changes a vector in the vertical gyro frame to the body frame
$\mathbf{R_{IB}}$	Rotation matrix that changes a vector in the body frame to the inertial frame
$\dot{\mathbf{R}}_\mathbf{IB}$	Derivative of the rotation matrix $\mathbf{R_{IB}}$ with respect to time
$\mathbf{R_{ICable}}$	Rotation matrix that changes a vector in the cable frame to the inertial frame
$\mathbf{R_{SI}}$	Rotation matrix that changes a vector in the inertial frame to the vertical gyro frame
Re	Reynolds Number
S_b	The reference area of the towfish body
S_f	Area of the two horizontal or vertical fins

S_J	JONSWAP wave spectrum
t	Thickness of the fin
T	Total kinetic energy of the towfish
T_c	Tension of the cable acting at the nose of the towfish
T_d	Derivative time
T_i	Integral time
$T_{\theta d}$	Pitch channel derivative time
$T_{\theta i}$	Pitch channel integral time
$T_{\phi d}$	Roll channel derivative time
$T_{\phi i}$	Roll channel integral time
T_1	Modal wave period
$\mathbf{T_2}$	Transformation matrix relating the body fixed angular velocity to the Euler rate vector
u	Velocity of the towfish in the x direction
$\mathbf{U_{depressor}}$	Depressor inertial velocity
U_0	Reference velocity
v	Velocity of the towfish in the y direction
$\mathbf{V}$	The velocity vector of the towfish represented in the body frame
Vol	Volume of the towfish body
w	Velocity of the towfish in the z direction
W	Weight of the Towfish
W_A	Weight of the towfish at point A
W_{added}	Weight added to point B
W_B	Weight of the towfish at point B
W_ε	Weight of the differential element of cable
x	Inertial x position of the towfish
x_b	The x position of the towfish in the body frame
x_{BA}	Distance from point A to point B in the longitudinal direction
x_c	The x position of the towfish in the water current frame
x_{cb1}	Center of buoyancy in the longitudinal direction from point A (in inches)

x_{cg}	Center of gravity in the x direction from the body axis center
x_{cg1}	Center of gravity in the longitudinal direction from point A (in inches)
x_{depth}	Depressor depth
x_f	The x distance from the orgin of the bdoy frame to the towfish to the hydrodynamic center of the horizontal fins
x_i	The x distance from the towfish nose to the depressor for a specific towing speed
x_{pcb}	Center of buoyancy in the longitudinal direction from the front of the power housing
x_{pcg}	Center of gravity in the longitudinal direction from the front of the power housing
x_{random}	Random depressor position in the inertial x direction
$\mathbf{X_{aci}}$	Vector that represents the distance from the body axis origin to the hydrodynamic center of the ith fin
$\mathbf{X_{cg}}$	Vector that represents the distance from the body axis center to the center gravity
$\mathbf{X_{depressor}}$	Inertial position of the depressor
$\mathbf{X_I}$	Inertial position of the towfish
$\dot{\mathbf{X}}_\mathbf{I}$	Inertial velocity of the towfish
$\mathbf{X_{nom}}$	Nominal motion of the towfish
$X_{\dot{u}b}$	Added mass associated with the body x direction
y	Inertial y position of the towfish
y_b	The y position of the towfish in the body frame
y_c	The y position of the towfish in the water current frame
y_{cg}	Center of gravity in the y direction from the body axis center
y_{random}	Random depressor position in the inertial y direction
$Y_{\dot{r}f}$	Added mass in the y_b direction due to yaw acceleration
$Y_{\dot{v}b}$	Added mass associated with the body y direction
$Y_{\dot{v}f}$	Added mass associated with the fins y direction
$Y_{\dot{v}f}^{2D}$	Added mass of the fins when assuming the fins are a 2-D plate

Y_{90}	Thickness at 90 percent of the chord divided by the chord length
Y_{99}	Thickness at 99 percent of the chord divided by the chord length
z	Inertial z position of the towfish
z_b	The z position of the towfish in the body frame
z_c	The z position of the towfish in the water current frame
z_{cg}	Center of gravity in the z direction from the body axis center
z_{ccb}	Center of buoyancy location in the z direction measured from the top of the computer housing
z_{ccg}	Center of gravity location in the z direction measured from the top of the computer housing
z_{random}	Random depressor position in the inertial z direction
$Z_{\dot{w}b}$	Added mass associated with the body z direction
$Z_{\dot{w}f}$	Added mass associated with the fins z direction

Greek Symbols

α	Angle of attack
α_c	Angle between the projection of the velocity vector into the plane of symmetry and the x_b axis
β_c	Angle between the velocity vector and the plane of symmetry with respect to the towfish body frame
$\delta_{\mathbf{nom}}$	Nominal vector of control inputs
δ_1	Requested fin deflection of the right fin
δ_2	Requested fin deflection of the left fin
ΔE	Angle from horizontal in which the horizontal fins are deflected
$\mathbf{\Delta x}$	Position vector from the towfish nose to the depressor
$\mathbf{\Delta X}$	Deviations from the nominal values of state
$\mathbf{\Delta u}$	Difference between the depressor speed and the towpoint speed
$\mathbf{\Delta}\delta$	Deviations from the nominal values of the control variables
η	Efficiency factor of the fins in the flow from the body
γ	Flight path angle

$\Lambda_{1/2}$	Sweep at 1/2 the chord
μ	Angle between the velocity vector and the x_b axis
μ_1	Dynamic viscosity of the ocean
ω_{dep}	Depressor pendulum frequency
ω_n	Angular frequency
ω_w	Wave frequency
$\mathbf{\Omega}$	The angular velocity of the towfish in the body fixed coordinate frame
ϕ	Roll angle of the towfish
$\dot{\phi}$	Change in roll angle of the towfish with respect to time
ϕ_c	Angle which the cable makes with vertical
ϕ_{TE}	The trailing edge angle of the fins
$\mathbf{\Phi_I}$	The angular position
$\mathbf{\dot{\Phi}_I}$	The change in angular position with respect to time
$\mathbf{\Pi}$	Body angular momentum of the towfish
$\mathbf{\dot{\Pi}}$	The derivative of the body angular momentum at the center of buoyancy of the towfish with respect to time
$\mathbf{\Pi_0}$	Body angular momentum of the towfish in the inertial frame
ψ	Yaw angle of the towfish
$\dot{\psi}$	Change in yaw angle of the towfish with respect to time
σ	Angle between the distance vector (from the towfish nose to the depressor) and the plane of symmetry with respect to the towfish body frame
ρ	Density of the fluid
τ	Response time constant
θ	Pitch angle of the towfish
$\dot{\theta}$	Change in pitch angle of the towfish with respect to time
θ_c	Angle that the tension force in the cable makes with horizontal
υ	Body fixed velocities
ε	Span efficiency factor
ξ	Angle between the projection of the distance vector (from the

	towfish nose to the depressor) into the plane of symmetry and the x_b axis
ζ	Weight per unit length of the cable
ζ_d	Damping ratio

List of Figures

List of Tables

1 Introduction

The goal of this project is to create a towed sensor platform that can hold a five-beam acoustic Doppler current profiler (VADCP) used to measure small-scale ocean turbulence. The towfish design has a streamlined body, two fixed vertical stabilizers and two independently actuated stern planes. The fully assembled towfish out of the water can be seen in Figure 1.

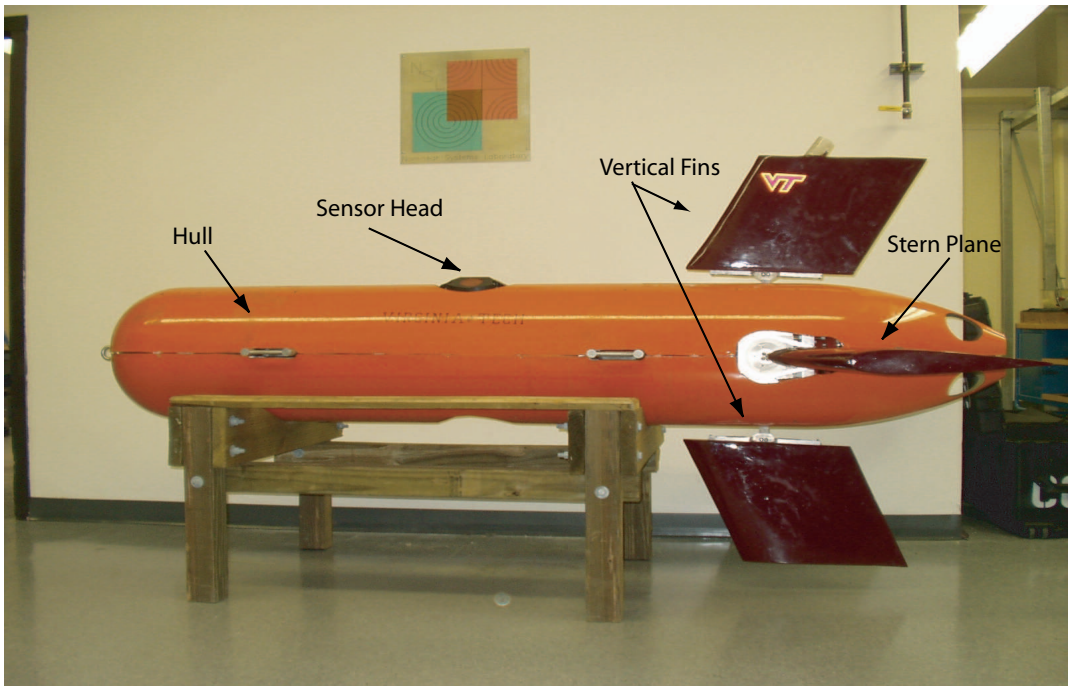

Figure 1: Fully assembled towfish out of the water

Performance specifications for the towfish include the ability to operate at depths of 660 feet ($\approx$ 200 m) and speeds from 2 to 6 knots ($\approx$ 3 ft/s to $\approx$ 10 ft/s). To allow accurate measurements to be made by the sensor to observe small-scale ocean turbulence in a vertical column, the towfish also needs to maintain plus or minus one degree of attitude in pitch and roll. For recovery purposes, the towfish is designed to be 5 percent buoyant.

1.1 System configuration

The towfish for this project was designed as a two-part tow where an umbilical cable runs from the research vessel to the towfish, with a depressor fastened along the cable; see Figure 2. The section of the cable from the ship to the depressor is known as the "main catenary" and the portion of the cable from the depressor to the towfish is labelled the "pigtail".

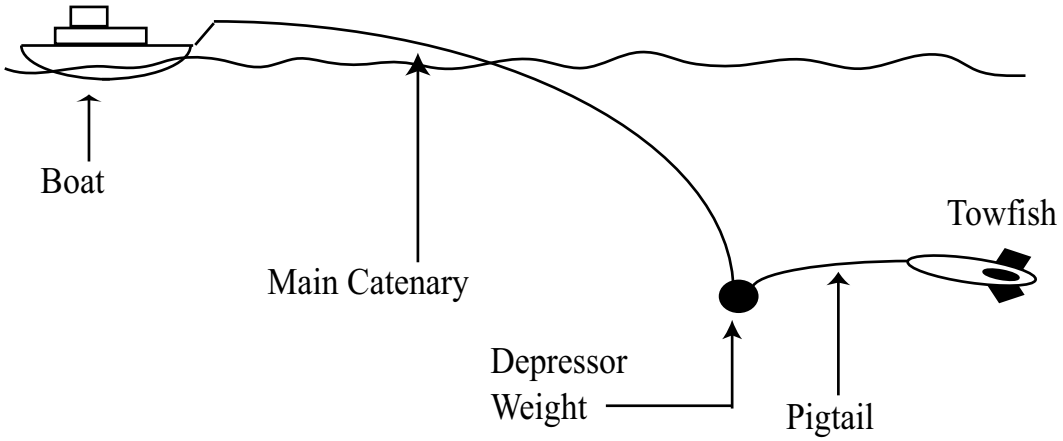

Figure 2: Two-part towing arrangement

This design was developed with four fins to give the towfish more stability and the ability to reject disturbances. This is necessary in order to make accurate measurements with the VADCP. The VADCP measures three components of fluid velocity that scientists can use to observe small-scale ocean turbulence in a vertical column. Figure 3 shows a sketch of the towfish taking measurements.

In order to make these measurements, the fins on the towfish are used to stabilize the vehicle within plus or minus one degree of pitch and roll. If the fins are unable to maintain the attitude in this range, the turbulence measurements will be corrupted and unusable. The two horizontal fins of the towfish are controlled by two servo-actuators through a sprocket/chain assembly. The two vertical fins are fixed and the top fin holds a VHF(very high frequency) pinger with a Xenon strobe light. Along with the VADCP, the towfish contains an on-board computer, an altimeter, a depth

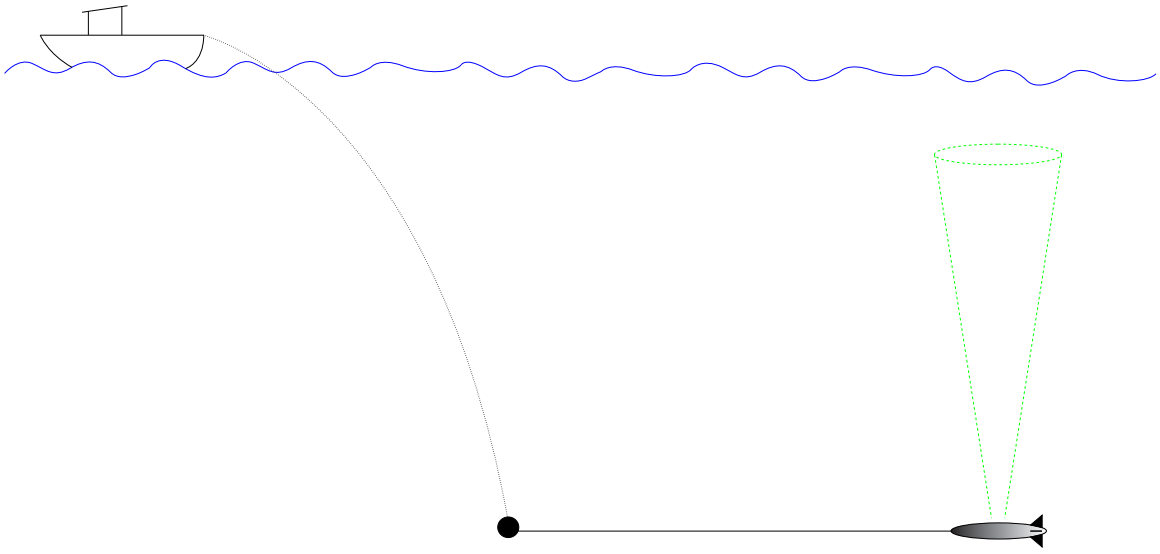

Figure 3: A sketch of the towfish taking measurements

sensor, and an inertial measurement unit. The altimeter measures the distance the towfish is from the bottom of the ocean. The depth sensor measures the depth of the towfish relative to the surface. The research vessel which tows the system, supplies AC power which is converted locally into 144, 48 and 12 volts DC to power the various onboard components. The power converters, computer, and a tilt sensor are enclosed in two watertight pressure housings that were designed to fit inside of the aluminum frame of the towfish.

The towfish was originally designed by Eric Schuch as described in his Masters thesis [20]. Figure 4 shows the original design of the towfish. A detailed description of the towfish components has been included in Section 5 of this thesis.

1.2 Literature review

Traditionally, ocean turbulence has been measured by dropping a tethered instrument at a point in the ocean, letting it fall to a specified depth and then retrieving the instrument. This type of data collection takes a lot of time. Recently, scientists have begun to measure fluid velocity using acoustic doppler current profilers (ADCPs),

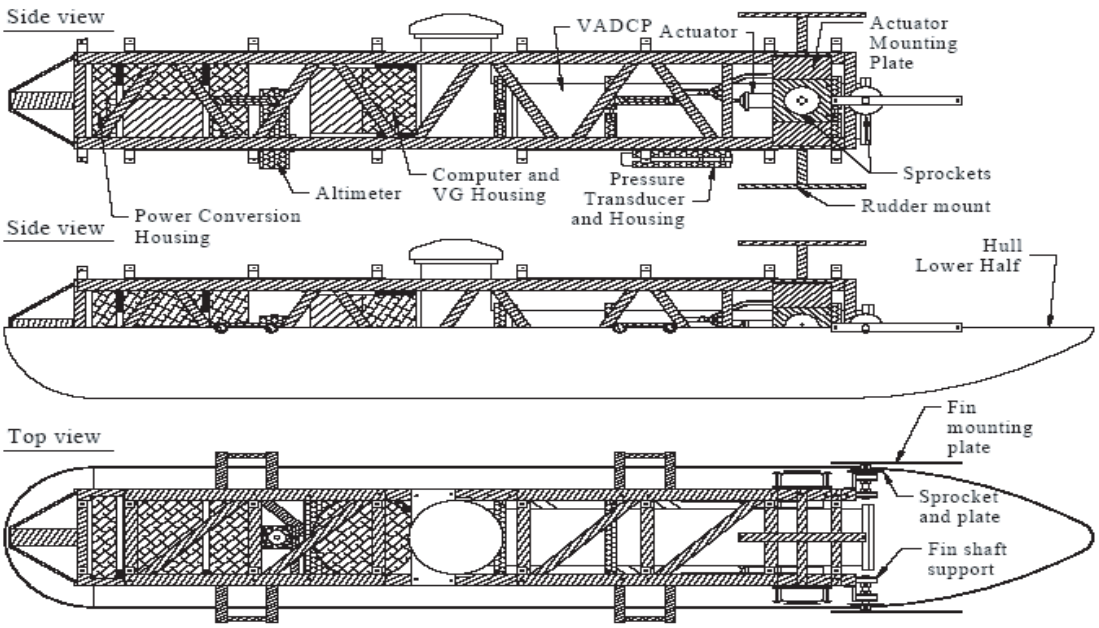

Figure 4: Top and side views of the towfish and its components [20]

which give them data at a grid of points in a vertical plane. Old Dominion University's Center for Coastal Physical Oceanography (CCPO) has a five-beam ADCP that can produce maps of the turbulence quantities such as vertical momentum stresses, turbulent kinetic energy, and the dissipation rate. The vertical shear and the mean current can also be measured with this sensor. A VADCP gives scientists the ability to map turbulence in offshore environments by identifying pockets of turbulence in the ocean quickly. The towfish can look for turbulent spots at a moderate speed and then when a turbulent area is found, it can gather higher resolution data at a lower speed. The VADCP was custom built by RD Instruments and is a one-of-a-kind sensor. The five beams of this sensor run at 1200 kHz. Figure 5 shows a photograph of the actual sensor.

The VADCP measures three components of fluid velocity. Four beams in a tetrahedral arrangement measure two components of velocity and the fifth beam provides the third velocity component. To accurately resolve small-scale ocean turbulence, the fifth beam must be precisely aligned with the local direction of gravity. The

Figure 5: Sensor used to make fluid velocity measurements

turbulent fluctuations are orders of magnitude larger in the lateral direction; a small misalignment of the sensor can irreversibly corrupt the data.

A few different approaches were considered for carrying the VADCP. These different approaches included remotely operated vehicles (ROVs), autonomous underwater vehicles(AUVs) and one and two-part towing arrangements. An ROV requires a cable winch and enough power from the boat to allow the ROV to go far below the ocean's surface. ROVs do allow for large exchanges of data since a large amount of power can be run from the research vessel to the ROV, however ROVs are best used for speeds of 3.28 ft/s ($\approx$ 1 m/sec) or less [1]. This speed of 3.28 ft/s falls at the low end of the operating range in which the towfish is desired to travel. A second option that was considered to hold the VADCP was an AUV. Two major drawbacks of using an AUV are their inability to transmit a large amount of data and the amount of money it costs to buy or make one. Although AUVs have come a long way over the years, they do not have the ability to transfer the recorded data in the necessary time. It is important that this data be transferred so scientists can analyze the fluid velocity measurements and change the survey plan accordingly [20].

Other designs explored were one and two-part towing arrangements. Towing arrangements however, create disturbances from the cable. A single towing arrangement with the towing point in front of or at the cg can cause the surge and heave from the research vessel to be transferred to the towfish. Pitch disturbances at the fins can be

caused from the surge and heave of the research vessel [18]. A two-part towing arrangement with a well-shaped catenary allows the surge and heave effects from the research vessel to be reduced by the depressor. The longer the length of the pigtail, the fewer disturbances that are likely to be transferred to the towfish [20]. The shape of the main catenary and pigtail in a two-part tow helps to reduce the pitch disturbance created from the main research vessel, however the yaw disturbances will still be transmitted to the towfish [18]. It should be noted, however that the change in yaw angle is not of importance for the VADCP to make accurate fluid velocity measurements.

Dr. Ann Gargett of CCPO used a metal frame as a towfish and was able to maintain this vehicle within plus or minus two degrees of tilt through using a two-stage towing arrangement. This process for towing the sensor was tedious because it had to be iteratively trimmed, launched and recovered to minimize the bias [9]. By adding servo-actuated stern planes, the biases of the towfish can be actively adjusted which will increase the stability of the towfish [19]. For this project, it was concluded that a two-part towing arrangement was best.

1.3 Outline of thesis

The towfish was designed by Eric Schuch in 2002 and 2003 and then fabricated by students and machinists. The towfish was then tested in November 2004. At this point, a number of issues were identified which needed to be fixed, such as, the flotation of the towfish and some control software issues. This thesis explains how the flotation of the towfish issue has been addressed along with a few other mechanical changes. It also discusses significant improvements to the numerical simulation that was developed to validate the control algorithms. This simulation is then used to investigate how varying critical parameters will affect the results obtained by the towfish when used in the ocean.

Section 2 discusses the nonlinear kinematic and dynamic equations for a 6 degree of freedom rigid body. This section develops the translational and rotational kinematic

equations and then derives the linear and angular momentum equations. There is also a detailed description of the forces and moments that act on the towfish.

Section 3 describes a detailed static analysis of the depressor-pigtail-towfish system. This analysis provides an improved model for the dynamic effect of the pigtail. There is also an explanation of how the equations were linearized about the equilibrium for the development of a PID controller that is used to increase the stability of the towfish.

Section 4 describes the numerical parametric analysis of the effects of the sea state, towing speed, the distance between the center of gravity (cg) and the center of buoyancy (cb) and a PID controller on the towfish performance.

Section 5 describes the process involved in constructing the hull and the fins of the towfish. This section also includes a description of major components of the towfish.

Section 6 covers the trimming and ballasting of the towfish. This section goes into detail on where the initial cg and cb were located in the towfish and what has been done to move these points so the towfish would be easier to keep within plus or minus one degree in pitch and roll. This section includes calculations that determined the two pressure housings' and sensor's cg and cb location.

Finally, section 6 provides conclusions on what limitations have been found from the simulations along with suggestions.

Appendix A includes the Matlab code that was written to calculate the cb and the cg of the towfish. This appendix also includes the Mathematica code that was written to determine the variation in towing force at the towfish nose due to change in speed.

Appendix B includes a detailed description of the Simulink simulation along with the Matlab code used with the simulation.

Appendix C explains how the vertical gyro has been used to measure the pitch and roll angles of the towfish. This appendix describes in detail how the the pitch and roll angles determined by the vertical gyro can be related to body frame. This is

important since the vertical gyro is oriented differently than the tilt sensor in the VADCP.

2 Kinematic and Dynamic Equations

In order to validate the two-part towing arrangement and to develop an understanding of its performance and limitations a Simulink simulation of the system was created. This Simulink simulation is described in detail in Appendix B. The following section develops the nonlinear equations needed to model this setup. The parameters for the towfish have been included in Appendix B along with the Simulink simulation description.

2.1 Kinematics

The kinematic equations for a rigid body with 6 degrees of freedom have been developed. The body-fixed coordinate system for the towfish was assumed to be at the cb which lies close to the geometric center. This coordinate frame can be seen in Figure 6. The x_b axis points out of the nose of the towfish, the y_b points out of the side, therefore the z_b axis points down and is in the plane of symmetry with the vertical fins. The position of the towfish is denoted by $\mathbf{X_I} = [x, y, z]^T$ and is relative to the inertial frame. The attitude with respect to the inertial frame is defined by $\mathbf{\Phi_I} = [\phi, \theta, \psi]^T$. The linear velocity relative to the inertial frame is labelled as $\mathbf{V} = [u, v, w]^T$ and is defined in the body fixed frame. The angular velocity is defined in the body fixed frame as $\mathbf{\Omega} = [p, q, r]^T$ with reference to the inertial axes.

The body frame vector components are mapped to the inertial frame vector components through the Euler angles (ϕ, θ, ψ). Conventionally, a 3-2-1 rotation is defined for guidance and control as the rotation from the inertial frame to the body frame.

$$\mathbf{R_{BI}} = \begin{bmatrix} \cos[\theta]\cos[\phi] & \cos[\theta]\sin[\phi] & -\sin[\theta] \\ \sin[\psi]\sin[\theta]\cos[\phi] - \cos[\psi]\sin[\phi] & \sin[\psi]\sin[\theta]\sin[\phi] + \cos[\psi]\cos[\phi] & \sin[\psi]\cos[\theta] \\ \cos[\psi]\sin[\theta]\cos[\phi] + \sin[\psi]\sin[\phi] & \cos[\psi]\sin[\theta]\sin[\phi] - \sin[\psi]\cos[\phi] & \cos[\psi]\cos[\theta] \end{bmatrix}$$

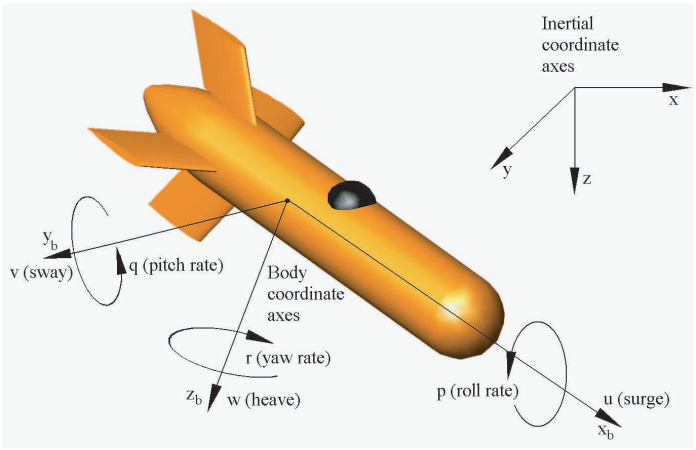

Figure 6: Location of the body and inertial coordinate frames on the towfish [20]

From this the translational kinematic equation is defined as follows:

$$\dot{\mathbf{X}}_{\mathbf{I}} = \mathbf{R}_{\mathbf{BI}}^{-\mathbf{1}}\mathbf{V} = \mathbf{R}_{\mathbf{BI}}^{\mathbf{T}}\mathbf{V} = \mathbf{R}_{\mathbf{IB}}\mathbf{V} \tag{1}$$

where $\mathbf{R_{IB}} = \mathbf{R_{BI}^{T}}$. The body fixed angular velocity vector is then related to the Euler rate vector, $\dot{\mathbf{\Phi}}_{\mathbf{I}} = [\dot{\phi}, \dot{\theta}, \dot{\psi}]^T$, through a transformation matrix $\mathbf{T_2}$. The matrix $\mathbf{T_2}$ can be derived through

$$\mathbf{\Omega} = \begin{bmatrix} \dot{\phi} \\ 0 \\ 0 \end{bmatrix} + R_1(\phi) \begin{bmatrix} 0 \\ \dot{\theta} \\ 0 \end{bmatrix} + R_1(\phi)R_2(\theta) \begin{bmatrix} 0 \\ 0 \\ \dot{\psi} \end{bmatrix}$$

where

$$\mathbf{R_1}(\phi) = \begin{bmatrix} 1 & 0 & 0 \\ 0 & \cos\phi & \sin\phi \\ 0 & -\sin\phi & \cos\phi \end{bmatrix}$$

and

$$\mathbf{R_2}(\theta) = \begin{bmatrix} \cos\theta & 0 & -\sin\theta \\ 0 & 1 & 0 \\ \sin\theta & 0 & \cos\theta \end{bmatrix}$$

Therefore,

$$\mathbf{\Omega} = \begin{bmatrix} 1 & 0 & -\sin[\theta] \\ 0 & -\cos[\theta] & \cos[\theta]\sin[\phi] \\ 0 & -\sin[\phi] & \cos[\theta]\cos[\phi] \end{bmatrix} \dot{\mathbf{\Phi}}_\mathbf{I}$$

Denote the 3×3 matrix as $\mathbf{T_2^{-1}}$. By taking the inverse of this three by three matrix the following equation is found:

$$\dot{\mathbf{\Phi}}_\mathbf{I} = \mathbf{T_2}\mathbf{\Omega} = \begin{bmatrix} 1 & \sin[\phi]\tan[\theta] & \cos[\phi]\tan[\theta] \\ 0 & \cos[\phi] & -\sin[\phi] \\ 0 & \sin[\phi]/\cos[\theta] & \cos[\phi]/\cos[\theta] \end{bmatrix} \mathbf{\Omega} \tag{2}$$

The above equation is known as the rotational kinematic equation. It should be noted that the transformation matrix $\mathbf{T_2}$ is undefined for a pitch angle of θ equal to plus or minus ninety degrees. Therefore at these two angles a singularity occurs. This however should not be a problem for the towfish since it is necessary to keep it within plus or minus one degrees in pitch and roll in order for the VADCP to make accurate measurements to observe small-scale ocean turbulence in a vertical column.

2.2 Dynamics

The dynamic equations for the simulation have assumed:

- The towfish is a streamlined rigid body with four fins
- The towfish is being towed through an ideal fluid
- The towfish has been approximated as an ellipsoid

The basic dynamic equations of the towfish can be found from Kirchhoff's equations of motion for a rigid body in an ideal fluid. These equations will be developed in this section. The total kinetic energy is

$$T = 1/2 \upsilon^T \bar{\mathbf{M}} \upsilon$$

where υ is the body-fixed velocities (u, v, w, p, q, r). Through expansion,

$$T = 1/2(\mathbf{\Omega}^T \mathbf{J} \mathbf{\Omega} + 2\mathbf{\Omega}^T \mathbf{D} \mathbf{V} + \mathbf{V} \mathbf{M} \mathbf{V}) \tag{3}$$

By then taking the partial derivative of the total kinetic energy with respect to the linear velocity and the angular velocity, the linear and angular momentum are developed:

$$\begin{bmatrix} \mathbf{P} \\ \mathbf{\Pi} \end{bmatrix} = \begin{bmatrix} \frac{\partial \mathbf{T}}{\partial \mathbf{V}} \\ \frac{\partial \mathbf{T}}{\partial \mathbf{\Omega}} \end{bmatrix} = \begin{bmatrix} \mathbf{M} & \mathbf{D}^T \\ \mathbf{D} & \mathbf{J} \end{bmatrix} \begin{bmatrix} \mathbf{V} \\ \mathbf{\Omega} \end{bmatrix} \tag{4}$$

where $\mathbf{M}$ is the mass and added mass matrix, $\mathbf{J}$ is the rotational inertia matrix, and $\mathbf{D}$ is the coupling that occurs when the cg and cb are not at the same location due to the translational and rotational motion and the added mass terms. The added mass comes from the forces and moments due to the acceleration of the fluid around the body. The generalized inertia matrix for this 6 DOF underwater vehicle can be defined by:

$$\bar{\mathbf{M}} = \begin{bmatrix} \mathbf{M} & \mathbf{D}^T \\ \mathbf{D} & \mathbf{J} \end{bmatrix}$$

The 3×3 $\mathbf{M}$ matrix for this underwater vehicle that includes the rigid body mass and added mass matrix is developed on the assumption that the rigid body is an ellipsoid. The only terms that appear in the added mass and mass matrix for this vehicle are on the diagonal since the rigid body is symmetric. The mass and added mass matrix for the towfish body is

$$\mathbf{M} = \begin{bmatrix} m + X_{\dot{u}b} & 0 & 0 \\ 0 & m + Y_{\dot{v}b} + Y_{\dot{v}f} & 0 \\ 0 & 0 & m + Z_{\dot{w}b} + Z_{\dot{w}f} \end{bmatrix}$$

where m is the mass of the towfish. The added mass terms due to the body are defined as $X_{\dot{u}b}$, $Y_{\dot{v}b}$ and $Z_{\dot{w}b}$ associated with the body x, y, and z direction respectively. The added mass terms due to the fins are defined as $Y_{\dot{v}f}$ and $Z_{\dot{w}f}$. The terms $m+Y_{\dot{v}b}+Y_{\dot{v}f}$ and $m + Z_{\dot{w}b} + Z_{\dot{w}f}$ in the above matrix are the same since the body of the towfish and the fins are symmetric. For a spheroidal body,

$$X_{\dot{u}b} = \frac{-\alpha_0}{2 - \alpha_0} m$$

and

$$Y_{\dot{v}b} = Z_{\dot{w}b} = \frac{-\beta_0}{2 - \beta_0} m$$

where α_0 and β_0 are constants that depend on eccentricity. From reference [6],

$$e = \sqrt{1 - \left(\frac{d_b}{l_b}\right)^2}$$

thus,

$$\alpha_0 = 2\frac{(1-e^2)}{e^3}(\frac{1}{2}\ln\left(\frac{1+e}{1-e}\right) - e)$$

$$\beta_0 = \frac{1}{e^2} - \frac{1-e^2}{2e^3}\ln\left(\frac{1+e}{1-e}\right)$$

The added mass terms of the fins, $Y_{\dot{vf}}$ and $Z_{\dot{wf}}$, are assumed to be equal due to symmetry. To estimate these values for the fins, it is assumed that each fin is a 2-dimensional plate. The added mass of the fins was calculated by

$$Y_{\dot{vf}}^{2D} = \pi\rho(c/2)^2$$

where ρ is the density of the water and c is the chord length of the fins [16]. Through following reference [6], $Y_{\dot{vf}}^{2D}$ is used to find $Y_{\dot{vf}}$.

$$Y_{\dot{vf}} = \int_{b/2}^{b/2} Y_{\dot{vf}}^{2D} dx = Y_{\dot{vf}}^{2D} b$$

The 3×3 rotational inertia matrix for the towfish can be defined by

$$\mathbf{J} = \mathbf{J_0} + \mathbf{J_{Ab}} + \mathbf{J_{Af}} \tag{5}$$

where $\mathbf{J_0}$ is the rigid body rotational inertia matrix, $\mathbf{J_{Ab}}$ denotes the added rotational inertia matrix from the body and $\mathbf{J_{Af}}$ represents the added rotational inertia matrix for the fins. Explicitly,

$$\mathbf{J} = \begin{bmatrix} J_x & -J_{xy} & -J_{xz} \\ -J_{xy} & J_y & -J_{yz} \\ -J_{xz} & -J_{yz} & J_z \end{bmatrix} + \begin{bmatrix} 0 & 0 & 0 \\ 0 & M_{\dot{qb}} & 0 \\ 0 & 0 & N_{\dot{rb}} \end{bmatrix} + \begin{bmatrix} K_{\dot{pf}} & 0 & 0 \\ 0 & M_{\dot{qf}} & 0 \\ 0 & 0 & N_{\dot{rf}} \end{bmatrix}$$

Note that it is assumed the principal axes are the same as the body axes in the Simulink simulation so the terms J_{xy}, J_{xz}, and J_{yz} have been set equal to zero. The added rotational inertia terms due to the body are defined as

$$N_{\dot{rb}} = M_{\dot{qb}} = -1/5 \left(\frac{(d_b^2 - l_b^2)^2(\alpha_0 - \beta_0)}{2(d_b^2 - l_b^2) + (d_b^2 + l_b^2)(\beta_0 - \alpha_0)} \right) m$$

where α_0 and β_0 are constants that have been previously defined, d_b is the diameter of the towfish and l_b is the length of the towfish.

Following reference [12], the added rotational inertia terms due to the fins are

$$N_{\dot{qr}} = M_{\dot{qf}} = l_f^2 Y_{\dot{vf}}$$

where l_f is the length from the origin of the body axis to the fin's geometric center. The added rotational inertia from the fins in the longitudinal direction, is taken from reference [6] as:

$$K_{\dot{pf}} = \int_{c/2}^{c/2} K_{\dot{pf}}^{2D} dx = K_{\dot{pf}}^{2D} c$$

thus, from reference [16],

$$K_{\dot{pf}}^{2D} = \frac{2}{\pi} \rho \left(\frac{b}{2} \right)^4$$

where b is the fin span. Note also that the values J_y and J_z are equal for a prolate spheroid with uniformly distributed mass. The towfish is not an exact prolate spheroid, however it can be assumed to be one.

The 3×3 matrix $\mathbf{D}$ is defined to represent the coupling that occurs when the cg and cb are not at the same location due to the translational and rotational motion of the vehicle along with the added mass terms $M_{\dot{wf}}$ and $N_{\dot{vf}}$.

$$\mathbf{D} = \begin{bmatrix} 0 & -mz_{cg} & my_{cg} \\ mz_{cg} & 0 & -mx_{cg} + M_{\dot{wf}} \\ -my_{cg} & mx_{cg} + N_{\dot{vf}} & 0 \end{bmatrix}$$

where x_{cg}, y_{cg}, and z_{cg} are the position of the cg relative to the body axis frame. Reference [12] defines the added mass term $N_{\dot{vf}}$ as

$$N_{\dot{vf}} = M_{\dot{wf}} = l_f Y_{\dot{vf}}$$

Note that $Y_{\dot{rf}} = l_f Y_{\dot{vf}}$.

The 6×6 generalized inertia matrix, $\bar{\mathbf{M}}$, is defined as follows:

$$\begin{bmatrix} m + X_{\dot{ub}} & 0 & 0 & 0 & mz_{cg} & -my_{cg} \\ 0 & m + Y_{\dot{vb}} + Y_{\dot{vf}} & 0 & -mz_{cg} & 0 & mx_{cg} + N_{\dot{vf}} \\ 0 & 0 & m + Z_{\dot{wb}} + Z_{\dot{wf}} & my_{cg} & -mx_{cg} + M_{\dot{wf}} & 0 \\ 0 & -mz_{cg} & my_{cg} & J_x + K_{\dot{pf}} & 0 & 0 \\ mz_{cg} & 0 & -mx_{cg} + M_{\dot{wf}} & 0 & J_y + M_{\dot{qb}} + M_{\dot{qf}} & 0 \\ -my_{cg} & mx_{cg} + N_{\dot{vf}} & 0 & 0 & 0 & J_z + N_{\dot{rb}} + N_{\dot{rf}} \end{bmatrix}$$

From the above definitions, the equations of motion for this rigid body can be derived through the following process:

$$\dot{\mathbf{P}}_I = \mathbf{f_{ext}}$$

where $\dot{\mathbf{P}}_\mathbf{I}$ is the derivative of the total linear momentum of the system in the inertial frame and $\mathbf{f_{ext}}$ is the external forces that are acting on the towfish.

The linear momentum can now be related from the body frame to the inertial frame by the following equation:

$$\mathbf{P_I} = \mathbf{R_{IB}P}$$

Through taking the derivative of this relationship

$$\dot{\mathbf{P}}_\mathbf{I} = \dot{\mathbf{R}}_\mathbf{IB}\mathbf{P} + \mathbf{R_{IB}}\dot{\mathbf{P}}$$

Next, each side of the equation is multiplied by $\mathbf{R}_\mathbf{IB}^\mathbf{T}$ and $\dot{\mathbf{R}}_\mathbf{IB} = \mathbf{R_{IB}}\hat{\mathbf{\Omega}}$ is substituted into the above equation. Therefore, the following expression is developed:

$$\mathbf{R}_\mathbf{IB}^\mathbf{T}\dot{\mathbf{P}}_\mathbf{I} = \mathbf{R}_\mathbf{IB}^\mathbf{T}[\mathbf{R_{IB}}\hat{\mathbf{\Omega}}\mathbf{P} + \mathbf{R_{IB}}\dot{\mathbf{P}}] = \hat{\mathbf{\Omega}}\mathbf{P} + \dot{\mathbf{P}}$$

The relationship $\hat{\mathbf{\Omega}}\mathbf{P} = \mathbf{\Omega} \times \mathbf{P}$ and $\mathbf{R}_\mathbf{IB}^\mathbf{T}\dot{\mathbf{P}}_\mathbf{I} = \mathbf{R}_\mathbf{IB}^\mathbf{T}\mathbf{f_{ext}} = \mathbf{F_{ext}}$ can be substituted into the previous equation. Through this process the following equation is developed.

$$\dot{\mathbf{P}} + \mathbf{\Omega} \times \mathbf{P} = \mathbf{F_{ext}}$$

therefore by rearranging this equation it becomes:

$$\dot{\mathbf{P}} = \mathbf{P} \times \mathbf{\Omega} + \mathbf{F_{ext}} \tag{6}$$

$\mathbf{F_{ext}}$ is the external forces acting on the towfish in the body frame. The external forces can be defined as follows:

$$\mathbf{F_{ext}} = \begin{bmatrix} F_{axial} \\ F_{lateral} \\ F_{normal} \end{bmatrix} = \mathbf{F_{body}} + \mathbf{F_{fin}} + \mathbf{F_{tow}} + \mathbf{F_{weight}} + \mathbf{F_{buoyancy}}$$

Note, these forces have been defined in the nomenclature section of this thesis.

At this point, the derivative of the angular momentum expression can be developed. Figure 7 shows the angular momentum acts at the center of buoyancy which is the center of the body frame.

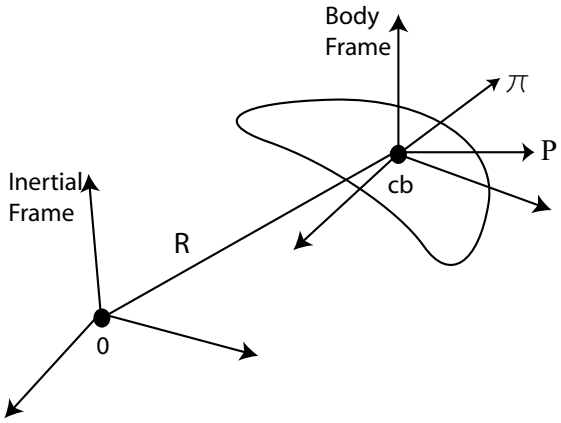

Figure 7: The body angular momentum related to the inertial frame

In Figure 7 the linear momentum $\mathbf{P}$ is denoted with respect to the body frame and the variable $\mathbf{R}$ is the position vector from the center of the inertial frame to center of buoyancy which is the origin of the body frame. From Figure 7 one can see that

$$\mathbf{\Pi_0} = \mathbf{\Pi} + \mathbf{R} \times \mathbf{P}$$

where $\mathbf{\Pi_0}$ is the angular momentum at point 0 which is the center of the inertial frame and $\mathbf{\Pi}$ is the angular momentum at the center of buoyancy of the rigid body. This equation can then be differentiated and the following relationship is produced:

$$\frac{d}{dt}(\mathbf{\Pi_0}) = \mathbf{M_0} = \frac{d}{dt}(\mathbf{\Pi}) + \frac{d}{dt}(\mathbf{R} \times \mathbf{P})$$

which can be written as:

$$\mathbf{M_0} = \dot{\mathbf{\Pi}} + \mathbf{\Omega} \times \mathbf{\Pi} + \mathbf{R} \times \frac{d}{dt}(\mathbf{P}) + \frac{d}{dt}(\mathbf{R}) \times \mathbf{P}$$

therefore, this gives

$$\mathbf{M_0} = \dot{\mathbf{\Pi}} + \mathbf{\Omega} \times \mathbf{\Pi} + \mathbf{R} \times \mathbf{F_{ext}} + \mathbf{V} \times \mathbf{P}$$

where it is known that $\mathbf{M_0} = \mathbf{R} \times \mathbf{F_{ext}} + \mathbf{M_{cb}} + \tau_t$. Through substituting this expression into the above equation the following equation is developed:

$$\dot{\mathbf{\Pi}} = \mathbf{\Pi} \times \mathbf{\Omega} + \mathbf{P} \times \mathbf{V} + \mathbf{M_{cb}} + \tau_t \tag{7}$$

The external moments $\mathbf{M_{ext}} = \mathbf{M_{cb}} + \tau_\mathbf{t}$ can be defined as follows:

$$\mathbf{M_{ext}} = \begin{bmatrix} M_{roll} \\ M_{pitch} \\ M_{yaw} \end{bmatrix} = \mathbf{M_{body}} + \mathbf{M_{fin}} + \mathbf{M_{tow}} + \mathbf{M_{damping}} + \mathbf{M_{weight}}$$

These forces and moments are described in the nomenclature section of this thesis.

Finally through substituting the relationships developed in equation (4) and their derivatives into equations (6) and (7), the equations of motion for a rigid body in a fluid become:

$$\mathbf{M}\dot{\mathbf{V}} + \mathbf{D}^T\dot{\mathbf{\Omega}} = (\mathbf{M}\mathbf{V} + \mathbf{D}^T\mathbf{\Omega}) \times \mathbf{\Omega} + \mathbf{F_{ext}} \tag{8}$$

$$\mathbf{J}\dot{\mathbf{\Omega}} + \mathbf{D}\dot{\mathbf{V}} = (\mathbf{J}\mathbf{\Omega} + \mathbf{D}\mathbf{V}) \times \mathbf{\Omega} + (\mathbf{M}\mathbf{V} + \mathbf{D}^T\mathbf{\Omega}) \times \mathbf{V} + \mathbf{M_{ext}} \tag{9}$$

2.3 Forces and moments from the towfish hull

The forces and moments from the towfish hull were calculated by using the lift coefficient, the drag coefficient, and the pitch moment coefficient data from the 1/40-scale model of the U.S. Airship Akron. These values were found through the NACA Report Number 432 reference [8]. The report explains the wind tunnel tests that were conducted at different pitch angles to obtain these coefficients. This vehicle seemed to be comparable to the towfish by its fineness ratio, the geometry of the hull and the Reynolds numbers in which it was tested. The major difference between the two vehicles was the hull of the 1/40-scale model of the U.S. Airship Akron is very smooth and had been sanded down. The towfish hull is made of fiberglass that is not faired therefore, the drag coefficient will be higher. This extra amount of drag was accounted for through the following equation from reference [10]:

$$C_{Db0} = 0.44\left(\frac{d_b}{l_b}\right) + 4C_f\left(\frac{l_b}{d_b}\right) + 4C_f\left(\frac{d_b}{l_b}\right)^{0.5} \tag{10}$$

In equation (10) d_b is the diameter of the hull, l_b is the length of the body, and C_f is the skin friction coefficient of the vehicle. This is the additional zero degree angle of attack drag coefficient for a rigid body.

The following data were taken from Table 1 of the NACA No. 432 Report [8] for the Reynolds number of 3.05×10^6 which is close to the Reynolds number of 2.91×10^6, that was calculated for a speed of 6.6 ft/s ($\approx$ 2 m/s) for the towfish. The lift coefficient, drag coefficient and pitching moment coefficient data of the 1/40-scale model of the U.S. Airship Akron were used as a good approximation for the towfish. Therefore

the data points were plotted for drag coefficient, lift coefficient and pitching moment coefficient versus pitch angle in Figures 8, 9, and 11. The lift and drag are non-dimensionalized through dividing by the dynamic pressure and the cube root of the volume squared. Thus, the pitching moment about the center of buoyancy can be divided by the dynamic pressure and the volume to obtain the pitching moment coefficient. The data from the 1/40-scale model of the U.S. Akron Airship was used from 0 degrees to 12 degrees angle of pitch [8]. The data for the drag coefficient versus the pitch angle is fitted with a second order polynomial in Excel. Figure 8 shows the plot of the data with the quadratic fit of the data.

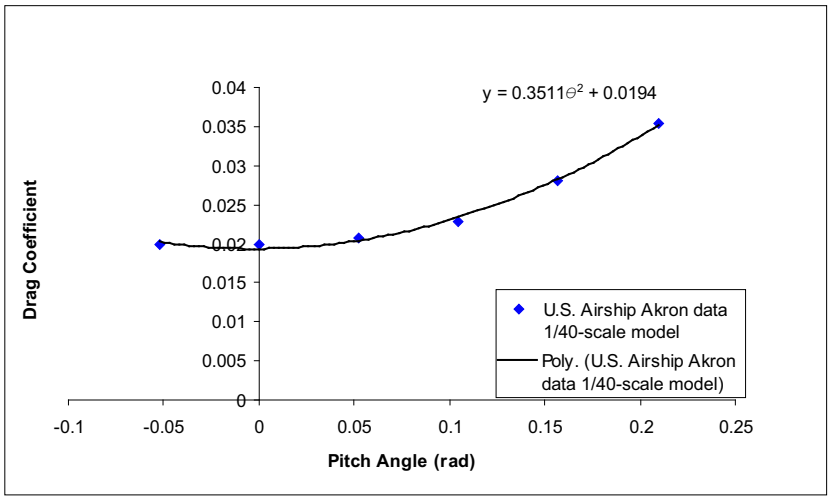

Figure 8: The U.S. Airship Akron 1/40-scale model drag coefficient data versus pitch angle with a quadratic fit

Figure 8 shows that the quadratic fit goes through all the data points therefore this seemed more accurate than the linear fit so it was used for the Simulink simulation. The data points were fitted to the following quadratic equation:

$$C_{Db} = 0.3511\theta^2 + 0.0194 \tag{11}$$

Thus, if the pitch angle of the U.S. Airship Akron 1/40-scale model is assumed to be the angle of attack of the towfish it could be concluded that the drag coefficient of

the body ($C_{D\alpha b}$) was 0.3511 and the drag coefficient at zero angle of attack due to the body (C_{D0}) was equal to 0.0194. However the additional drag from the hull of the towfish from equation (10) also needs to be included in the total drag coefficient of the body of the towfish.

A second plot of the U.S. Airship Akron 1/40-scale model data was created that showed the lift coefficient versus the pitch angle [8]. This plot is shown in figure 9. The data points plotted were linearly and quadratically fit. The quadratic fit proved to be a more accurate fit, therefore this was used in the Simulink simulation.

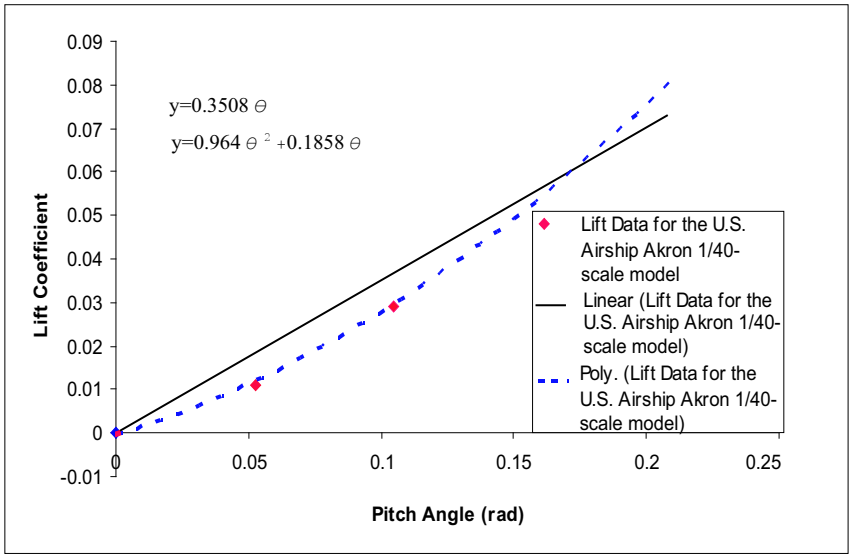

Figure 9: The U.S. Airship Akron 1/40-scale model lift coefficient data versus pitch angle with a linear and a quadratic fit

From Figure 9, the coefficients of lift due to the body are best approximated from the quadratic curve fit where $C_{L\alpha b1}$ was 0.1858 and $C_{L\alpha b2}$ was 0.964. It was assumed that the curve went through (0,0). The value for the lift coefficients of the body are determined on the assumption that the pitch angle is equivalent to the angle of attack of the towfish. Note that, due to symmetry of the towfish about the x_b axis, the side force that acts on the towfish, can be assumed to have the same relationship that the

lift force of the towfish has with the angle of attack.

In order to relate these forces of lift and drag on the body, a frame due to the water current was defined. This frame has an origin fixed to the body at the cb of the towfish. In the water current frame, the x_c axis points in the direction of the velocity vector of the towfish relative to the local body of water. The z_c axis is chosen to lie in the plane of symmetry of the towfish and the y_c axis points to the right of the plane of symmetry, completing the right-handed coordinate frame. For this reference frame, x_c may not always lie in the plane of symmetry. It is dependent on whether the relative water current changes, however z_c always lies in the plane of symmetry. Therefore, the angles α_c and β_c are defined as hydrodynamic angles that relate the water current frame to the body frame of the towfish. The angle between the velocity vector and the plane of symmetry with respect to the towfish body frame can be defined as β_c. The angle between the projection of the velocity vector into the plane of symmetry and the x_b axis is denoted as α_c. This angle is positive when the current is below the x_b axis [4]. Figure 10 shows how α_c and β_c can be defined in terms of $\mathbf{V}$, v, u, and w. Thus, $\mathbf{V}$ is the vector of the linear velocities u, v and w in the x_b, y_b and z_b directions.

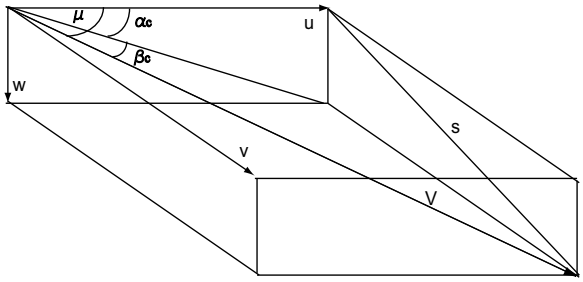

Figure 10: Hydrodynamic angles

From this figure, the hydrodynamic angles α_c and β_c are defined as:

$$\alpha_c = \arctan(\frac{w}{u})$$

$$\beta_c = \arcsin(\frac{v}{|\mathbf{V}|})$$

where

$$|\mathbf{V}| = \sqrt{u^2 + v^2 + w^2}$$

Some other relations that can be developed from Figure 10 that prove to be useful are the following:

$$s = \sqrt{v^2 + w^2}$$

$$\sin(\mu) = \frac{s}{|\mathbf{V}|}$$

$$\mu = \arcsin(\sqrt{\frac{v^2 + w^2}{|\mathbf{V}|^2}})$$

Thus, for small angles it can be assumed that

$$\mu \approx \sqrt{\beta_c^2 + \alpha_c^2}$$

The rotation from the local water current frame to the body frame can therefore be defined as

$$\mathbf{R_{BC}} = \begin{bmatrix} \cos[\alpha_c]\cos[\beta_c] & -\cos[\alpha_c]\sin[\beta_c] & -\sin[\alpha_c] \\ \sin[\beta_c] & \cos[\beta_c] & 0 \\ \cos[\beta_c]\sin[\alpha_c] & -\sin[\alpha_c]\sin[\beta_c] & \cos[\alpha_c] \end{bmatrix}$$

From the defined forces that act on the U.S. Airship Akron 1/40-scale model and the correction term of drag due to the towfish the forces acting on the towfish in the body frame can be defined as

$$\mathbf{F_{body}} = \mathbf{R_{BC}} \left(\begin{bmatrix} -C_{D\alpha b}\mu^2 + C_{D0} \\ -(C_{L\alpha b1}\beta_c + C_{L\alpha b2}\beta_c^2) \\ -(C_{L\alpha b1}\alpha_c + C_{L\alpha b2}\alpha_c^2) \end{bmatrix} \bar{q} Vol^{2/3} + \begin{bmatrix} -C_{Db0} \\ 0 \\ 0 \end{bmatrix} \bar{q} S_b \right)$$

where $\bar{q}$ is the dynamic pressure defined as $\bar{q} = 1/2\rho|\mathbf{V}|^2$, Vol stands for the volume of the vehicle and S_b is the reference area of the body. The reference area of the body is defined as $S_b = \pi d_b^2/4$.

Next, the moments acting on the body of the towfish are defined. This is done by first plotting the pitching moment coefficient data of the U.S. Airship Akron 1/40-scale model versus pitch angle [8]. Figure 11 displays these data points along with the linear fit to the data.

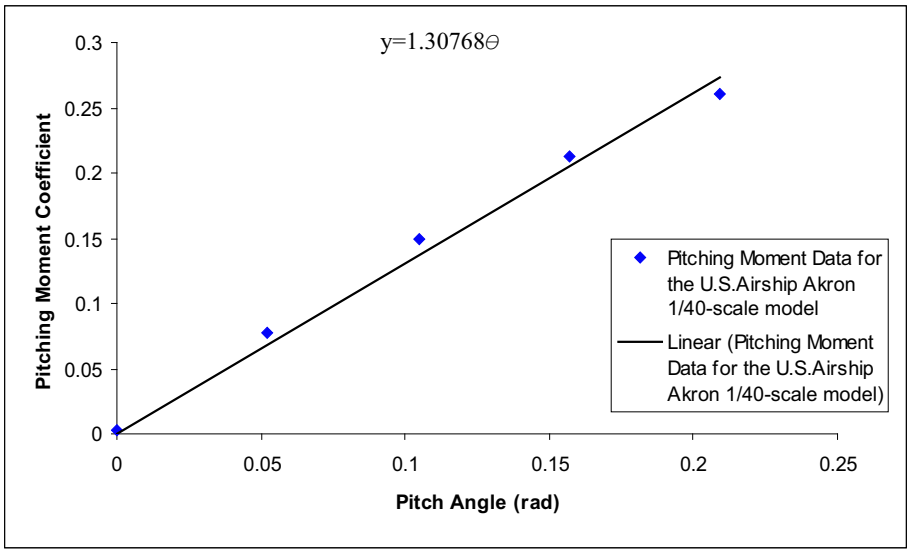

Figure 11: The U.S. Airship Akron 1/40-scale model pitching moment coefficient data versus pitch angle with a linear fit

From this plot, the pitching moment coefficient of the body is determined to be $C_{m\alpha b} = 1.3076$ where the equation for the pitching moment coefficient is calculated as $C_m = 1.3076\theta$. The moments on the body can be defined as follows

$$\mathbf{M_{body}} = \begin{bmatrix} 0 \\ C_{m\alpha b}\alpha \\ -C_{m\alpha b}\beta \end{bmatrix} \bar{q} Vol$$

2.4 Forces and moments from the fins

The force due to the fins include lift, side force and induced drag. The two vertical fins have a side force acting on them from side slip and drag. The two stern planes are affected by a lifting force and induced drag force. The lift curve slope for the fins can be approximated as follows:

$$C_{L\alpha f} = \frac{2\pi}{(1 + \frac{2\pi}{\pi AR})}$$

where AR in the above equation is the aspect ratio. In the water current frame, the (nondimensional) force acting on each vertical fin is:

$$\mathbf{C_{vf}} = \begin{bmatrix} \frac{-C_{L\alpha f}\beta_c^2}{\pi \varepsilon AR} \\ -C_{L\alpha f}\beta_c \\ 0 \end{bmatrix}$$

The two stern planes have force coefficients in the water current frame that are:

$$\mathbf{C_{spl}} = \begin{bmatrix} \frac{-C_{L\alpha f}(\alpha_c + d_1)^2}{\pi \varepsilon AR} \\ 0 \\ -C_{L\alpha f}(\alpha_c + d_1) \end{bmatrix}$$

and

$$\mathbf{C_{spr}} = \begin{bmatrix} \frac{-C_{L\alpha f}(\alpha_c+d_2)^2}{\pi\varepsilon AR} \\ 0 \\ -C_{L\alpha f}(\alpha_c + d_2) \end{bmatrix}$$

The variables d_1 and d_2 represent the fin deflection of the right and left fins and ε is the span efficiency factor. Positive fin deflection angles d_1 and d_2 are defined as the leading edge of the fin being up and the trailing edge is down. These four fins create a force on the towfish.

$$\mathbf{F_{fin}} = \mathbf{R_{BC}}(2\mathbf{C_{vf}} + \mathbf{C_{spl}} + \mathbf{C_{spr}})1/2S_f\bar{q}$$

The fins on the aft end of the hull create a moment on the towfish. This moment is

$$\mathbf{M_{fin}} = 1/2\bar{q}S_f(\mathbf{X_{ac1}} \times \mathbf{R_{BC}}\mathbf{C_{vf}} + \mathbf{X_{ac2}} \times \mathbf{R_{BC}}\mathbf{C_{vf}} + \mathbf{X_{ac3}} \times \mathbf{R_{BC}}\mathbf{C_{spl}}\mathbf{X_{ac4}} \times \mathbf{R_{BC}}\mathbf{C_{spr}})$$

where $\mathbf{X_{aci}}$ is the distance vector from the body axis origin to the hydrodynamic center of the ith fin. First order actuator dynamics are defined in equations (12) and (13).

$$\dot{d_1} = \frac{1}{\tau}(\delta_1 - d_1) \tag{12}$$

$$\dot{d_2} = \frac{1}{\tau}(\delta_2 - d_2) \tag{13}$$

The time constant τ can be approximated to account for manufacturer-specified rate limit of 90 deg/sec. This is done through first defining the stall angle of the fins at 20 degrees. Thus, with a rate limit at 90 deg/sec it would take 0.22 seconds for the actuators to move 20 degrees. The rate at which the response approaches the final value is determined by a time constant. For a first order system 99.3 percent of the

command angle can be reached in 5τ seconds [20]. This shows that the time constant, τ, is approximately 0.044 seconds. This allows the simulation to account for the rate limit of 90 degrees/second when the stall angle of the fins is set at 20 degrees [20].

2.5 Gravitational and buoyant forces and gravitational moment

The weight and buoyancy force have been calculated for the towfish in Section 6. They are defined symbolically as:

$$\mathbf{F_{weight}} = \mathbf{R_{IB}}^T \begin{bmatrix} 0 \\ 0 \\ W \end{bmatrix}$$

$$\mathbf{F_{buoyancy}} = -1.05\mathbf{R_{IB}}^T \begin{bmatrix} 0 \\ 0 \\ B \end{bmatrix}$$

Since the cg lies below the cb (this is calculated in Section 6) a restoring moment is created when the towfish pitches or rolls. This moment is found by

$$\mathbf{M_{weight}} = \mathbf{X_{cg}} \times \mathbf{F_{weight}}$$

where $\mathbf{X_{cg}}$ is the distance vector from the body axis origin (the cb) to the cg.

2.6 Moments due to damping

As the towfish moves through the water it will be caused to pitch, roll and yaw which will result in damping moments. These damping moments occur because there is a

resistance of motion caused from towing the towfish through a fluid. These moments due to roll, pitch and yaw can be defined as follows:

$$L_p p = \left(C_{lp} \bar{q} S_b b \frac{b}{2U_0} \right) p$$

$$M_q q = \left(C_{mq} \bar{q} S_b l_b \frac{l_b}{2U_0} \right) q$$

$$N_r r = \left(C_{nr} \bar{q} S_b l_b \frac{l_b}{2U_0} \right) r$$

where C_{lp},C_{mq}, and C_{nr} are non-dimensional stability derivatives. The damping moment coefficient due to roll is approximated as

$$C_{lp} = -\frac{C_{L\alpha f}}{12} \frac{1 + 3(c_t/c_r)}{1 + (c_t/c_r)}$$

where c_t and c_r are the tip and root chords of the fins [5]. The term C_{mq} is the pitch damping moment coefficient and can be approximated as

$$C_{mq} = -2\eta C_{L\alpha f} \frac{l_t^2 S_f}{l_b S_b c}$$

The hydrodynamic center of the fins is a distance l_t aft of the towfish body frame center, l_b is the length of the towfish body, S_f is the planform area of the stern planes or the vertical fins, and S_b is the planform area of the towfish body. The variable c denotes the chord length of the fins and the reference velocity is defined as U_0. Also note that due to symmetry, $C_{mq} = C_{nr}$.

3 Cable Modeling

The towing force which acts at the nose of the towfish is affected by the length of the cable, the weight of the depressor, and the motion of the research vessel that is towing it. The two-part towing arrangement can be seen in Figure 12.

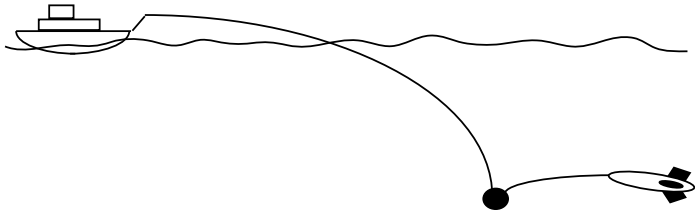

Figure 12: Towing configuration

A model of this arrangement was previously developed in reference [20]. This model assumed a linear spring-damper system from the nose of the towfish to the depressor, unless the distance from the nose of the towfish to the depressor became less than the length of the pigtail, in which case the force vanished. The spring constant for a steel cable in tension is

$$\bar{k} = \frac{EA_c}{L}$$

where E is the Young's modulus for steel, A_c is the cross-sectional area and L is the length of the cable from the depressor to the towfish nose. The Young's modulus for steel was recorded from reference [2] to be 29×10^6 psi. Therefore the spring constant $\bar{k}$ was calculated as 86,086 lb_f/ft for a 164.04 foot cable. This $\bar{k}$ was then used as the spring stiffness of the cable. This spring constant is only accurate if the towing cable that runs from the depressor to the towfish is perfectly horizontal or vertical. Therefore, this modeling method is incorrect since it has neglected the curvature and hydrodynamics of the cable. This thesis uses the spring-damper model, but the spring stiffness is determined by computing cable tension for a sequence of static cable profiles. The change in tension versus the change in length from the towfish to the depressor gives the equivalent spring stiffness at a given operating condition.

The static cable modeling approach has been used to better approximate the spring constant by including curvature and hydrodynamics of the cable. It should be noted however, that this static approach is a crude approximation for determining the spring constant which is used to find the force and moment on the towfish from the towing cable. The behavior of the system is better captured by a model which includes the infinite dimensional tether dynamics, but such an approach was beyond the scope of this thesis.

3.1 Static cable modeling for a two-part tow

The profiles of the main catenary and pigtail are functions of the system parameters and state. In order to obtain an equivalent spring stiffness for the pigtail, the equations are derived for the equilibrium configuration at various speeds. A free-body diagram of the towfish can be seen in Figure 13.

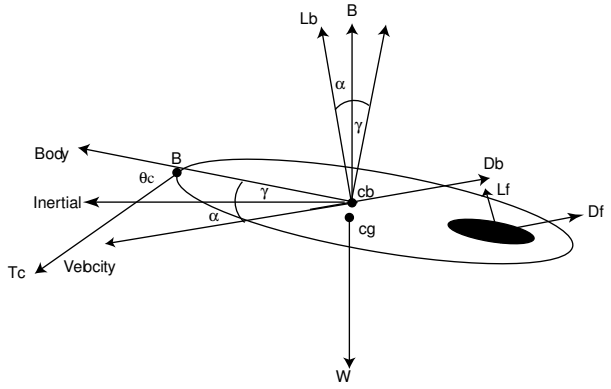

Figure 13: Free-body diagram of the towfish

The free-body diagram shows a weight force (W), a buoyant force (B), a lift force (L_b), a drag force(D_b), and a tension force from the cable (T_c). It is assumed that the lift force, drag force and buoyancy force all act at the cb of the towfish which is shown in the Figure 13. The weight force is assumed to be acting 1 inch below the cb at the cg . The cg is the point where the net weight force acts on the towfish. The buoyant force and weight force for the towfish have been calculated through trimming

and ballasting the towfish in the tank and these calculations are shown in Section 6. The lift and drag force are

$$L_b = C_{lb}\frac{1}{2}\rho V^2 S_b \tag{14}$$

$$D_b = C_{db}\frac{1}{2}\rho V^2 S_b \tag{15}$$

where ρ is the density of the fluid, V is speed, S_b is a body reference area, C_{db} and C_{lb} are the lift and drag coefficients for the body. Thus,

$$C_{lb} = C_{L\alpha b}\alpha \tag{16}$$

$$C_{db} = C_{D0b} + KC_{lb}^2 \tag{17}$$

K is a constant that defines the drag polar curve and C_{D0b} is the zero degree angle of attack coefficient of drag for the body. The zero degree angle of attack coefficient of drag was defined in section 2.3.

Also seen in the free-body diagram, Figure 13, are the forces of lift and drag acting on the stern planes of the towfish. These forces are assumed to act at the stern planes hydrodynamic center and can be defined through the following two equations:

$$L_f = C_{lf}\frac{1}{2}\rho V^2 S_f \tag{18}$$

$$D_f = C_{df}\frac{1}{2}\rho V^2 S_f \tag{19}$$

In equations (18) and (19), C_{lf} and C_{df} are the lift and drag coefficients of the fins and S_f is the area of the fins. The fins on the towfish have been designed to have the shape of a NACA 0012 airfoil. The coefficient of lift for the fins was approximated through three 2-D properties. First, the theoretical coefficient of lift was approximated by the following formula:

$$(C_{l\alpha f})_{theory} = 2\pi + 4.9\frac{t}{c} \tag{20}$$

where t and c are the thickness and chord length of the fin [5]. For the fins on the towfish, $(C_{l\alpha f})_{theory}$ was found to equal 6.90 per radian. Through reference [5], the trailing edge angle ϕ_{TE} was calculated by:

$$Tan[1/2\phi_{TE}] = \frac{(1/2Y_{90} - 1/2Y_{99})}{9} \tag{21}$$

where Y_{90} is the nondimensional thickness at 90 percent of the chord and Y_{99} is the nondimensional thickness at 99 percent of the chord. From this approximation and the approximated Reynolds number of the towfish, the empirical factor K_1 can be found through the graph on page 321 of reference [5]. The Reynolds number of the towfish was calculated through the following formula:

$$Re = \frac{\rho V l_b}{\mu_1} \tag{22}$$

where l_b is the length of the towfish and μ_1 is the dynamic viscosity of the water. The following table shows the Reynolds' numbers that were calculated for speeds from 3.28 ft/s to 9.84 ft/s (1 m/s to 3 m/s).

Table 1: Reynolds' numbers over the operating velocity range for the towfish

Velocity (ft/s)	Reynolds Number
3.28	1.5×10^6
6.56	2.9×10^6
9.84	4.4×10^6

From Figure B.1,1a in Appendix B of reference [5], K_1 was approximated as 0.915. Next, $C_{l\alpha f}$ was corrected for the trailing edge angle and the Reynolds number. The following is the equation that shows how to correct for these factors.

$$C_{l\alpha f} = 1.05 K_1 (C_{l\alpha f})_{theory} \tag{23}$$

The constant κ is also determined to find the lift coefficient of the stern planes.

$$\kappa = \frac{C_{l\alpha f}}{2\pi} \tag{24}$$

κ was calculated to be 1.05 for the fins of the towfish. Finally, the coefficient of lift of the fins is found through using the sectional lift-curve slope, the correction for the finite wing-span and the sweep angle. This is done through the following equation that was taken from reference [5].

$$C_{L\alpha f} = \frac{2\pi AR}{2 + \sqrt{(\frac{AR^2}{k^2})(1 + \tan[\Lambda_{1/2}]) + 4}} \tag{25}$$

Thus, AR is the aspect ratio of the fins which is defined by $AR = b/\bar{c}$ where b is the span of the fins and $\bar{c}$ is the average chord length. Also, in this equation $\Lambda_{1/2}$ is the sweep at 50 percent chord however, these fins have a constant sweep. The sweep of the fins was estimated as 25 degrees. The lift coefficient of the fins was computed through the previously explained process to be $C_{l\alpha f} = 2.28$.

The free-body diagram in Figure 13 shows that there are three unknowns: the tension of the cable pulling on the towfish (T_c) , the angle at which the cable is pulling the towfish (θ_c) and the angle in which the fins are deflected (ΔE). Through summing the forces in the x and y directions and summing the moments about the nose of the towfish the following equations are developed:

$\sum F_x = 0$

$$(L_b + L_f)\sin[\alpha] - (D_b + D_f)\cos[\alpha] + T_c \cos[\theta_c] + (B - W)\sin[\gamma] = 0 \tag{26}$$

$\sum F_y = 0$

$$(L_b + L_f)\cos[\alpha] + (D_b + D_f)\sin[\alpha] - T_c \sin[\theta_c] + (B - W)\cos[\gamma] = 0 \tag{27}$$

$\sum M_B = 0$

$$(B-W)\cos[\gamma]\frac{l_b}{2}+(L_b\cos[\alpha]+D_b\sin[\alpha])\frac{l_b}{2}+(L_f\cos[\alpha]+D_f\sin[\alpha])(x_f+\frac{l_b}{2})=0 \quad (28)$$

For this problem, α and γ are small angles. The towfish tilt angle must be less than one degree. In nominal, equilibrium motion, $\alpha = \gamma = 0$ and $L_b = 0$. The equilibrium condition is displayed in Figure 14.

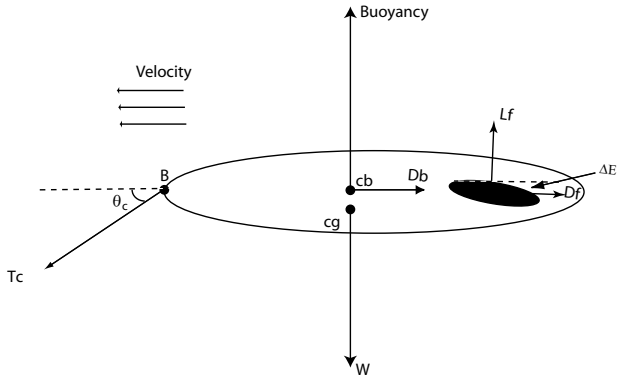

Figure 14: Free-body diagram of the towfish at equilibrium

In equilibrium motion,

$$-D_b - D_f + T_c\cos[\theta_c] = 0 \quad (29)$$

$$L_f - T_c\sin[\theta_c] + B - W = 0 \quad (30)$$

$$(B-W)\frac{l_b}{2} + L_b\frac{l_b}{2} + L_f(x_f + \frac{l_b}{2}) = 0 \quad (31)$$

From equation (31), ΔE can be solved for in terms of the velocity of the vehicle. This is possible since the buoyancy, the weight, the lift of the fins and and the vehicle geometry are all known. Substituting known values,

$$\Delta E = -1.63/V^2 \tag{32}$$

Using this result, equations (29) and (30) were used to solve for the tension in the cable and the cable angle. Through calculations in Mathematica it was found that:

$$\theta_c = \cot^{-1}[2.0775 \times 10^{-19}(\frac{3.4146 \times 10^{17}}{V^2} + 1.588 \times 10^{17}V^2)] \tag{33}$$

$$T_c = \frac{304.708}{\sin[\theta_c]} \tag{34}$$

These values provide boundary conditions for the boundary value problem describing the equilibrium cable profile.

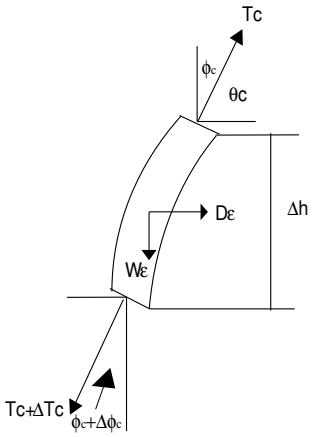

Figure 15: Diagram for a differential element of the cable

Consider the differential cable element shown in Figure 15. The weight and drag of this element are:

$$W_\varepsilon = \frac{-\zeta}{\cos[\phi_c]}\Delta h \tag{35}$$

$$D_\varepsilon = C_{Dc} 1/2 \rho V^2 d_c \Delta h \tag{36}$$

where ζ is the weight per unit length of the cable underwater, ϕ_c is the angle which the cable makes with vertical, and h is the depth below the towfish. The diagram that shows the definition of the length for the differential cable is shown in Figure 16. In the drag equation for the cable $d_c \Delta h$ is based off of the frontal area of the cable, where d_c is the diameter of the cable. The drag due to skin friction along the cable has been neglected for this problem.

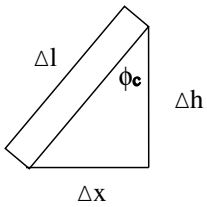

Figure 16: Definition of the length of a differential element of the cable

Next, by summing the forces in the x direction and y direction on the differential element, the follow equations are derived:

$\sum F_x = 0$

$$T_c \sin[\phi_c] + D_\varepsilon - (T_c + \Delta T_c) \sin[\phi_c + \Delta\phi_c] = 0 \tag{37}$$

$\sum F_y = 0$

$$T_c \cos[\phi_c] - W_\varepsilon - (T_c + \Delta T_c) \cos[\phi_c + \Delta\phi_c] = 0 \tag{38}$$

Because the differential angle $\Delta\phi_c$ is small, the following substitutions can be made in the above equations

$$\sin[\phi_c + \Delta\phi_c] \simeq \sin[\phi_c] + \cos[\phi_c]\Delta\phi_c \tag{39}$$

$$\cos[\phi_c + \Delta\phi_c] \simeq \cos[\phi_c] - \sin[\phi_c]\Delta\phi_c \tag{40}$$

Substituting these relationships into equations (37) and (38) and rearranging gives

$$C_{dc}1/2\rho V^2 d_c \Delta h - T_c \cos[\phi_c]\Delta\phi - \Delta T_c \sin[\phi_c] - \Delta T_c \cos[\phi_c]\Delta\phi_c = 0$$

$$\frac{\zeta}{\cos[\phi_c]}\Delta h + T_c \sin[\phi_c]\Delta\phi_c - \Delta T_c \cos[\phi_c] + \Delta T_c \sin[\phi_c]\Delta\phi_c = 0$$

Dividing by Δh and ignoring the higher order terms leads to the development of two ODE's:

$$T_c \cos[\phi_c]\frac{d\phi_c}{dh} + \sin[\phi_c]\frac{dT_c}{dh} = C_{Dc}d_c 1/2\rho V^2 \tag{41}$$

$$T_c \sin[\phi_c]\frac{d\phi_c}{dh} - \cos[\phi_c]\frac{dT_c}{dh} = \frac{-\zeta}{\cos[\phi_c]} \tag{42}$$

Equations (41) and (42) can be decoupled as

$$T_c\frac{d\phi_c}{dh} - C_{Dc}d_c 1/2\rho V^2 \cos[\phi_c] + \zeta \tan[\phi_c] = 0 \tag{43}$$

$$\frac{dT_c}{dh} - C_{Dc}d_c 1/2\rho V^2 \sin[\phi_c] - \zeta = 0 \tag{44}$$

A third equation was developed that gives x in terms of h. From Figure 16,

$$\frac{dx}{dh} - \tan[\phi_c] = 0 \tag{45}$$

Note in the above equations that T_c, ϕ_c and x all are functions of h. Using Mathematica's numerical differential equation solver, these equations were solved for a range of velocities. The cable diameter was assumed to be 0.0656 feet with a drag coefficient of $C_{Dc} = 1.05$ and $\zeta = 0.0001\ lb_f/ft$ for this program. The drag coefficient of the

cable was estimated by the drag coefficient of a circular cylinder [14]. In reality, the pigtail will be heavy in water, but with support floats located at a finite number of points along the cable. For simplicity of modeling, a cable with uniform density quite close to that of water was assumed.

To develop cable profiles for different speeds the differential cable elements were summed at every 0.001 feet in depth until the cable hit a set length of 164.0420 feet (50 m). This approach was used to obtain the curve of the cable at different speeds. Cable profiles for 3.3 ft/s to 10.3 ft/s in 0.5 ft/s increments are shown in Figure 17. The lowest velocity used for this problem, 3.3 ft/s, is denoted as the bottom curve in red. As the speed increased the depth of the cable decreased and the x distance increased. The curves in this figure start from the bottom by being defined by red and then vary to a gray color as the speed is increased. The top curve, with the largest x distance and least depth occurs at a velocity of 10.3 ft/s and is distinguished by a gray color. The towfish is assumed to be at the position (0,0) feet and the depressor is located at the opposite end of the cable, denoted by the black dot, for each curve in this plot. Figure 18 shows a close up view of the cable profiles at the end of the cable in which the depressor is attached. The depressor is represented by the black dot on the end of the cable.

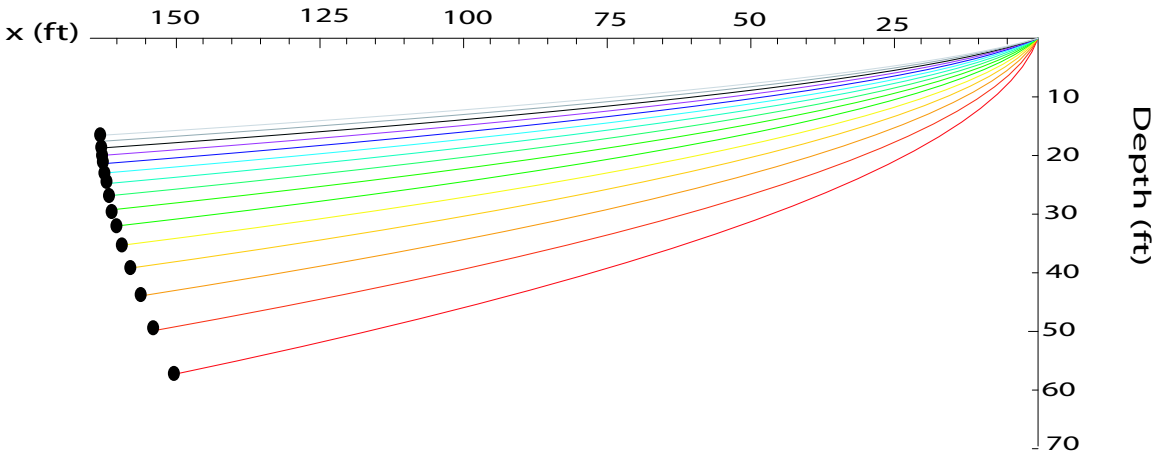

Figure 17: Cable profiles for speeds between 3.3 ft/s to 10.3 ft/s

Through developing these static cable profiles the force at the nose of the towfish

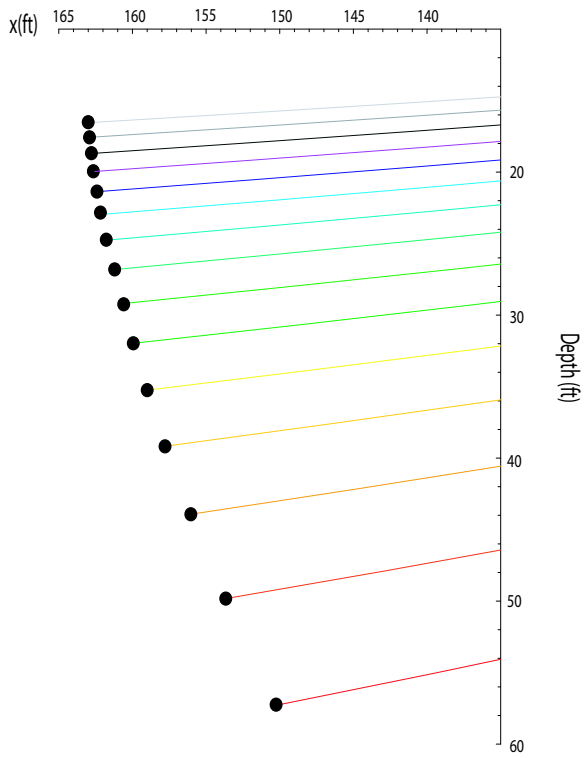

Figure 18: Cable profiles zoomed in at the end attached to the depressor

versus towing speed and the diagonal distance from the towfish nose to the depressor versus towing speed can be plotted separately and the spring constant function can be developed from the data. The tension force that acts at the nose of the towfish is first plotted versus the towing speed of the towfish. Figure 19 shows how the force acting on the towfish nose varies with towing speed.

This curve of data is approximated well by the following equation:

$$F = 400.7299 - 66.9169V + 13.2105V^2 \tag{46}$$

This quadratic equation was found through Mathematica's Polynomialfit function. The force versus velocity data along with the quadratic fit is shown in Figure 19.

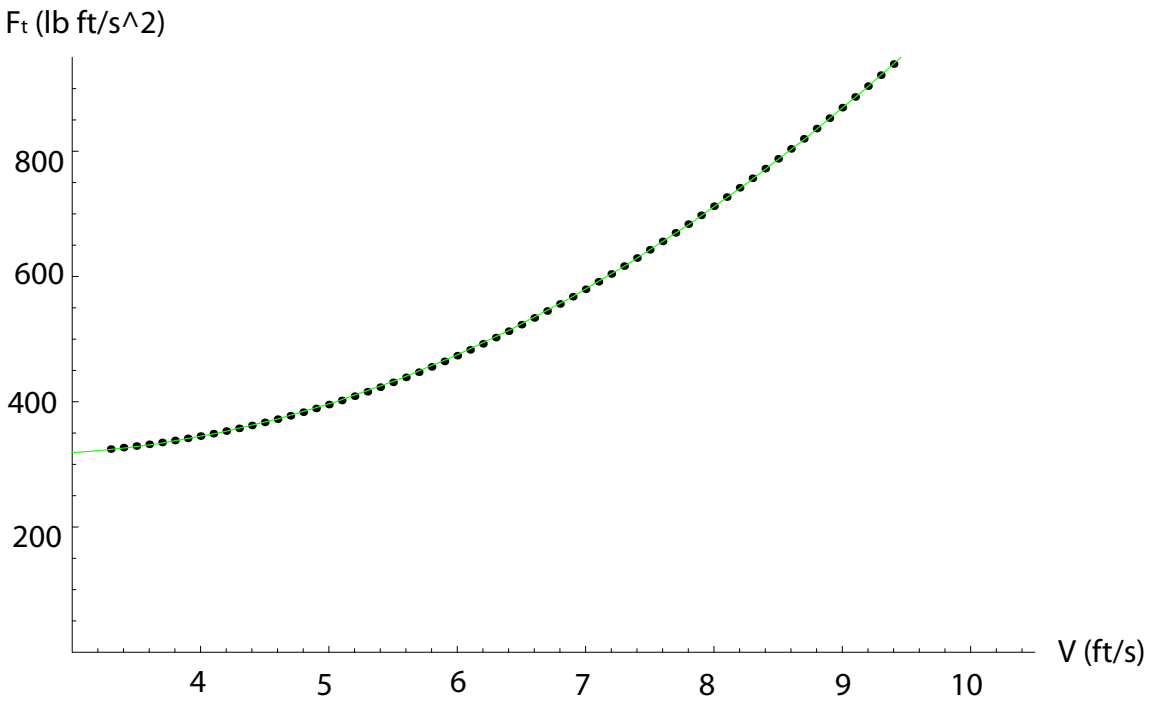

Figure 19: The quadratic fit of the force versus the velocity plotted with the original data

Next the diagonal distance (l_i) between the towfish nose and the depressor due to the change in force was determined for the data in the operating range of 3.3 ft/s to 10.3 ft/s (roughly a range of 2 to 6 knots). The value l_i was found through the following formula:

$$l_i = \sqrt{x_i^2 + h_i^2}$$

where x_i and h_i define the x position and depth between the towfish nose and the depressor at a specific towing speed, which is shown in Figure 20. Note that as the towing speed increased the cable profile from the towfish nose to the depressor changed. As the towing speed increased the x position of the depressor relative to towfish nose increased where the depth of the depressor from the towfish nose decreased. Figure 17 shows a slight variation in x position and h distance at the end

of the cable. Figure 18 better displays how the x distance and depth change at the depressor when the towfish nose is assumed to held at the same place for this static analysis.

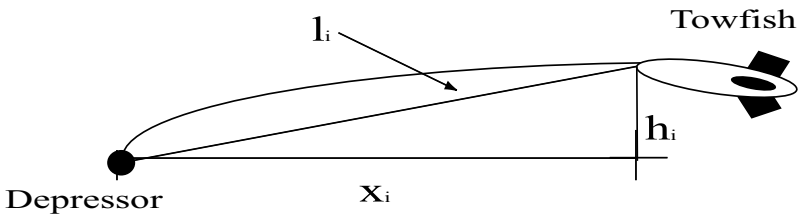

Figure 20: The diagonal distance measurement between the towfish nose and the depressor

This diagonal distance from the towfish nose to the depressor (l_i) versus the velocity was plotted in Figure 21.

The data found for the diagonal distance from the towfish nose to the depressor versus the towfish velocity is approximated through:

$$l = 153.0040 + 3.5322V - 0.3967V^2 + 0.01524V^3 \tag{47}$$

Figure 21 shows along with the diagonal distance versus the velocity data, the third order polynomial fit for this data.

To develop the spring constant the derivative of the force and the diagonal distance equations were taken with respect to V and the following two equations were produced:

$$\frac{\partial F}{\partial V} = -66.9169 + 26.421V \tag{48}$$

$$\frac{\partial l}{\partial V} = 3.5322 - 0.7934V + 0.04572V^2 \tag{49}$$

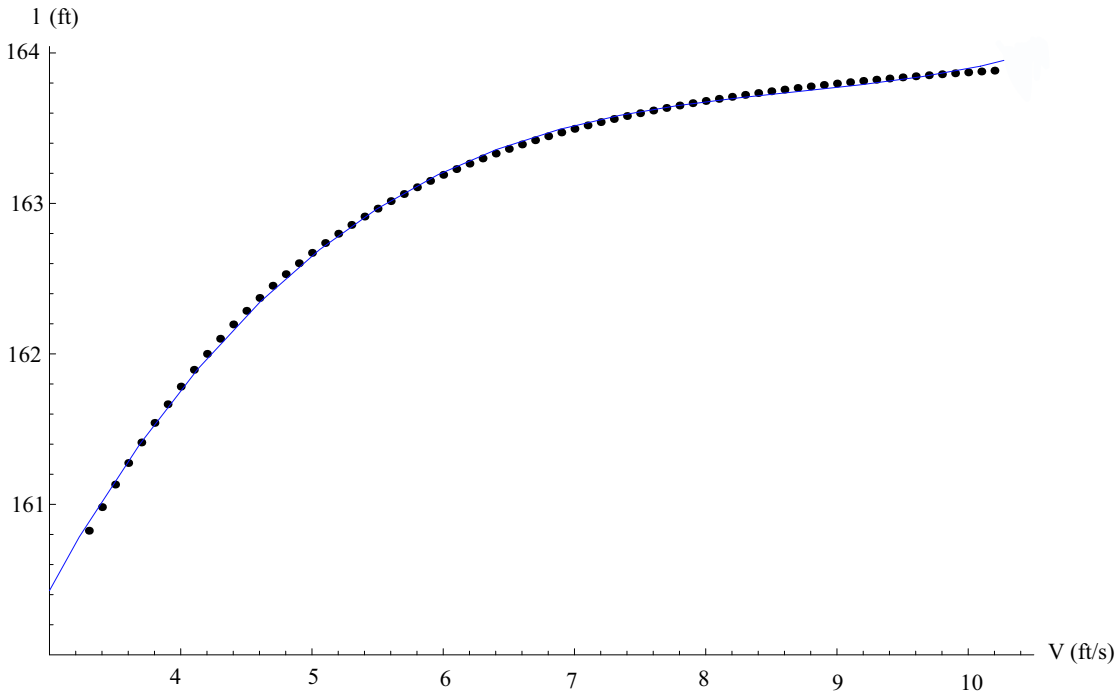

Figure 21: The polynomial fit of the diagonal distance versus the velocity plotted with the original data

Through assuming that these two equations are well defined, $\partial F/\partial V$ can be divided by $\partial l/\partial V$ to obtain:

$$\frac{\partial F}{\partial l} = \frac{-66.9169 + 26.421V}{3.5322 - 0.7934V + 0.04572V^2} \tag{50}$$

This expressions assumes that $\partial F/\partial l$ is the same as the spring constant for a linear spring, therefore from the above equation the spring constant can be approximated by a set value at each towing speed.

3.2 Force and moment due to the cable

This section examines the movement of the depressor and how it affects the movement of the towfish. The pigtail is represented as a linear spring-damper that runs from the depressor to the towfish, where the spring constant was computed in Section 3.1. Figure 22 displays how the system was modeled to simulate the effects from the main catenary and the pigtail.

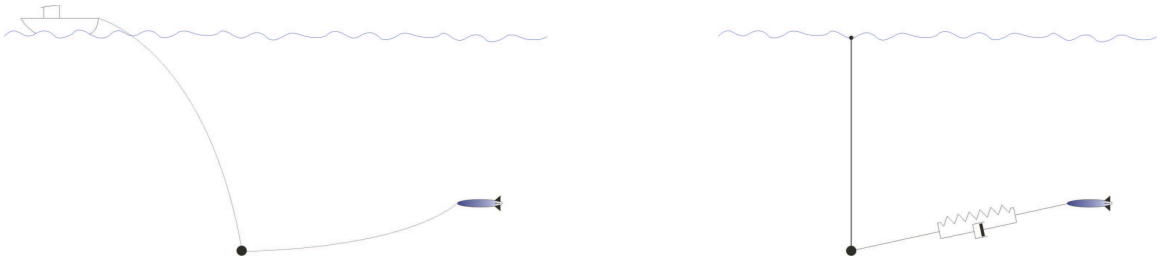

Figure 22: A diagram showing how the system has been modeled in comparison to the actual system

The motion caused by the research vessel and the main catenary has been approximated in this simulation by moving the depressor. The motion of the depressor is approximated by the wave motion created from the sea state along with a harmonic oscillation that is intended to model the "pendulum" motion. The depressor model also includes effects from surge disturbances.

The pigtail is modeled with a linear spring-damper. The spring force requires the vector from the towfish nose to the depressor, which is given by

$$\mathbf{\Delta x} = \mathbf{X_{depressor}} - \left(\mathbf{X_I} + \mathbf{R_{IB}} \begin{bmatrix} \frac{l_b}{2} \\ 0 \\ 0 \end{bmatrix} \right)$$

where $\mathbf{X_{depressor}}$ is the position of the depressor, $\mathbf{X_I}$ is the inertial position, and l_b is the length of the towfish. The damping force requires the difference between the depressor speed and the tow point speed:

$$\mathbf{\Delta u} = \mathbf{U_{depressor}} - \left(\mathbf{R_{IB}V} + \mathbf{R_{IB}} \left(\mathbf{\Omega} \times \left| \begin{array}{c} \frac{l_b}{2} \\ 0 \\ 0 \end{array} \right| \right) \right)$$

where $\mathbf{U_{depressor}}$ is the velocity of the depressor. To calculate the towing force from the pigtail the spring and damping coefficients are defined as

$$\bar{k} = \frac{-66.9169 + 26.421U_0}{3.5322 - 0.7934U_0 + 0.04572U_0^2}$$

and

$$\bar{b} = 2m\zeta_d\omega_n$$

where

$$\omega_n = \sqrt{\frac{\bar{k}}{m}}$$

The damping ratio, ζ_d, was chosen to be one, corresponding to a critically damped system. In a coordinate frame where the x-axis points from the towfish nose to the depressor, the towing force is

$$\mathbf{F_{td}} = \left[\begin{array}{c} \bar{k}(|\Delta x| - L) + \bar{b}\left(\Delta u \cdot \frac{\Delta x}{|\Delta x|}\right) \\ 0 \\ 0 \end{array} \right]$$

where L is the total length of the pigtail. This coordinate frame is shown in Figure 23.

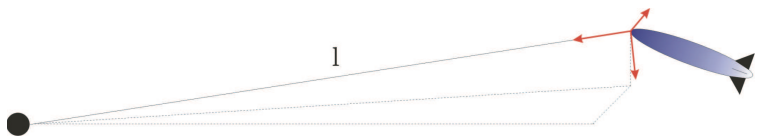

Figure 23: Cable coordinate frame where the x-axis points from the towfish nose to the depressor

The motion of the research vessel at various sea states depends on where the waves hit the ship and the type of research vessel that is being used. The motion of the depressor for the simulation was assumed to match the wave motion. The JONSWAP wave spectrum provides an energy density spectrum of wave amplitudes at specific sea states. A sea state is defined by the significant wave height and the modal wave period [13].

The Joint North Sea Wave Project (JONSWAP) spectrum describes non-fully developed seas. This makes the spectrum more peaked than other spectrums that are used to describe fully developed seas. The JONSWAP spectrum represents wind-generated waves under the assumptions that there is a finite water depth and limited fetch [7]. The spectral density function is defined as follows:

$$S_J = 155\frac{H_s^2}{T_1^4}\omega_w^{-5}\exp(\frac{-944}{T_1^4}\omega_w^{-4})3.3^{Y_w} \tag{51}$$

where H_s is significant wave height, T_1 is the modal wave period, and ω_w is the modal frequency. The expression that represents Y_w is defined through reference [7] as

$$Y_w = \exp[-(\frac{0.191\omega_w T_1 - 1}{\sqrt{2}\sigma_w})^2]$$

where

$$\sigma_w = 0.07 \text{ for } \omega_w \leqq 5.24/T_1$$
$$\sigma_w = 0.09 \text{ for } \omega_w > 5.24/T_1$$

The modal wave period can be related to the significant wave height through the following formula:

$$T_1 = 1.668\pi\sqrt[4]{\frac{5H_s^2}{12.44}}$$

The modal frequency for this spectrum is developed by defining the spectrum range and then dividing the spectrum into bins of random width The center frequencies are then selected. A random signal is generated through summing the sinusoids at N different frequencies within the significant frequency content of this spectrum. The signal provides an estimate of wave heights in fully developed seas. The signal that was generated from the JONSWAP spectrum for the x, y and z axes were assumed to be x_{random}, y_{random} and z_{random}.

Through assuming steady forward motion of the depressor with random lateral motion,

$$\mathbf{X_{depressor}} = \begin{bmatrix} x_{random} + \sin\phi_{w1}\cos\phi_{w2}H_{RP} + U_0 t \\ y_{random} + \sin\phi_{w2}H_{RP} \\ z_{random} + \cos\phi_{w1}\cos\phi_{w2}H_{RP} \end{bmatrix}$$

where ϕ_{w1} and ϕ_{w2} are the two angles that describe the spherical pendulum motion and H_{RP} is the random pendulum amplitude. The superimposed harmonic oscillation is intended to model the "pendulum" motion of the depressor. The frequency of the oscillation is $\omega_d = \sqrt{\frac{g}{x_{depth}}}$, where x_{depth} is the depth of the depressor. The oscillation frequency accounts for the natural frequency of the depressor [20]. The length x_{depth} was set to a maximum of 660 feet ($\sim$ 200 m) in the simulation since this was determined to be the maximum operating depth of the depressor that was needed for this project. Figure 24 shows the sample motion of the depressor in three-dimensions, without the steady component in the x direction.

To transfer the towing force determined previously to the body coordinate frame the following rotation from the cable frame to the inertial frame must be applied:

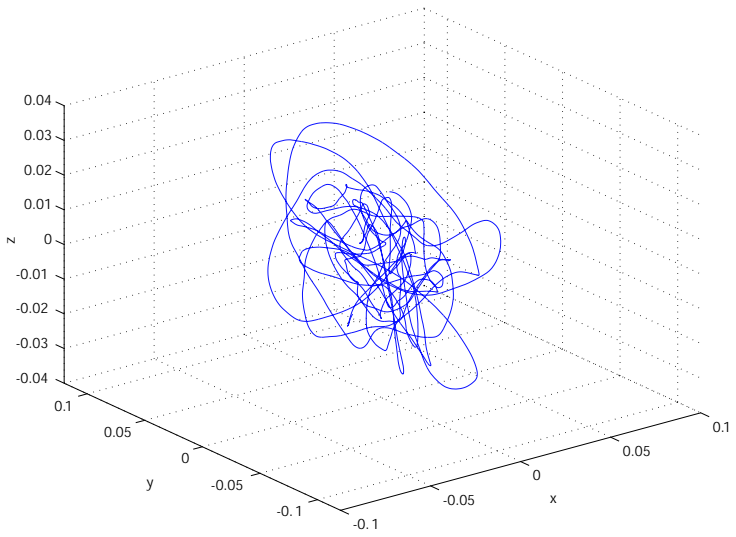

Figure 24: Motion of the depressor, minus the steady component in the x-direction

$$R_{ICable} = \begin{bmatrix} \cos[\xi]\cos[\sigma] & -\cos[\xi]\sin[\sigma] & -\sin[\xi] \\ \sin[\sigma] & \cos[\sigma] & 0 \\ \cos[\sigma]\sin[\xi] & -\sin[\xi]\sin[\sigma] & \cos[\xi] \end{bmatrix}$$

where the angles ξ and σ can be defined by

$$\xi = \arctan\left(\frac{\Delta x_3}{\Delta x_1}\right)$$

$$\sigma = \arcsin\left(\frac{\Delta x_2}{|\Delta x|}\right)$$

Figure 25 shows these angles with respect to the towfish and the depressor.

The towing force on the body of the towfish in the body frame is

$$\mathbf{F_{tow}} = \mathbf{R_{IB}}^T \mathbf{R_{ICable}} \mathbf{F_{td}}$$

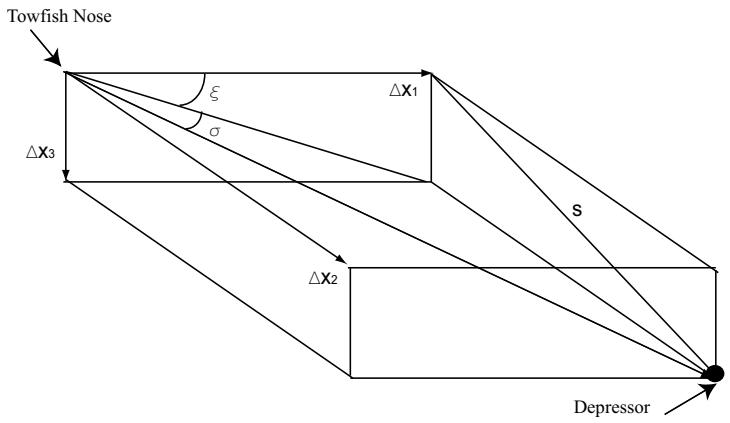

Figure 25: The angles that define the cable reference frame

The moment caused from the towing force is

$$\mathbf{M_{tow}} = \begin{bmatrix} \frac{l_b}{2} \\ 0 \\ 0 \end{bmatrix} \times \mathbf{F_{tow}}$$

3.3 Linearized equations

The equations of motion for the towfish are nonlinear, however they can be approximated by linear equations for small perturbations from the nominal operating condition. It is necessary to approximate the nonlinear equations by linear equations for designing the PID controller. This PID controller design will be explained in Section 4.1.

Through approximating the equations of motion by linear equations this simplifies the system and allows the system to be observed at specific conditions about which it has been linearized. The nominal motion is

$$\begin{aligned}\mathbf{X_{nom}} &= \left[\tilde{x}(t), \tilde{y}(t), \tilde{z}(t), \tilde{\phi}(t), \tilde{\theta}(t), \tilde{\psi}(t), \tilde{u}(t), \tilde{v}(t), \tilde{w}(t), \tilde{p}(t), \tilde{q}(t), \tilde{r}(t)\right]^T \\ &= [U_0 t, 0, 0, 0, 0, 0, U_0, 0, 0, 0, 0, 0]^T\end{aligned} \tag{52}$$

$$\delta_{\mathbf{nom}} = \left[\tilde{\delta_2}(t), \tilde{\delta_4}(t)\right] \tag{53}$$

where $\tilde{\delta_2}(t)$ and $\tilde{\delta_4}(t)$ are inputs.

The kinematic and dynamic equations were linearized. Written implicitly, the twelve first order equations are

$$\begin{aligned}\dot{x} &= f_1(x, y, z, \phi, \theta, \psi, u, v, w, p, q, r, \delta_1, \delta_2) \\ \dot{y} &= f_2(x, y, z, \phi, \theta, \psi, u, v, w, p, q, r, \delta_1, \delta_2) \\ &\vdots \\ \dot{r} &= f_{12}(x, y, z, \phi, \theta, \psi, u, v, w, p, q, r, \delta_1, \delta_2)\end{aligned}$$

Applying a multivariable Taylor series expansion, evaluating at the nominal conditions, and assuming small perturbations so that higher order terms may be ignored gives

$$\frac{d}{dt}(\mathbf{\Delta X}) = \mathbf{A_1 \Delta X} + \mathbf{B_1 \Delta} \delta$$

where

$$\mathbf{A_1} = \begin{bmatrix} \frac{\partial f_1}{\partial X_1} & \frac{\partial f_1}{\partial X_2} & \cdots \\ \frac{\partial f_2}{\partial X_1} & \ddots & \cdots \\ \vdots & \vdots & \vdots \end{bmatrix}_{nom}$$

and

$$\mathbf{B_1} = \begin{bmatrix} \frac{\partial f_1}{\partial \delta_1} & \frac{\partial f_1}{\partial \delta_2} \\ \frac{\partial f_2}{\partial \delta_1} & \vdots \\ \vdots & \vdots \end{bmatrix}_{nom}$$

The variables $\mathbf{\Delta X}$ and $\mathbf{\Delta}\delta$ represent deviations from the nominal values of the state and control variables.

4 Simulations

A nonlinear Simulink simulation has been created using the equations developed in Section 2, to evaluate how parameters such as sea state, towing speed, cg position and feedback control change the pitch and roll stability of the towfish. A PID controller was developed by Eric Schuch [20] using the Zeigler-Nichols frequency response method. This PID controller is evaluated on its ability to maintain the tilt angle within plus or minus a half of a degree. To ensure the actual tilt angle of the towfish is within plus or minus one degree the PID controller needs to maintain the output tilt angle within a half of a degree since the vertical gyro has an uncertainty of a half of a degree when taking static measurement. Due to the fact that this system will have slow dynamics and needs to maintain a static equilibrium attitude for accurate measurements to be made the static accuracy is more relevant. A detailed description of the simulation is provided in Appendix B. The simulation includes actuator position, rate saturation, and encoder quantization. The actuator dynamics that were approximated through a 1st order model in Section 2 have been replaced in this simulation by position and rate limits.

4.1 PID control design

A proportional-integral-derivative (PID) controller was designed for this two-part towing arrangement. The integral control was needed to remove small errors in pitch and roll. The derivative control was important to help remove the high frequency disturbances that acted on the towfish due to the research vessel and the towing cable [20]. Figure 26 shows the PID controller structure.

Here, T_i stands for the integral time, T_d denotes the derivative time, and k_p is the proportional gain.

The performance specifications require that the actual pitch and roll angles be maintained between plus or minus one degree. The PID controller however needs to

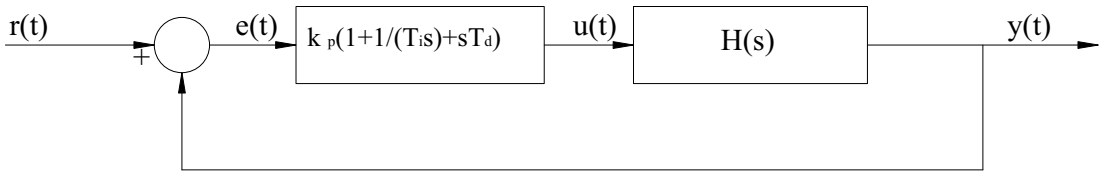

Figure 26: The PID controller structure [20]

maintain pitch and roll angle between plus or minus a half of a degree due to the uncertainty of the vertical gyro. To assess performance, the initial condition response of the simulation was taken for a neutrally buoyant towfish with an initial roll or pitch angle of one degree. The cg of the towfish was set to $X_{cg} = [0; 0; 3]$ inches in the body frame and the towing velocity was set to 6.6 ft/s (2 m/s). Gains were estimated using the Zeigler-Nichols method and the initial condition response was used to determine if the controller could bring the roll and pitch angle back to 0.1 degrees (10 percent of the design criteria of 1 degree) in an acceptable amount of time with little oscillation [20]. Note that the commanded fin deflections must be feasible. To tune the gains of the PID controller for this simulation, the Zeigler-Nichols frequency response method was used. This method involves setting the integral and derivative gain to zero and increasing the proportional gain until the system is constantly oscillating. The critical gain k_{cr} and the critical period of oscillations (P_{cr}) were used to calculate the three gains. The Zeigler-Nichols frequency response method defines the following equations for the proportional gain, the integral and the derivative time [20].

$$k_p = 0.6k_{cr} \tag{54}$$

$$T_i = 0.5P_{cr} \tag{55}$$

$$T_d = 0.125P_{cr} \tag{56}$$

The critical gain and the critical period of oscillation were calculated from the pitch

angle versus time graph and were used to find the proportional gain and the integral and derivative times. These gains however showed an oscillatory response and the fin deflections were large. Therefore to try and improve the system the following integral and derivative control gains were defined.

$$k_i = k_p/T_i \tag{57}$$

$$k_d = k_p T_d \tag{58}$$

The controller was then tuned until there was less oscillatory motion. The following proportional gain, integral and derivative times were developed.

$$\begin{aligned} k_{\theta p} &= 4 \\ T_{\theta i} &= 0.6 \quad seconds \\ T_{\theta d} &= 1 \quad second \end{aligned}$$

A similar approach was used to tune the roll channel of the PID controller. The proportional gain and the integral and derivative times for roll control were tuned to the following values.

$$\begin{aligned} k_{\phi p} &= 2 \\ T_{\phi i} &= 0.5 \quad seconds \\ T_{\phi d} &= 0.3 \quad seconds \end{aligned}$$

A more detailed analysis of how these values were achieved has been developed in reference [20].

4.2 The effect of various parameters on the stability of the towfish

A parametric study was conducted to see the effects of the sea state, towing speed, center of gravity position and a PID controller on the towfish dynamics. It should be noted that for all of the following simulations the towfish was assumed to be 5 percent buoyant with a dry weight of approximately 471 pounds. All of the initial conditions were set to zero except for the velocity of the towfish. The pigtail length was set to 164.04 feet (50 m) and it was assumed the depressor was travelling at a constant forward speed. Note the initial 20 seconds has been cut off all of the plots to allow time for the transient behavior associated with the non-equilibrium initial conditions to decay.

4.2.1 The effects of change in sea state on the stability of the towfish

The first parameter that was evaluated for its effect on the towfish's stability was the sea state. For this particular simulation the depressor depth was assumed to be 656.17 feet (200 m) and the PID controller was used to help the roll and pitch angle remain within their designed range. The cg was assumed to be a distance $X_{cg} = [0, 0, 1]^T$ inches away from the cb. The Simulink simulation was used to vary the sea state at three different velocities.

Table 3 shows data that were taken from reference [12] to use in this simulation to observe the stability of the towfish at different sea states. Data recorded for the North Atlantic open ocean region are used for this simulation since this is one of the areas the towfish will be used.

Figures 27, 28, and 29 display how the fluctuation in pitch angles changes for different sea states at towing speeds of 3.3 ft/s, 6.6 ft/s and 9.8 ft/s. The sea state was varied from 2 to 5 with these simulations and the average significant wave height was used to account for the different sea states. The assumption was made that the towfish would most likely be unable to be launched to take measurements if the sea state is

Table 2: Data of sea states from the North Atlantic

Sea state data for the North Atlantic			
Sea State	Avg Sig Wave Height (H_S)	Avg Period ($\bar{\mathrm{T}}$)	Range of Periods(s)
1	0.05	-	-
2	0.3	7.5	3.3-12.8
3	0.88	7.5	5.0-14.8
4	1.88	8.8	6.1-15.2
5	3.25	9.7	8.3-15.5
6	5	12.4	9.8-16.2
7	7.5	15	11.8-18.5
8	11.5	16.4	14.2-18.6
> 8	> 14	20	18-23.7

above 5, therefore it was unnecessary to concentrate on how large sea states affect the towfish's stability.

From Figure 27 it can be concluded that as the sea state increases the variation in pitch angle only slightly increases. The variation in pitch angle stays well within the desired range of plus or minus a half of degree therefore this plot shows the towfish could make accurate measurements up to sea state 5 at a towing speed of 3.3 ft/s. At this towing speed the forces and moments are smaller than at higher speeds therefore the desired pitch range is able to remain well within the desired range. It should be noted that the PID controller however was tuned for a velocity of 6.6 ft/s. To get a better sense of the variation in pitch angle of the towfish the gains would need to be tuned for the towing speed of 3.3 ft/s.

A second set of simulations were run under the same conditions with the exception of changing the towing speed to 6.6 ft/s. Thus the same range of sea states were observed and their effect on the pitch angle is displayed in Figure 28.

Figure 28 shows that the towfish is able to maintain the desired range in pitch for

ocean conditions of sea state 4 and below. At a sea state of 5 the pitch angle fluctuates outside of the desired region 17 times over the 100 second range. This shows that operating the towfish at sea state 5 conditions at a towing velocity of 6.6 ft/s will not allow accurate measurements to be made by the VADCP. The PID controller has been tuned for this towing speed however the cg relative to the cb of the system is different than the cg position in which the PID controller was tuned. In the future a more effective PID controller could be developed by using the actually cg position of the towfish when tuning the control gains.

A third set of simulations were then run for the max desired towing speed of 9.8 ft/s. Figure 29 displays how the variation in pitch angle changes for each sea state.

This towing speed proved to maintain the desired attitude range for sea state 2. For the sea states 3, 4, and 5 with a towing speed of 9.8 ft/s the pitch angle goes outside of the desired range of a half of a degree. The number of times that the pitch angle moves outside of the desired range of plus or minus a half of a degree versus the sea state over 100 seconds is show in Figure 30.

For the towing speed of 9.8 ft/s the number of times the pitch angle exceeds the necessary range greatly increases. The reason this is happening is due to the gains being tuned for a different speed and large moments that can be accounted for by the update rate of the system. To simulate the actual system the simulation only changes the fins orientation every 1/4 second to correct for the pitch and roll angles. This can cause large moments at higher speeds due to the orientation of the fins for that 1/4 of a second. At higher speeds the towfish would be more likely to stay within the desired range of attitude if the time constant was smaller. This would allow the system to reorient the fins more frequently to account for the error.

From the three different velocities it can be noted that the PID controller was tuned for the middle speed of 6.6 ft/s. To get a better idea of how sea state affects the other two towing speeds the gains for the PID controller need to be tuned for each speed. The PID controller would also be more beneficial if the gains were tuned while using the correct cg position.

4.2.2 The effects of change in towing speed on the stability of the towfish

A second parameter that was evaluated for its effect on the towfish's stability was the towing velocity. For this particular simulation the depressor depth was assumed to be 656.17 feet (200 m) and the PID controller was used to help the roll and pitch angle remain within plus or minus a half of a degree. The cg was assumed to be a distance $X_{cg} = [0, 0, 1]^T$ inches away from the cb. The towing speed was varied between 3.3 ft/s and 9.8 ft/s and the sea state was set at three. Figures 31 and 32 were developed to show how the roll and pitch angle vary at different speeds.

From Figure 31 it can be observed that as the towing speed increases the variation in roll angle of the towfish slightly increases. The roll angle however remains well within the desired range. The roll angle seems to fluctuate in a repetitive type motion. This is due to the encoder quantization of the actuators. The actuators of this system correct for the angle error, however there is a limit on the smallest amount the actuators can correct for. If the error angle is smaller than the smallest correction it causes this repetitive type motion since the actuators are always over correcting.

Figure 32 shows that the largest change in pitch angle occurs at a speed of 9.8 ft/s. The change in pitch angle increases from the towing speed of 3.3 ft/s to 9.8 ft/s. The reason for this is there are larger moments and forces that act on the fins at higher velocities due to the controllers inability to continuously correct for the error in pitch and roll angle. The towing speed of 9.8 ft/s goes outside of the desired pitch angle range 3 times over 100 seconds. The other two towing speeds remain within the desired pitch angle range. In conclusion, for the designated operating range of 3.3 ft/s to 9.8 ft/s the towfish will be able to accurately take measurements in sea state three.

4.2.3 The effects of change in center of gravity on the stability of the towfish

Another parameter that was evaluated for its effect on the towfish's performance was the placement of the center of gravity at different speeds. For this simulation the depressor depth was assumed to be 656.17 feet (200 m) and the PID controller was used to help the roll and pitch angle remain within plus or minus a half of a degree. The variation in the cg position was observed at three different towing speeds. At each velocity four different cg positions were evaluated. The first cg position, $X_{cg} = [0, 0, 1]^T$, was the desired cg location of the towfish after trimming and ballasting. The second cg position, $X_{cg} = [2, -0.26, 0.36]^T$, was the approximated cg location after the first set of sea trails. The third cg location, $X_{cg} = [0.145, -0.216, 0.46]^T$, was the assumed cg location of the towfish after modifications. The fourth cg location, $X_{cg} = [0, -1, 1]^T$, was used to observe how a 1 inch offset in the y and z directions would effect the variation in pitch and roll angle. Note, all cg locations are defined in inches. Figures 33, 34 and 35 show the pitch angle variation for these four cg positions at towing speeds of 3.3 ft/s, 6.6, ft/s and 9.8 ft/s.

As a generalization it can be concluded from Figures 33, 34, and 35 that a lower cg in the z direction helps to stabilize the towfish and helps to account for disturbances. The variation in pitch angle is less when the cg is well below the cb in the z direction. The desired cg location of $X_{cg} = [0; 0; 1]$ inches stayed within the desired pitch range for the 2 lower towing speeds and only fluctuates out of the desired region three times for the towing speed of 9.8 ft/s. The second cg location of $X_{cg} = [2; -0.26; 0.36]$ inches had the largest variation in pitch angle at a towing speed of 9.8 ft/s. This cg location exceeds the desired pitch range at this towing speed 8 times. This shows that moving the cg and cb closer longitudinally and further apart in the z direction allows for the towfish to be able to stay in the desired pitch range for the VADCP. The other two cg locations $X_{cg} = [0.145; -0.216; 0.46]$ inches and $X_{cg} = [0; -1; 1]$ inches fluctuated out of the desired region 4 times each at towing speeds of 6.6 ft/s and 9.8 ft/s. A bar chart of the number of times the pitch range was exceeded is shown in Figure 36 for a towing velocity of 9.8 ft/s. Note at the towing velocity of

6.6 ft/s the third and fourth cg positions went out of the desired range 4 times each.

From Figure 36, it can be seen that at higher towing speeds the 2nd cg position is the worst for maintaining the desired tilt attitude in pitch. This reemphasizes the importance of trimming and ballasting the towfish.

The effect of these cg positions on the roll angle were also observed. Figures 37, 38, and 39 display the variations in roll angle for each of the four cg positions.

Figures 37, 38 and 39 show that the change in cg location has little affect on the fluctuation of the roll angle unless it is moved a good amount in the y direction. All but one of the cg cases plotted over the range of towing speeds for roll angle versus time stayed within the region of plus or minus a half of a degree of roll. In Figure 38 the $X_{cg} = [0; -1; 1]$ inches goes outside of the desired range once at a towing speed of 6.6 ft/s over the 100 seconds plotted. It can be concluded from these roll angle versus time plots for the four different cg locations that the actual cg location of the towfish will be able to stay within the desired range of roll angle.

4.2.4 The effect of a PID controller on the stability of the towfish

Finally the PID controller was turned off for this simulation. The towing speed was set to 6.6 ft/s, the cg position was set to $X_{cg} = [0, 0, 1]$ inches and the depressor depth to 656 ft. Figures 40 and 41 display how turning off the control of the system affected the pitch angle and roll angle at sea state 3.

Figures 40 and 41 show that no control has a large affect on the variation in the pitch angle, however it doesn't seem to impact the roll angle at sea state 3. In order to maintain the pitch angle of plus or minus a half of a degree the PID controller is an important part of the system. Figure 40 shows that without a controller after the first initial 20 seconds that have been cut off to allow time for the transient behavior associated with the non-equilibrium initial condition to decay the towfish has a negative pitch angle from the towing force of the cable. It is noticed that Figure 41 shows a repetitive fluctuation due to the encoder quantization of the roll

angle versus the time. To get rid of this repetitive fluctuation between small angles within the desired roll angle range a dead zone was added. This dead zone sets a region where the controller wouldn't act if the input roll angle is within this region. Once the input roll angle was outside of the set region the controller would correct for the roll angle offset. Through adding the dead zone in this system it allowed the continuous fluctuation seen from roll to go away. Figure 42 shows the variation in roll angle for no controller, the PID controller and the PID controller with the dead zone for the towing speed of 6.6 ft/s. Figure 43 then compares no controller and the PID controller with the dead zone for a 6.6 ft/s towing speed.

Figures 42 and 43 show that adding a dead zone gets rid of the continuous fluctuation due to encoder quantization. It also improves the systems variation in roll angle from the no control case.

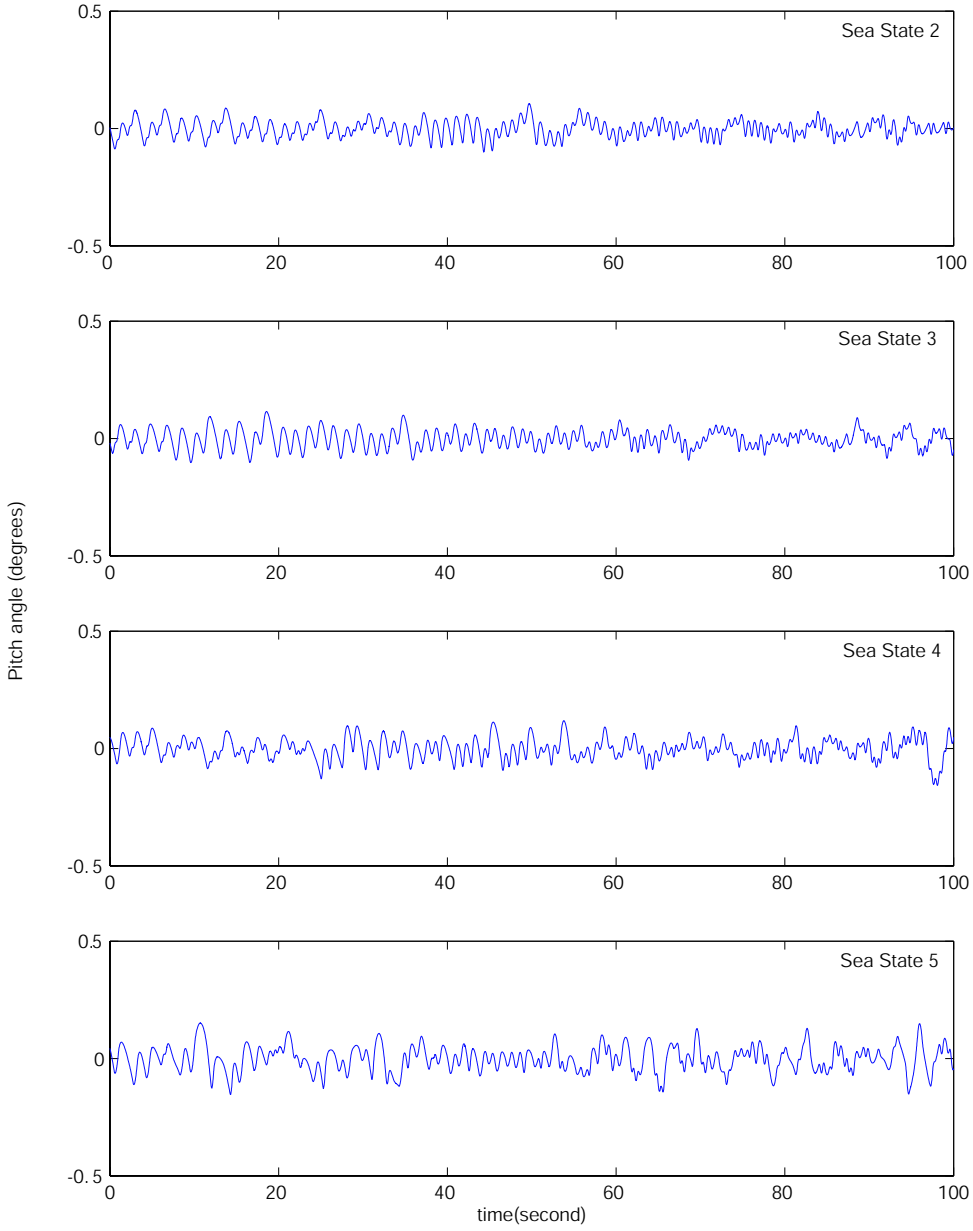

Figure 27: Variation in pitch angle at a velocity of 3.3 ft/s (1 m/s) for a range of sea states

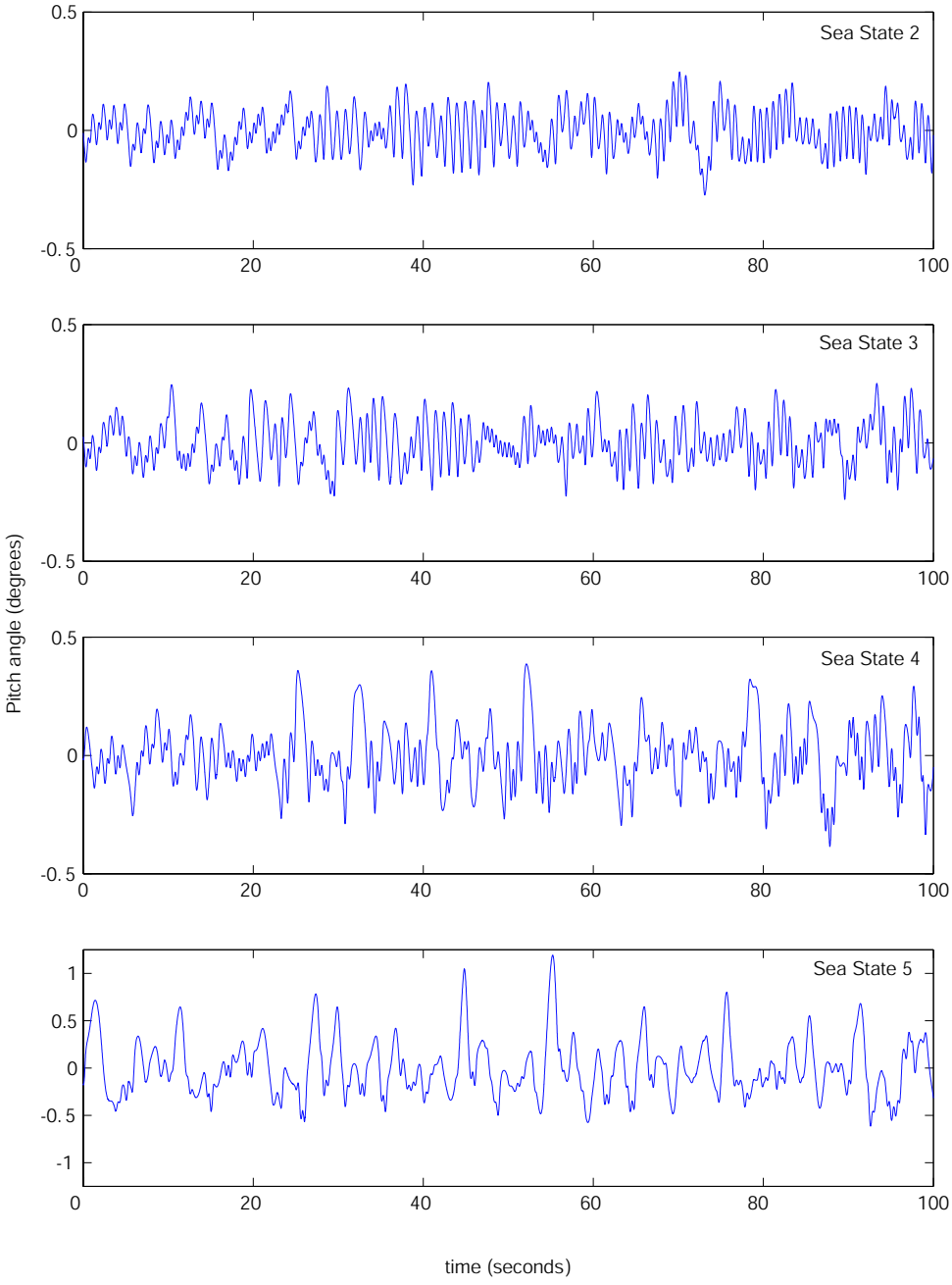

Figure 28: Variation in pitch angle at a velocity of 6.6 ft/s (2 m/s) for a range of sea states

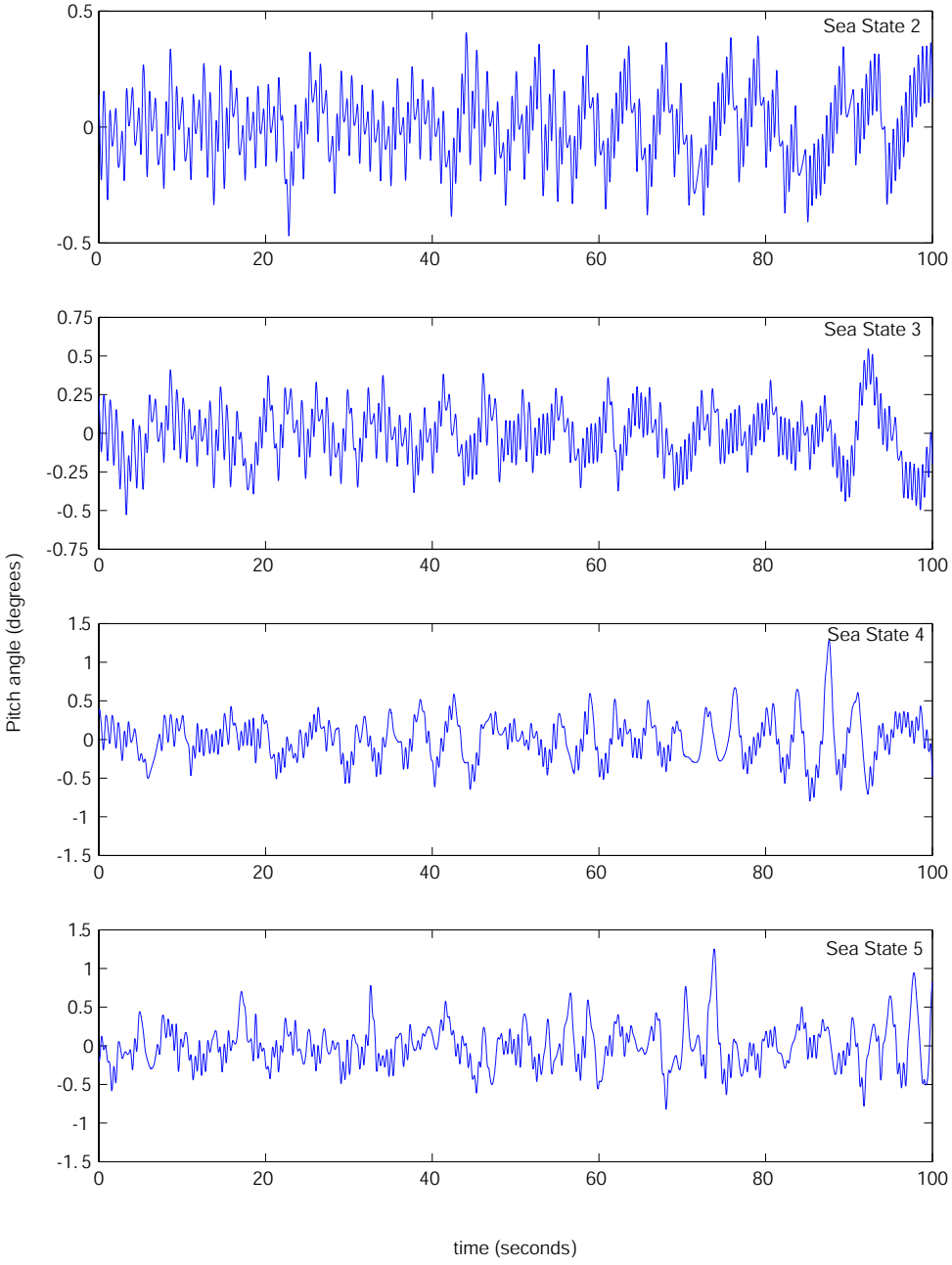

Figure 29: Variation in pitch angle at a velocity of 9.8 ft/s (3 m/s) for a range of sea states

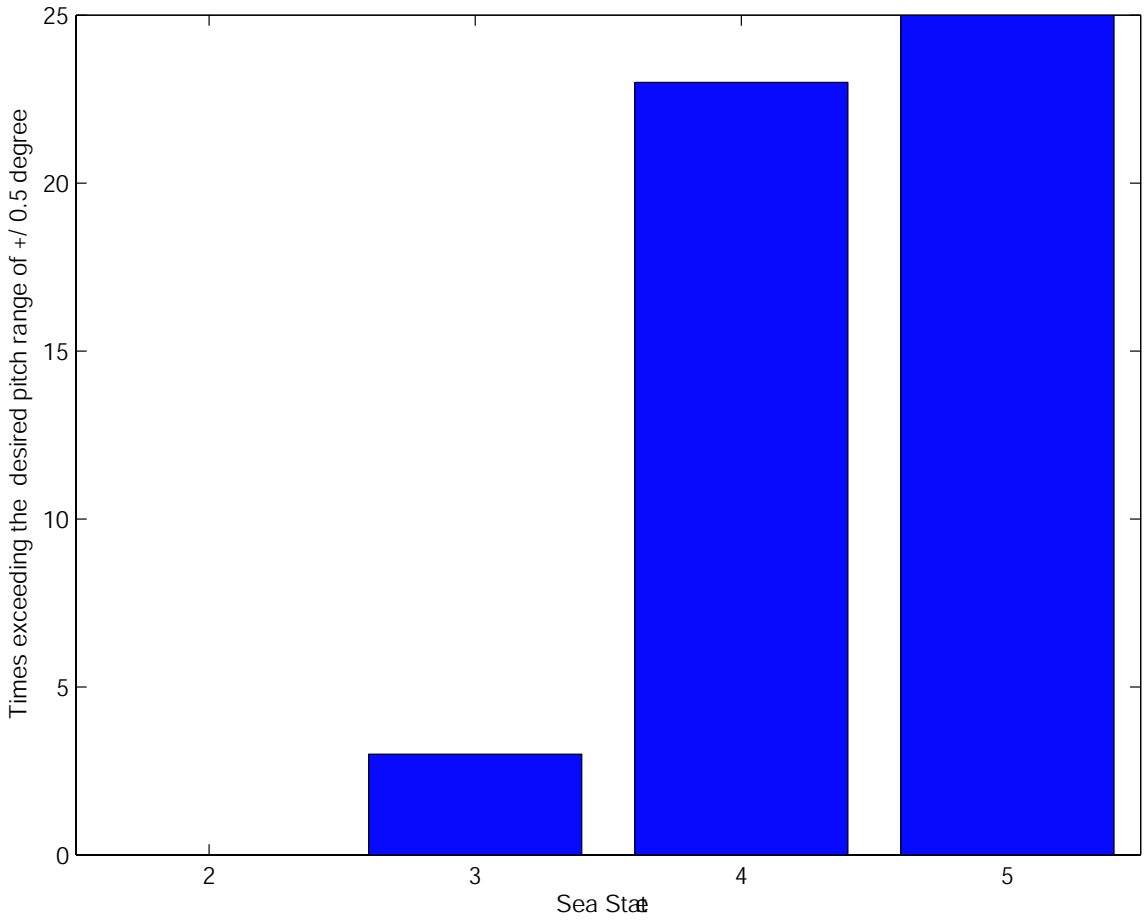

Figure 30: Times exceeding the desired pitch angle range of plus or minus 0.5 degrees versus Sea Sate at a velocity of 9.8 ft/s over 100 seconds

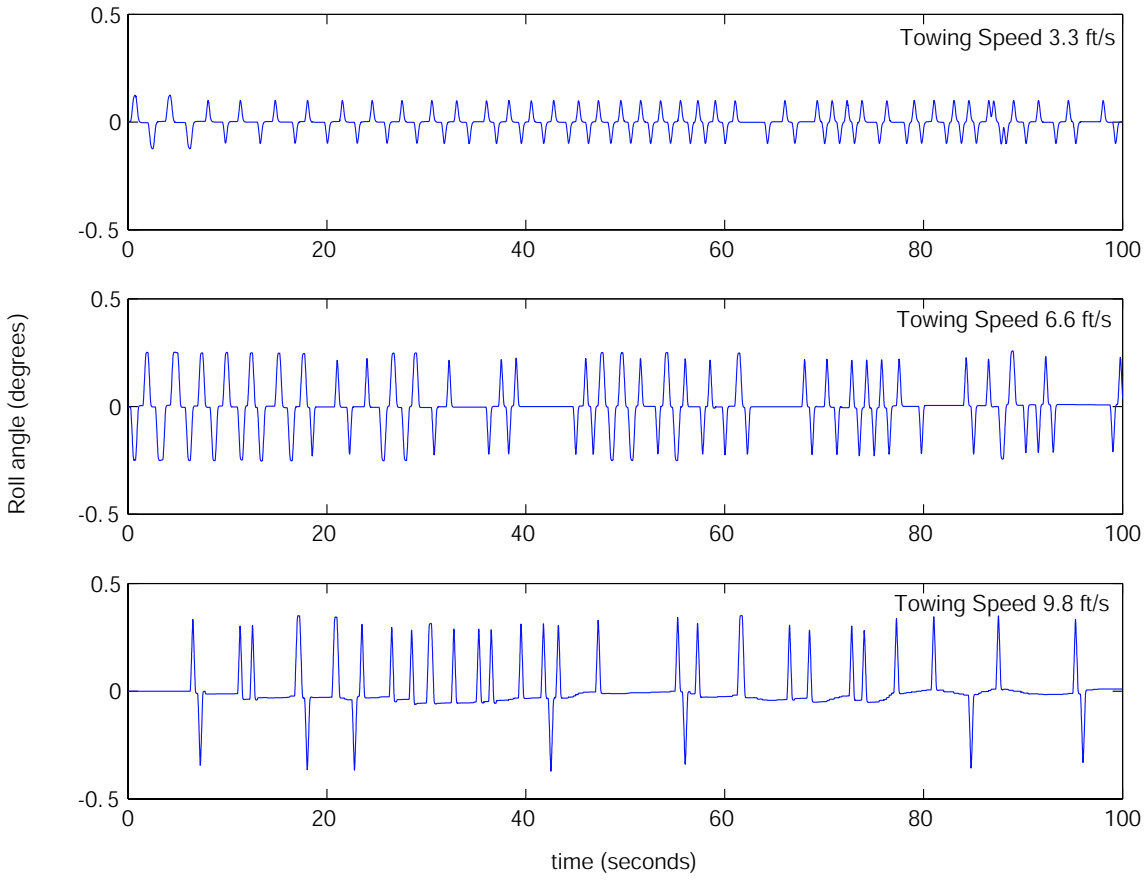

Figure 31: Variation in roll angle at sea state 3 for a range of velocity values

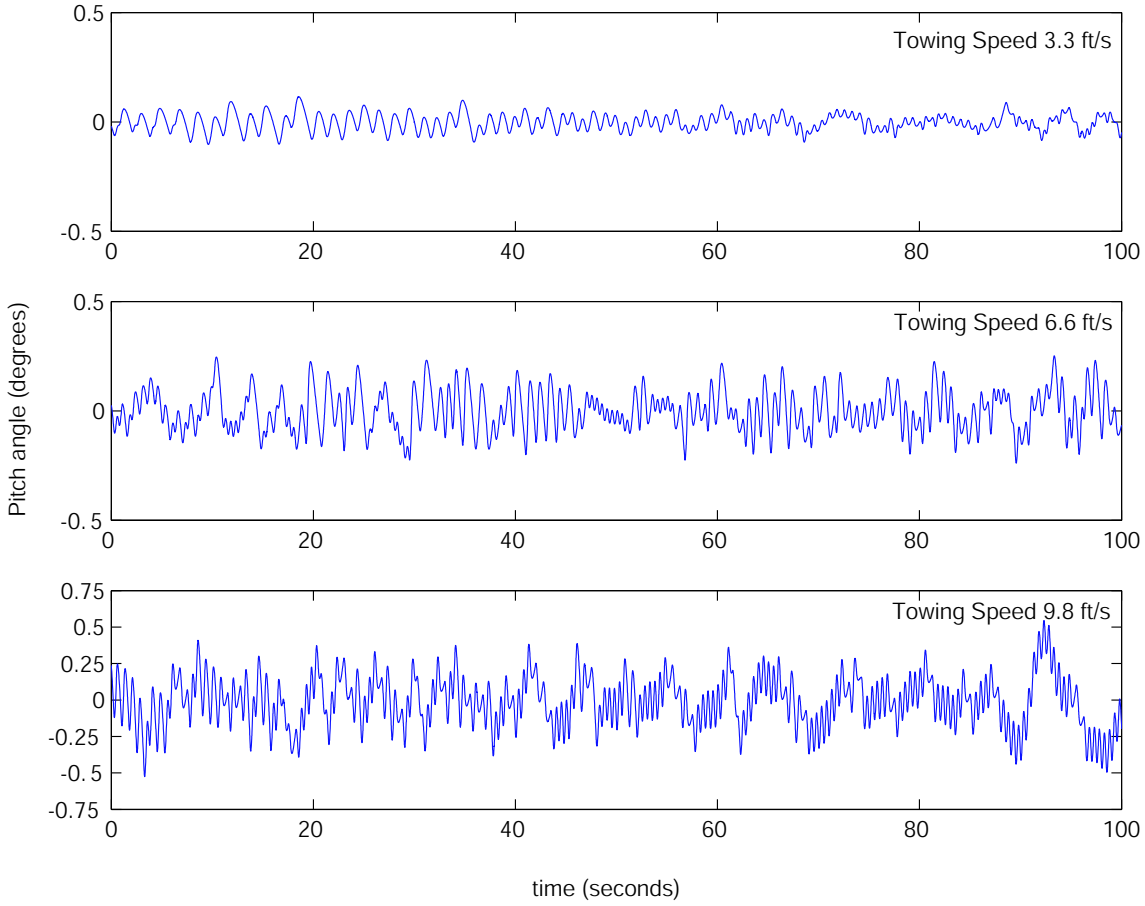

Figure 32: Variation in pitch angle at sea state 3 for a range of velocity values

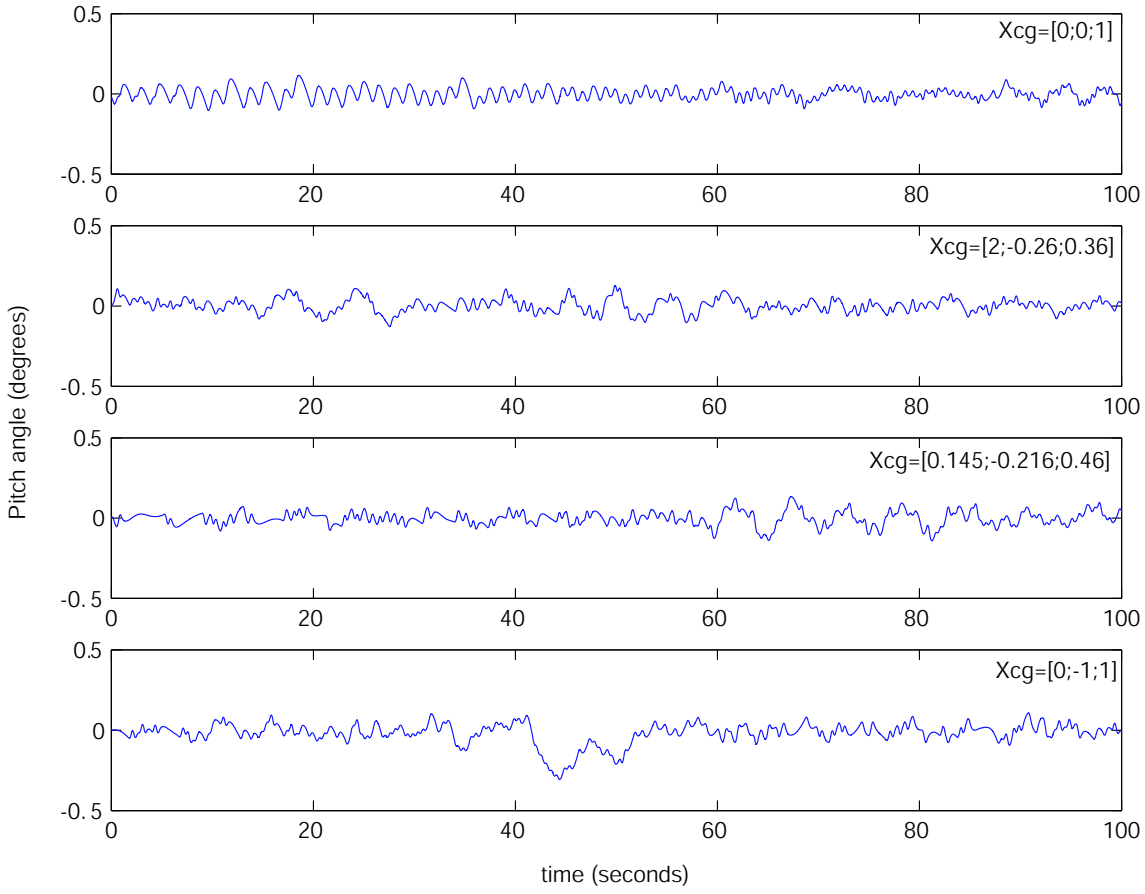

Figure 33: Variation in pitch angle for a towing velocity of 3.3 ft/s for four different cg locations

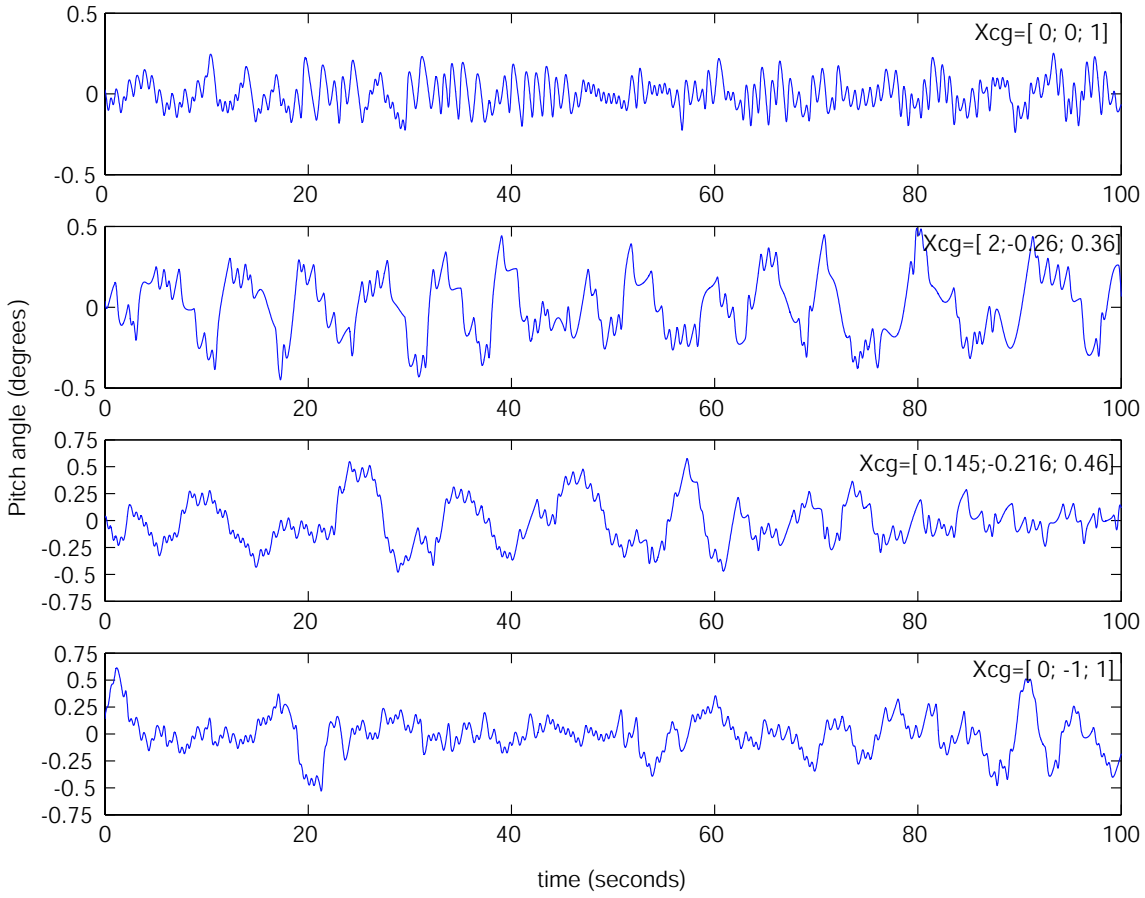

Figure 34: Variation in pitch angle for a towing velocity of 6.6 ft/s for four different cg locations

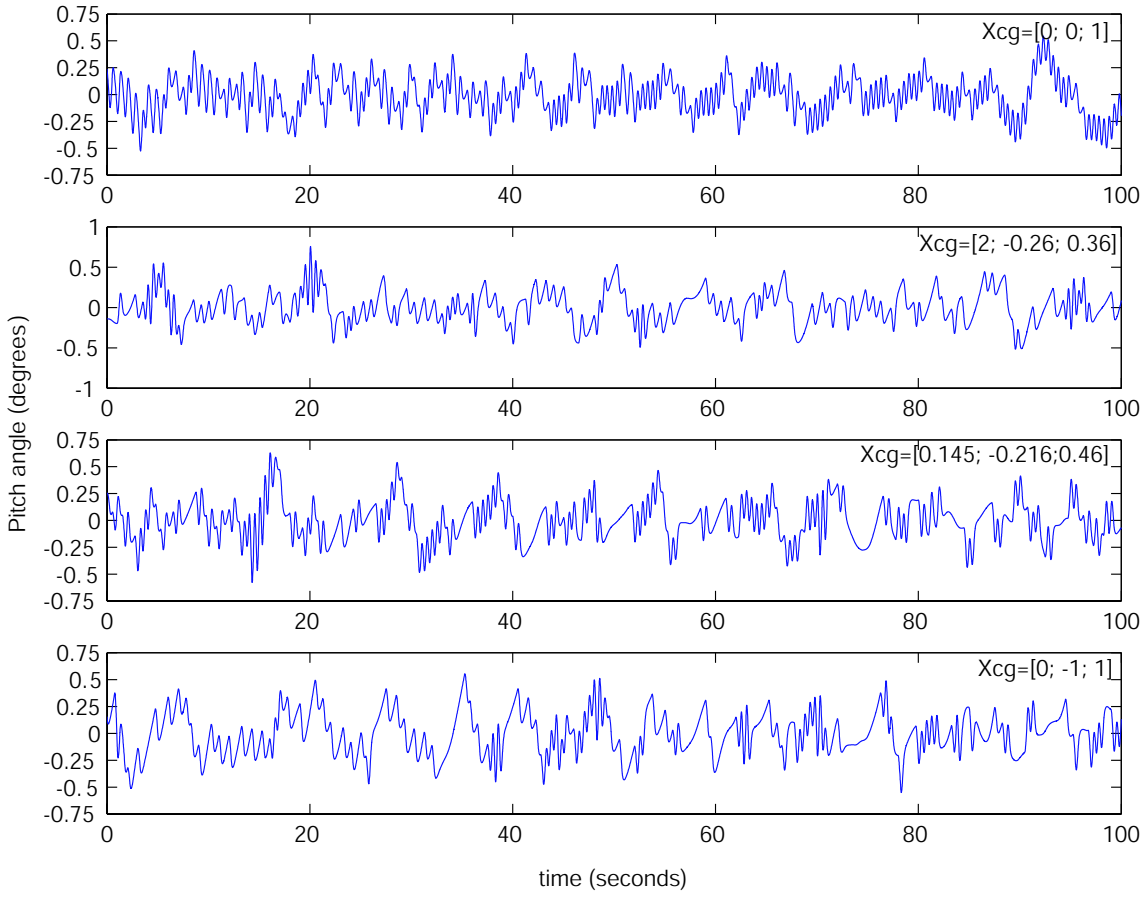

Figure 35: Variation in pitch angle for a towing velocity of 9.8 ft/s for four different cg locations

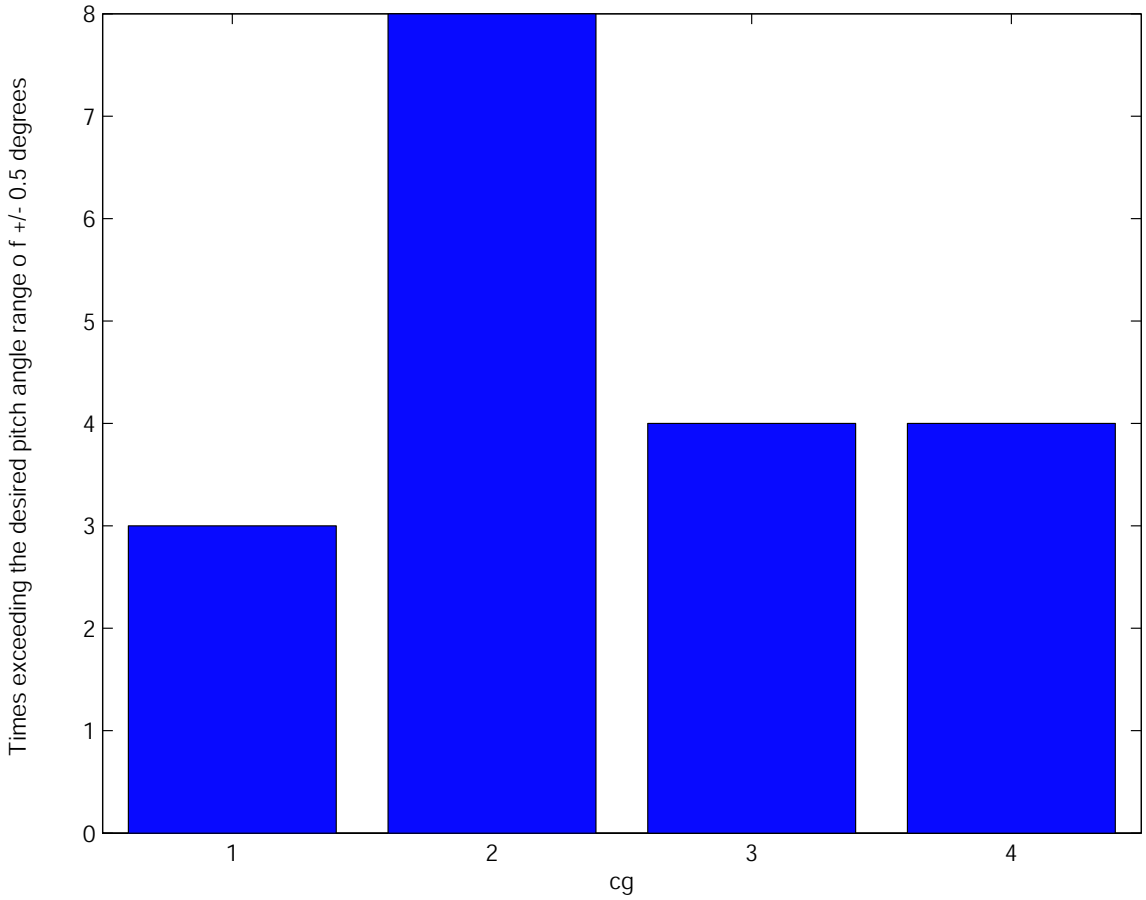

Figure 36: Times exceeding the desired pitch angle range of plus or minus 0.5 degrees versus cg position at a towing speed of 9.8 ft/s for 100 seconds where $X_{cg1} = [0; 0; 1]$ inches,$X_{cg2} = [2; -0.26; 0.36]$ inches,$X_{cg3} = [0.145; -0.216; 0.46]$ inches and $X_{cg4} = [0; -1; 1]$ inches.

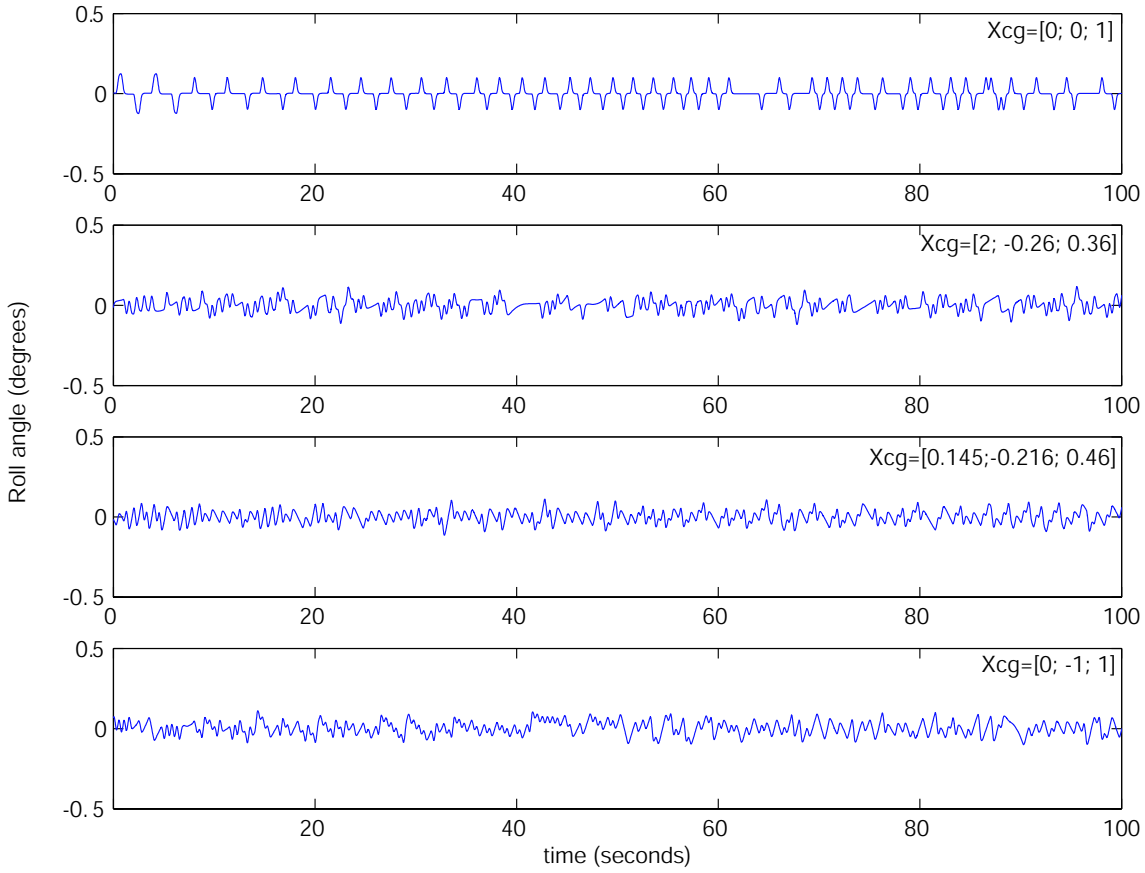

Figure 37: Variation in roll angle for a towing velocity of 3.3 ft/s for four different cg locations

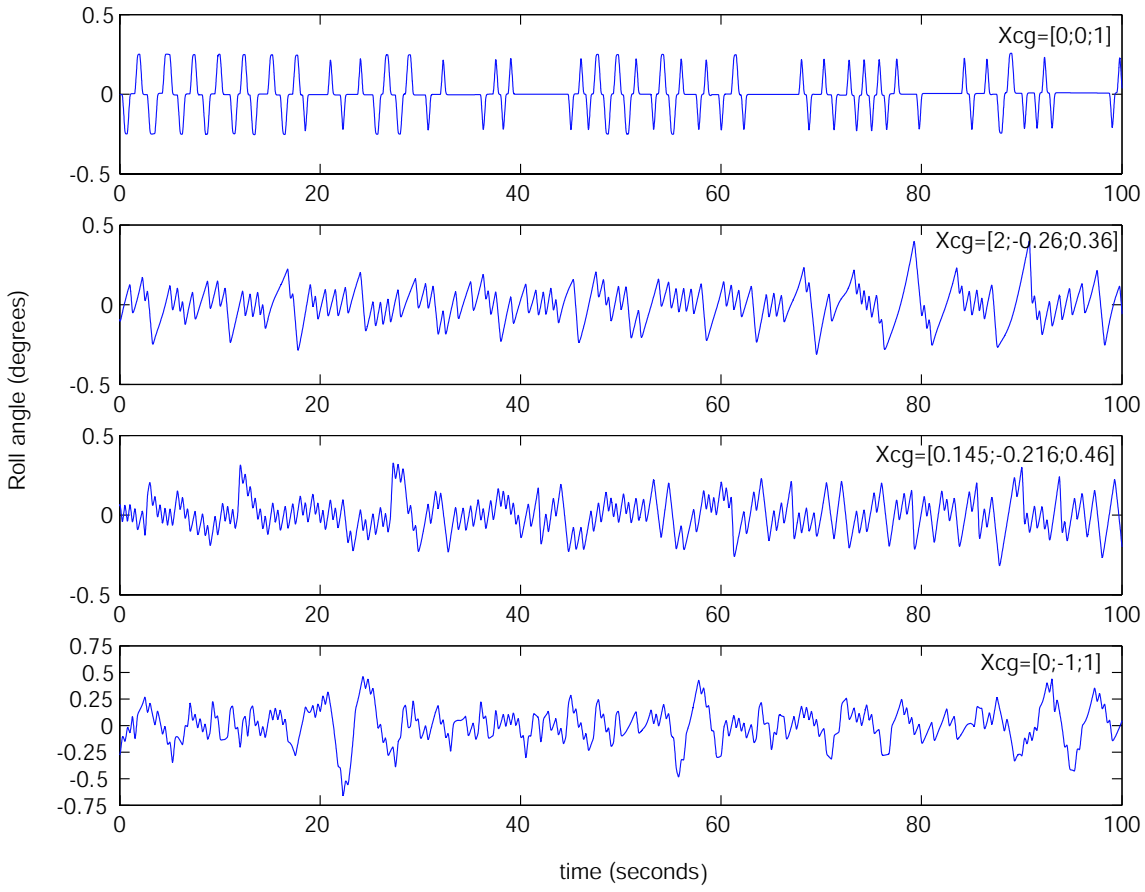

Figure 38: Variation in roll angle for a towing velocity of 6.6 ft/s for four different cg locations

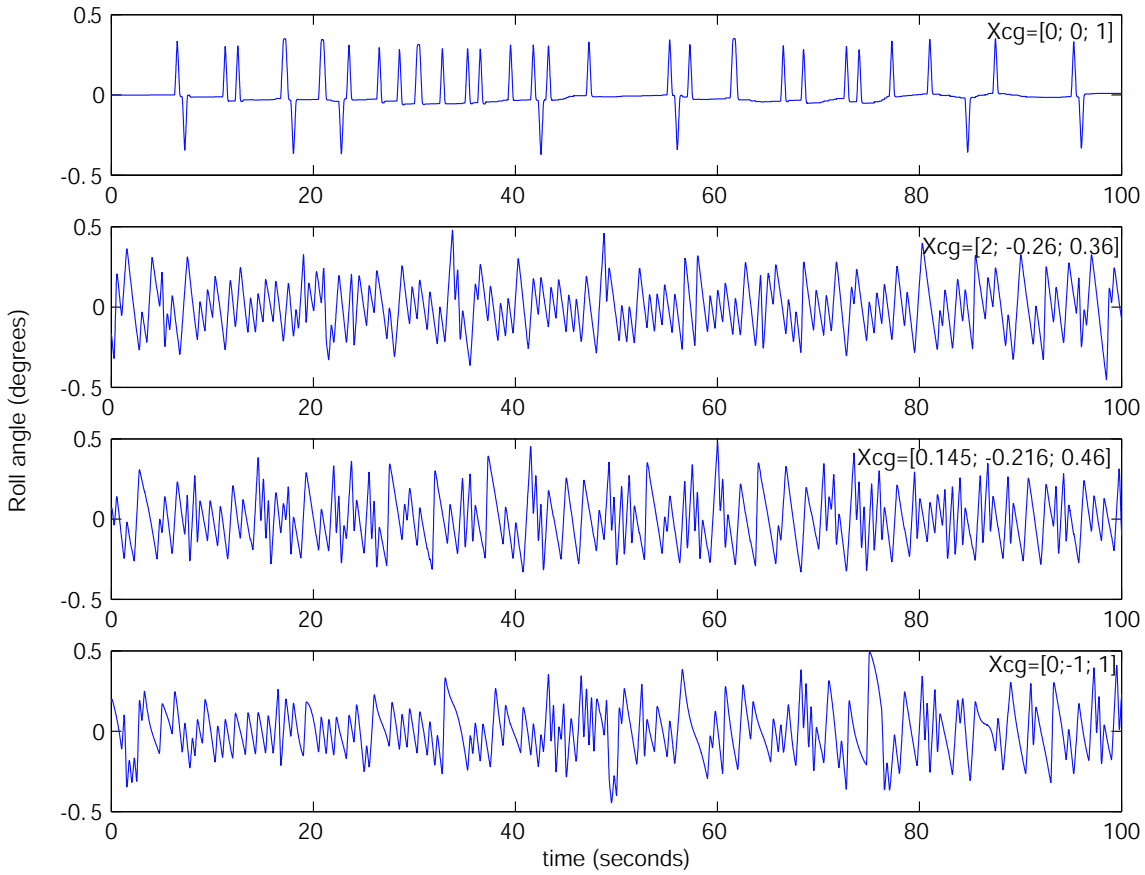

Figure 39: Variation in roll angle for a towing velocity of 9.8 ft/s for four different cg locations

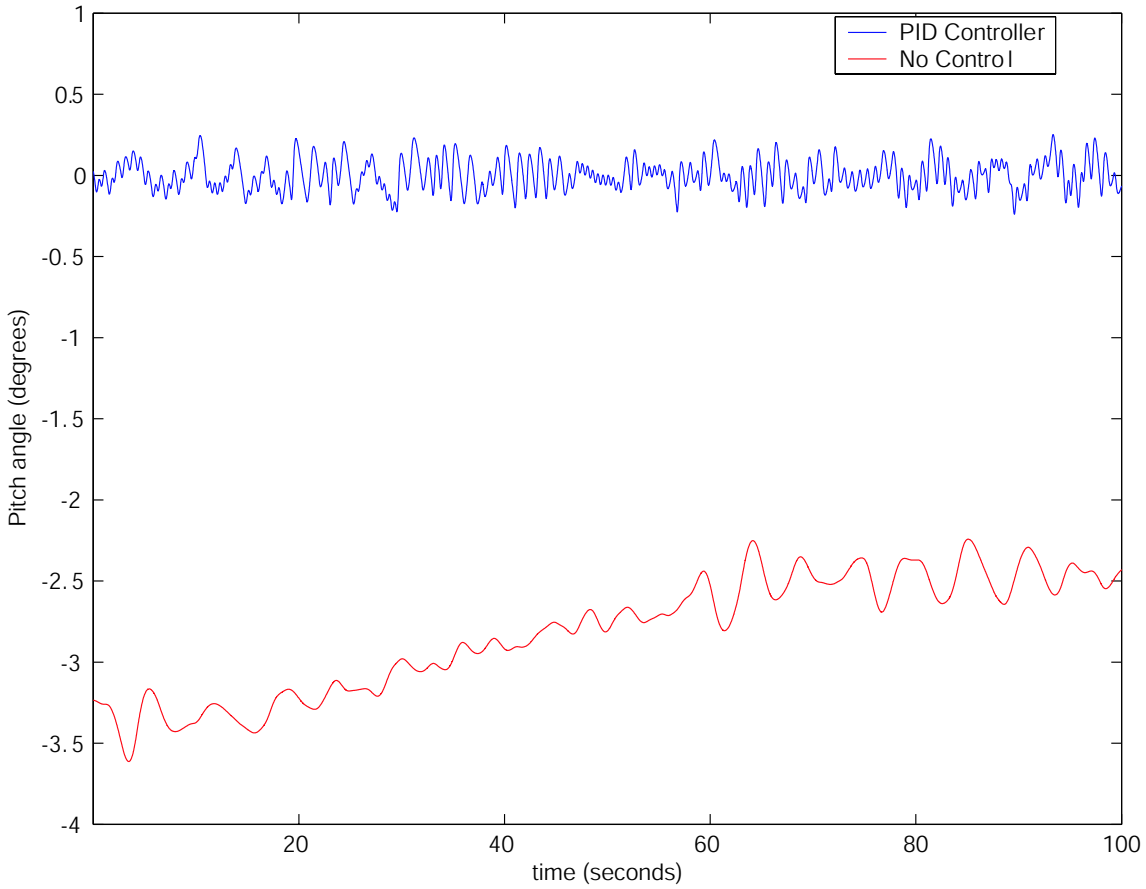

Figure 40: Variation in pitch angle for no controller versus a PID controller at a towing velocity of 6.6 ft/s

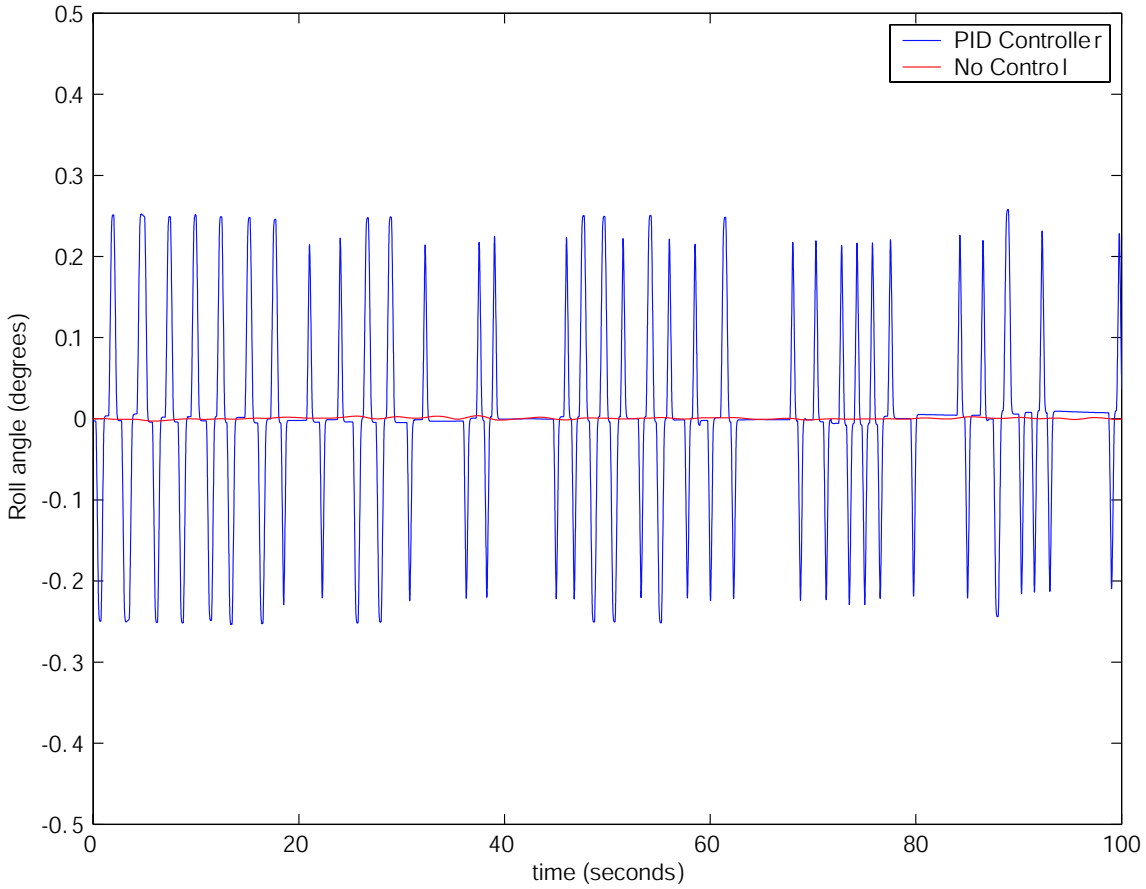

Figure 41: Variation in roll angle for a no controller versus a PID controller at a towing velocity of 6.6 ft/s

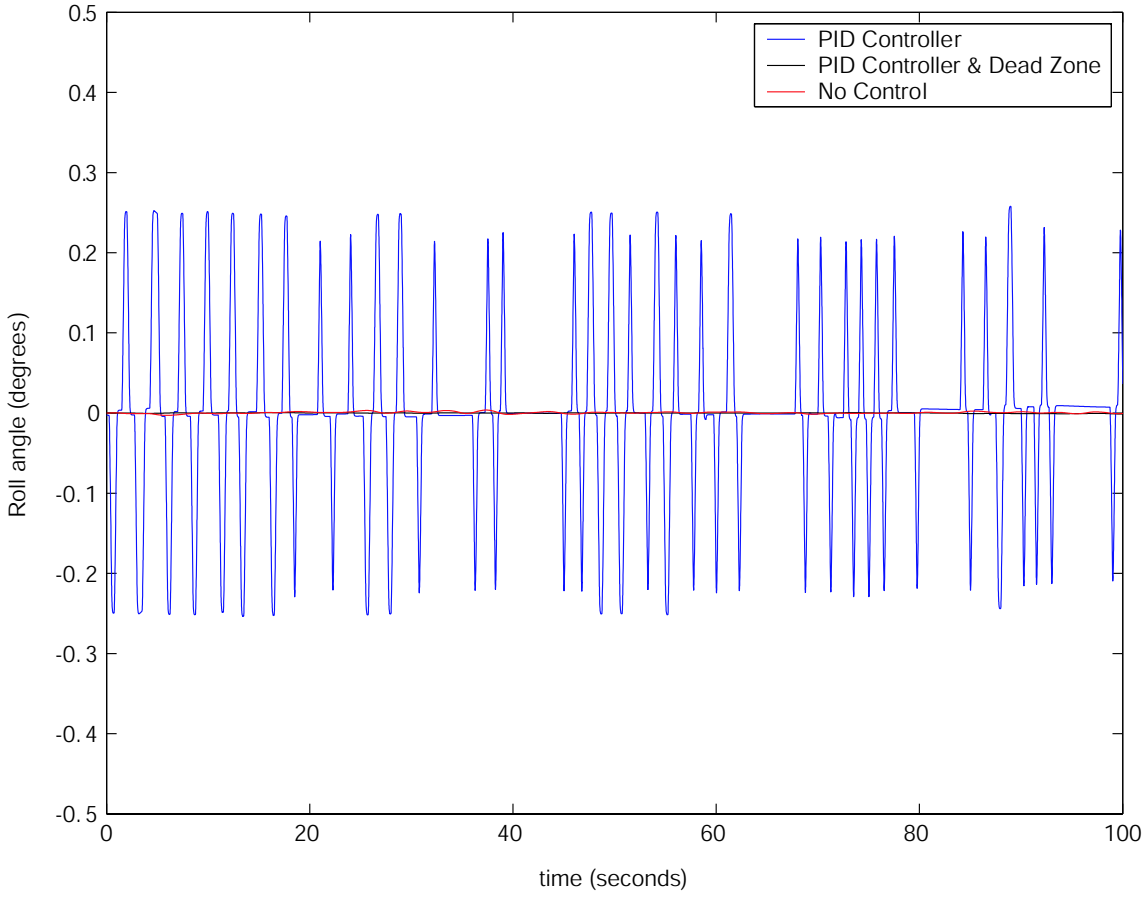

Figure 42: Variation in roll angle for no controller, a PID controller, and a PID controller with a dead zone at a towing velocity of 6.6 ft/s

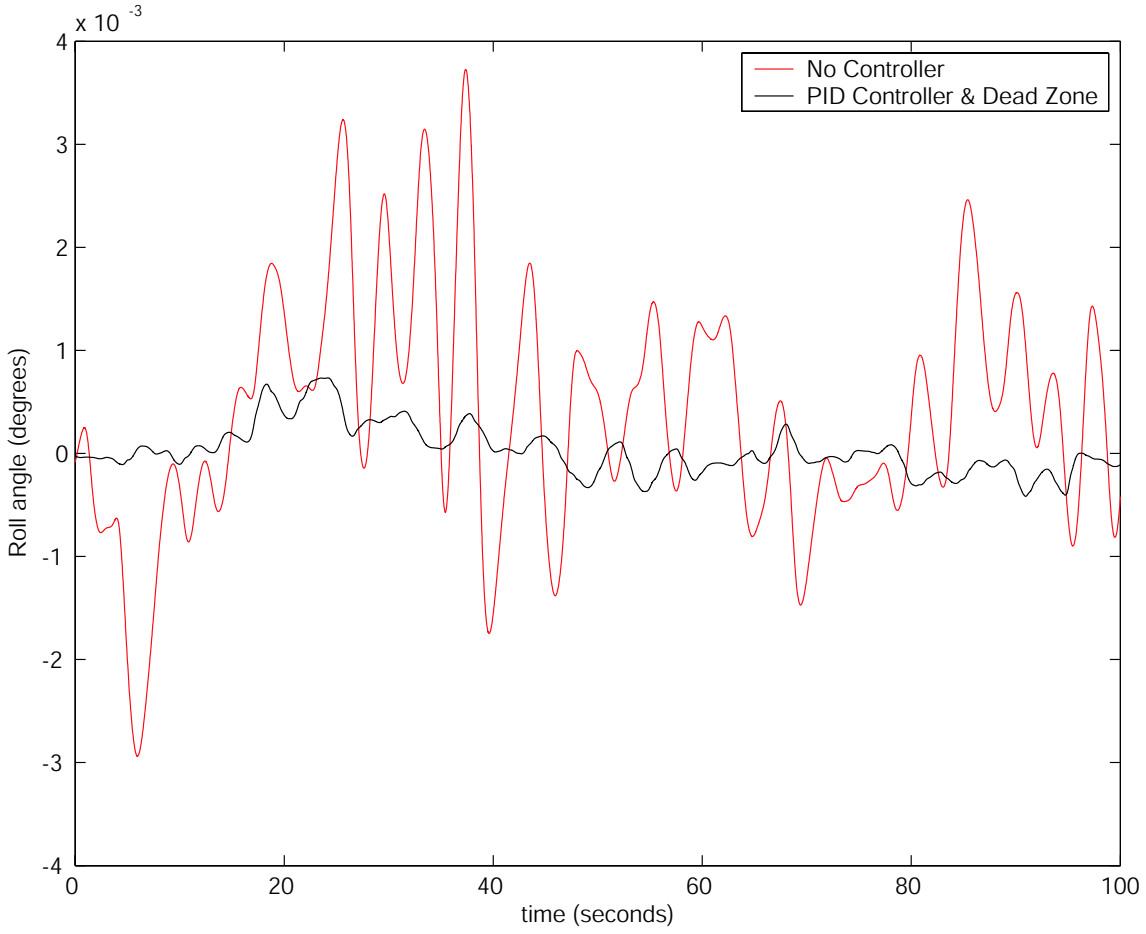

Figure 43: Variation in roll angle for no controller versus a PID controller with a dead zone at a towing velocity of 6.6 ft/s. Note the scale on the y axis is 10^{-3}.

5 Construction

5.1 Hull

The hull of the towfish was constructed by developing a shape that was reasonably hydrodynamic and was large enough to hold all the components needed for the towfish. A CAD drawing with the shape and dimensions of the hull was sent to Vectorworks a company that designs and manufactures male and female molds. A female mold was created for half of the hull since the two halves were symmetric. The makeup of the hull was fiberglass with a two-part epoxy resin. From this female mold, fiberglass lay-ups were done inside of the mold to create half of the hull. Fiberglass was used because it does not absorb water. One layer of heavy bi-directional weave fiberglass with a matte backing and two layers of medium fiberglass were used to make each half of the hull.

The pieces of fiberglass were carefully cut to the size of the hull. Mold release was spread over the female mold so that the hull formed of epoxy and fiberglass would come out of the female mold easily when the process was complete. The pieces of fiberglass were placed inside the hull after the mold release dried. Epoxy was poured and spread out over top of the layer of fiberglass. Next, peal ply and batting material were placed over the fiberglass and the area was vacuum sealed. This was done to help get any bubbles out of the fiberglass and to allow the epoxy to distribute evenly throughout the fiberglass while curing. Two vacuum fittings were used to give the surface a better finish and to help remove the air quickly inside the vacuum bag.

In between the heavy layer of fiberglass and the first layer of medium fiberglass, two aluminum bars were attached into the hull. The purpose of the these aluminum bars was to countersink holes so that the hull could be bolted to the frame.

A 8.9 inch diameter hole was cut out of the top and bottom of the hull to allow the VADCP head to protrude from the hull. At the aft end of the hull two holes were cut out for the shafts that were attached to the frame. These shafts were used to mount

Figure 44: Top half of the hull constructed of fiberglass

the vertical fins. Another two holes were cut out of each side of the aft end to allow the stern planes to attach to the actuators.

5.2 Fins

The fins were created by enlarging a NACA 0012 airfoil to a width that was slightly larger than the VHF pinger, since the VHF pinger needed to be put in the top vertical fin. For this airfoil shape, wood templates were cut out to use as guides when hot-wiring. Next, large sheets of foam were purchased and the fins were hot-wired out of them. These foam fins were then wrapped in two layers of heavy bi-directional weave fiberglass with matte backing to create an outside shell. Before fiberglassing, a nickel-chrominium wire was placed spanwise through all of the fins. This wire made it easier to hot-wire the foam out once the fiberglassing process was completed. This foam had to be removed because it would crush at 660 feet ($\approx$ 200 meters). At this point, once all the foam inside the fiberglass shell was removed, rods were machined to place inside the fins which would allow the fins to be attached to the hull. To

Figure 45: Half of the hull in the female mold

hold these rods in place while pouring the syntactic foam, a stand was made that allowed the fins to sit upright and allowed for the rods to be placed in the correct holes. Before pouring the syntactic foam, one end of the shell was fiberglassed over and holes were cut out for the rods. By doing this, the syntactic foam stayed inside the shell and hardened. This process was done for each fin until 5 fins were made (four plus one replacement). For the fin that was designed to hold the VHF pinger a PVC pipe was covered and placed inside the fin as a sleeve in which the VHF pinger would be able to fit into after the syntactic foam dried. After all of the fins were poured, they were all covered with fairing compound and faired down until they were smooth. Figure 46 shows the four fins attached to the hull looking from the aft end of the towfish.

The two vertical fins are fixed in place, however the two stern planes are independently actuated. The servo actuators are Tecnadyne Model 60 rotary actuators. Each actuator has eight Hall sensors on the input shaft and there is a 200 to 1 gear ratio

Figure 46: A rear view of the four fins attached to the hull

which gives 1600 pulses per revolution on the output shaft [20]. These actuators provide 60 ft-lbs of torque and can turn up to 90 degrees per second [20]. Two limit switches are mounted off of the frame to cause the stern planes to stop at a designated angle of 20 degrees, above which the planes may stall.

5.3 Frame

The frame for the towfish that fits inside of the fiberglass hull has a square cross section, with 11.5 inch sides and is 80 inches long. This frame was made of 6061 aluminum to protect it from corroding. The corners of the frame were made from angle aluminum. They were approximately 73 inches long and had 1.25 inch legs that came off the top and the bottom of the frame. These 1.25 inch legs were cut at an angle to allow the hull the ability to be screwed into the frame. The sides of the frame were made up of 1 inch wide by quarter inch thick aluminum bars that were welded to the angle aluminum bars. Four handles were attached to the side of the frame to help with recovering and lifting of the towfish. The bottom of the frame has

two square frame sections that were made from 1.25 inches height and 0.25 inches thick aluminum bars. These sections were welded to the bottom of the frame. The top of the frame has similar square frame sections that were removable to allow the VADCP, the power housing and the computer housing to be placed inside the frame. The nose of the frame is made of four, 2 inch wide by 0.25 inch thick by 7.25 inch long aluminum bars, that were welded to the four cross members and then welded to a 2 inch by 2.5 inch by 0.25 inch plate to make a pyramid shape [20]. This plate is the nose of the towfish. It has a hole in it that allows an eye-bolt to be attached to the frame. The eye-bolt secures the tether to the towfish. It is made of steel and is separated from the aluminum frame by a rubber washer to keep the steel eye-bolt and the aluminum frame from corroding. Two aluminum plates that are 5.5 inches by 11.5 inches by 0.13 inches have been welded to the rear sides of the frame with a 4.13 inch diameter hole [20]. These were attached so the head of the actuator would fit through each plate. The frame can be seen in Figure 47.

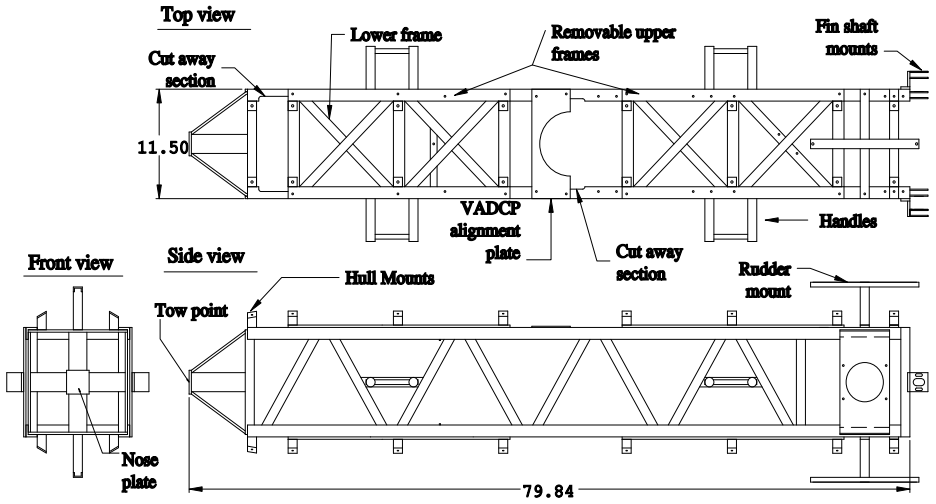

Figure 47: Aluminum frame of the towfish [20]

5.4 Electronic suite

Two pressure housings are secured into the frame of the towfish. They convert AC power from the research vessel to DC power to run the computer, sensors and actuators. The pressure housings hold the computer and attitude sensor to keep them in a watertight environment. The first pressure housing was used to supply power to the towfish. It is located at the nose of the towfish and is known as the power housing. The power housing was equipped with three conversions units. It receives 220 VAC from the research vessel through the umbilical cable that runs from the research vessel to the towfish. The power that has been supplied is converted into 144 VDC via an AC to DC converter. Next, the 144 VDC is reduced to 48 VDC and then the 48 VDC is reduced further to 12 VDC. Converters were purchased from Vicor [20].

The three power converters are attached to a rectangular bracket. Figure 48 shows that the AC to DC converter lies on top of the bracket and the DC to DC converters are attached below the bracket. Note that the heat exchanger is positioned to face away from the DC to DC converters [20].

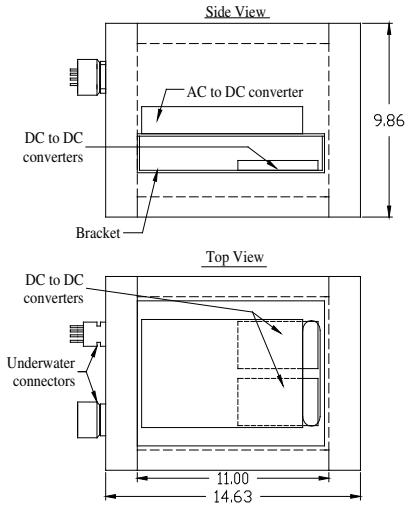

Figure 48: Inside view of the Power Housing [20]

The power housing fits inside the frame, where it sits on a semicircular piece of

aluminum. This semicircular piece of aluminum is 0.125 inches thick and is fastened at each end to a semicircular piece of Starboard. The Starboard pieces are attached to an aluminum L bracket that has been welded to the frame. The power housing is then secured to the aluminum piece by two quick-release hose clamps. Note the piece of aluminum is covered with neoprene to keep the steel hose clamps off of the aluminum. Figure 49 shows how the power housing is secured inside of the frame [20].

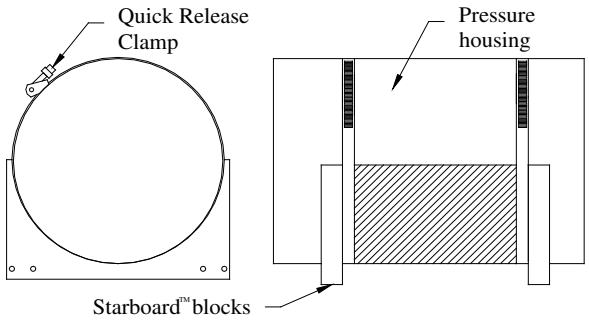

Figure 49: The power housing sitting in the Starboard mount [20]

The second pressure housing holds the computer and the attitude sensor. The Crossbow VG400-CC-100 is a vertical gyro (VG) that is used to measure the attitude and angular rate. It allows for the pitch and roll of the towfish to be measured within a half of degree statically and within 2 degrees dynamically. Due to the fact that this system will have slow dynamics and needs to maintain a static equilibrium attitude for accurate measurements to be made the static accuracy is therefore more relevant. Note that the pitch and roll angle outputs from the vertical gyro will need to be within plus or minus a half of a degree to ensure the actual tilt angle of the towfish is within plus or minus one degree. The vertical gyro also measures the pitch and roll rate. This pressure housing also holds a PC-104 computer that runs Labview in Linux for data collection. The computer includes the CPU module (a Micro 886ULP from Advanced Micro Peripherals), the power board (a HE5120V5120T from Diamond

Systems), a serial expansion card (an Emerald-MM-8, also from Diamond Systems) and a two-axis motor control card (a 4I27A from Mesa Electronics) [20].

A bracket is mounted under the upper end cap of the computer housing to which the PC-104 is attached. The bottom end cap is used to mount the Crossbow vertical gyro. Impulse brand right angle connectors are attached to the outside of the computer housing, the right angle connectors allow for space to be conserved outside of the computer housing. Figure 50 shows the inside view of the computer housing. This computer housing was mounted upright in the frame to allow for easier cable connections within the hull of the towfish. It was secured in place by two quick-release hose clamps that went around a vertical aluminum semicircular piece. This aluminum piece was attached to two Starboard pieces which were then attached to the frame. This setup is similar to how the power housing is attached in the frame with the exception that this pressure housing sits vertical.

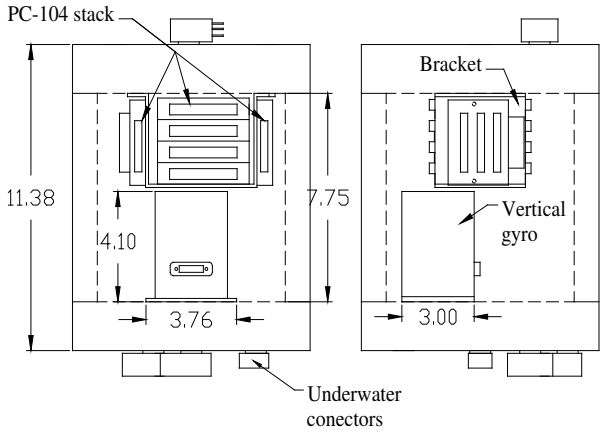

Figure 50: The inside of the computer housing [20]

The connectors between the pressure housings and the VADCP are waterproof and purchased from Impulse except for the connectors attached to the actuators. These connectors are Seacon connectors. Figure 51 shows an electronics schematic of the towfish setup.

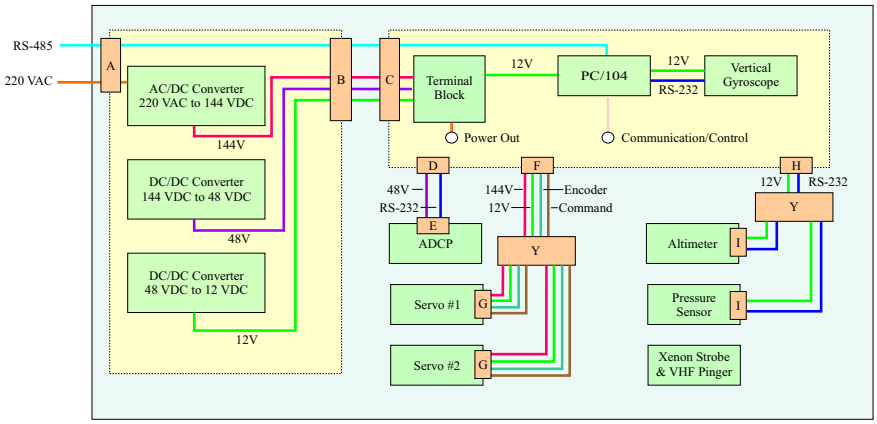

Figure 51: Electronics diagram [20]

5.5 Main sensor

The VADCP was custom built by RD Instruments and is a one-of-a-kind sensor. The five beams of this sensor run at 1200 kHz. Four beams in a tetrahedral arrangement measure two components of velocity and the fifth beam provides the third velocity component. To accurately resolve small-scale ocean turbulence, the fifth beam must be precisely aligned with the local direction of gravity. This instrument has a length of approximately 42.5 inches, a diameter of 6.75 inches and a height of roughly 15 inches. A detailed diagram of this sensor can be seen Figure 52.

This sensor has the ability to either face up or face down in the towfish. The sensor is secured into the frame of the towfish by tightening quick-release hose clamps around aluminum rods that have been attached inside the Starboard pieces. The Starboard pieces then attach to the frame.

5.6 Flotation

Flotation was a necessary component of the towfish to help make it 5 percent buoyant. This is important in case the cable parts after the depressor; it would allow the towfish

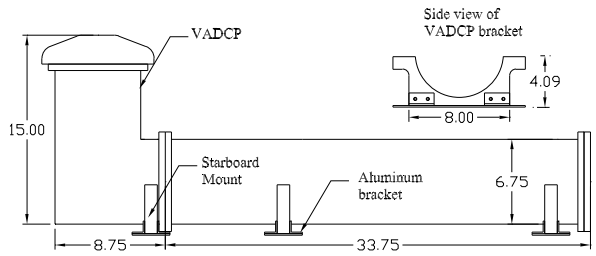

Figure 52: Detailed diagram of the VADCP (units in inches). *Adapted from reference [20]

to float to the surface and be recovered. For this to be possible under the condition that the towfish would be going to depths of 660 feet ($\approx$ 200 m), syntactic foam was decided upon since it had a low density and was rated well beyond this depth. Cuming Corporation was the supplier of the foam. For this project, TP-24 and TP-38 foam was used to help make the towfish more buoyant. C-Foam TP-24 is a syntactic foam that is packed in place with a density of 24 pounds per cubic foot. The depth rating for TP-24 foam is about 2,700 feet (822.96 m) which is based off the maximum pressure rating of the micro balloons utilized within the foam matrix. The C-Float TP-38 is a pour in place product with a density of 38 pounds per cubic foot. This foam uses the same mirco balloons as the C-Foam TP-24; the depth rating of this foam is greater than that of the C-Foam TP-24.

C-Float TP-38 was originally poured in the top of the hull to help make the towfish more buoyant see Figure 53. Two side pieces of C-Foam TP-24 were constructed that fit between the towfish hull and the side of the frame to help with buoyancy issues, which is shown in Figure 54.

A large block of C-Foam TP-24 was finally placed above the VADCP. These were the original places that foam was placed but the relative cg and cb locations were found to be unacceptable. A trim and ballast analysis of the towfish is presented in Section

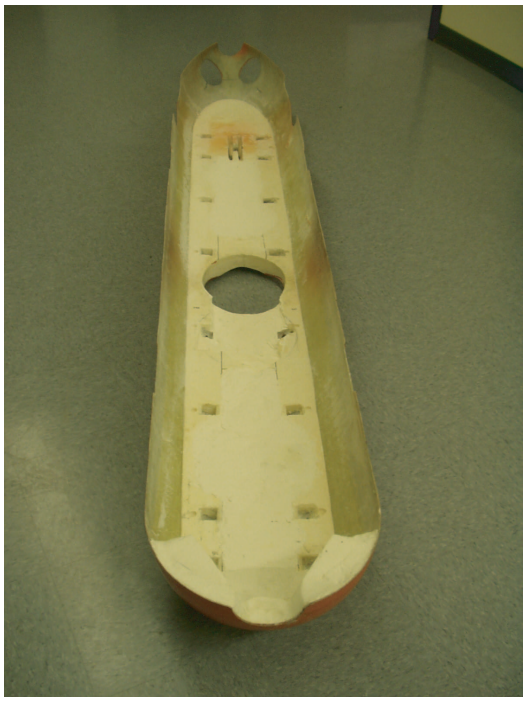

Figure 53: A view of the top hull with foam inside

6 that describes where foam was added to evenly ballast the towfish.

5.7 Other equipment

Some other components of the towfish which are necessary are an altimeter, a VHF pinger and a RF-700C1 light. A Benthos Datasonics PSA-916 altimeter is another component that is used to determine the altitude of the towfish, shown in Figure 55. This is used to measure the distance from the towfish to the bottom. A Novatech designed RF-700C1 light and a VHF pinger are two other components of the towfish that are used for recovery purposes.

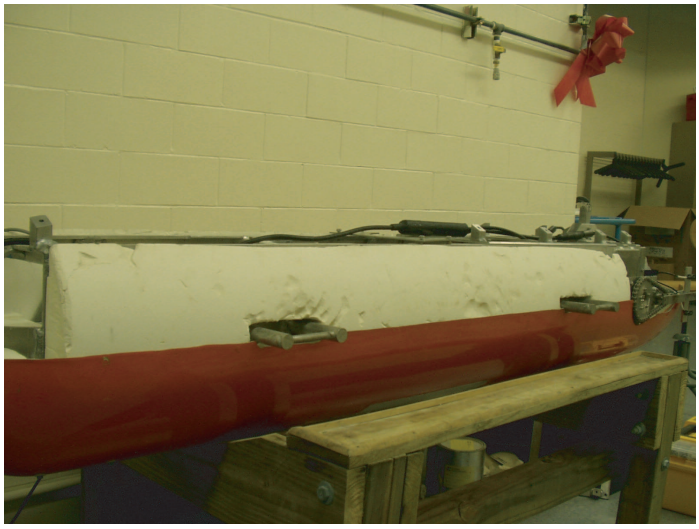

Figure 54: A piece of foam that was constructed to fit between the inside of the towfish hull and the outside of the frame

Figure 55: The Benthos Datasonic PSA-916 altimeter

6 Trimming the Towfish

After an initial sea trial it was determined that the towfish was improperly trimmed. The towfish was excessively nose-heavy. The towfish was assembled and placed in a water tank. Two rachet straps were wrapped around the the towfish at the handles and attached to two scales. Figure 56 shows the exact setup.

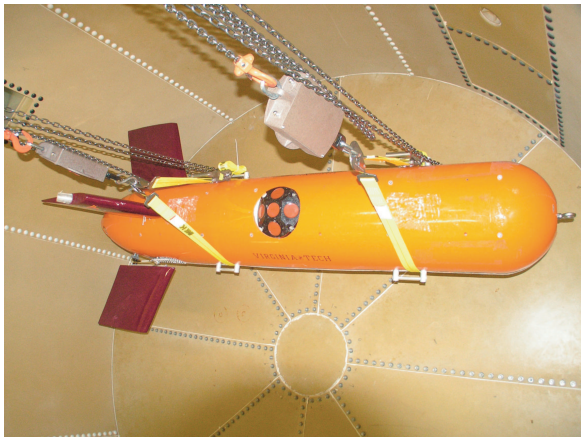

Figure 56: Towfish setup in the water tank to find the dry weight

6.1 Dry and wet weight of the fully assembled towfish

The towfish was weighed and its total weight with all its components was 482 pounds. For the towfish to be 5 percent buoyant, it needed a buoyant force of 506 pounds. The tank was then filled up with water so the wet weight could be measured. At this point, it was observed the aft end of the towfish was floating, however the nose was fully submerged. A wet weight was measured by attaching 63 pounds of dive weights at point B shown in Figure 57, the point of the aft set of handles. This weight was evenly distributed on both sides of the towfish.

Attaching this weight caused the aft end of the towfish to sink and allowed for the net wet weight to be measured. The following measurements were recorded in Table 3 from the wet and dry measurements.

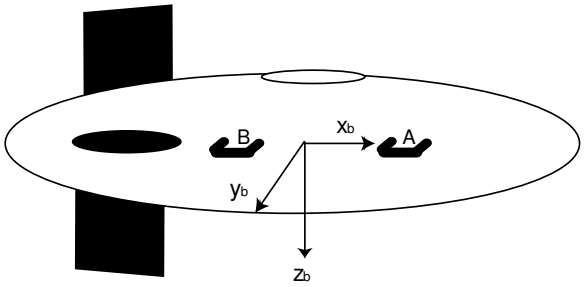

Figure 57: Towfish trim and ballast diagram

Table 3: Dry and wet weight measurements for the fully assembled towfish

Type of Measurement	Scale A (lbs)	Scale B (lbs)	Weight Added
Dry Weight	160	322	0
Wet Weight	18	19	+62.84 lbs added to B

These measurements allowed for the longitudinal cg and cb location to be calculated. The following equations show how these values were calculated.

Dry Calculations:

$$\sum F_z = 0 = W - W_A - W_B = 0 \tag{59}$$

W = 482 lbs

$$\sum M_A = 0 = W x_{cg1} - W_B x_{BA} \tag{60}$$

x_{cg1} = 25.0519" aft from point A

The weight measured at point A is defined as W_A, W_B represents the weight acting at point B and W is the total weight of the towfish. The cg in the longitudinal direction from point A is denoted above as x_{cg1} and x_{BA} is the distance in the longitudinal direction from point A to B.

Wet Calculations:

$$\sum F_z = 0 = W + W_{added} - W_A - B - W_B \tag{61}$$

B = 508 lbs

$$\sum M_A = 0 = W x_{cg1} - B x_{cb1} + (W_{added} - W_B) x_{BA} \tag{62}$$

x_{cb1} = 27.1" aft from point A

The weight added at point B to cause the aft end of the towfish to sink is defined as W_{added} and B is the buoyancy of the towfish. The cb of the towfish in the longitudinal direction from point A is defined as x_{cb1}.

In conclusion, from the calculations that were made above the difference longitudinally between the x_{cg1} and x_{cb1} was a little over 2 inches, with the cg being in front of the cb. Therefore from this ballasting experiment it was concluded that buoyancy needed to be added to the nose of the towfish. The overall buoyancy of the towfish however was just slightly over 5 percent. Therefore, to keep the total buoyancy of the towfish at approximately 5 percent it was determined that foam should be added to the nose of the towfish and foam should be removed from the aft end of towfish. This would allow the towfish to be more equally buoyant.

The difference in vertical distance between the cg and cb was also of interest for the towfish. It is very important that the cg lie below the cb to be able to stabilize the vehicle in roll and pitch and also to make the vehicle more robust to disturbance. For a good approximation of the distance vertically between the cg and cb, the vehicle without the fins was rolled 90 degrees and released. The towfish body was allowed to damp out to a small angle of $\approx$ 10 to 15 degrees and then the period was measured for two oscillations. This experiment was performed three times.

From the data, the average time period, 3.387 seconds, was used to find the vertical distance between the cg and cb. It was assumed that the towfish rotates about the centerline. Therefore the following equation was developed:

Table 4: Period measurements without the fins

Trail	Period(sec)
1	3.335
2	3.385
3	3.44

$$I_o\ddot{\phi} = r_{cg}Wsin\phi - r_{cb}Bsin\phi \tag{63}$$

where I_o was the moment of inertia of the towfish body, r_{cb} denotes the distance from the cb to the center of the body axis frame and r_{cg} denotes the distance from the cg to the center of the body axis frame. The buoyancy of the towfish is approximately five percent more than the weight, but it was assumed that the weight equaled the buoyancy for this calculation. It was also assumed that ϕ was a small angle, which means $\sin[\phi] \cong \phi$. This allowed equation (63) to be simplified to the following

$$I_o\ddot{\phi} = (r_{cg} - r_{cb})W\phi \tag{64}$$

where

$$(r_{cb} - r_{cg}) = l_d \tag{65}$$

This can then be rewritten as

$$I_o\ddot{\phi} + l_dW\phi = 0 \tag{66}$$

therefore

$$\omega_n = \sqrt{\frac{l_dW}{I_0}} \tag{67}$$

The moment of inertia (I_o) was assumed to equal to that of a cylinder with an offset distance of l_d. By using the parallel axis theorem the moment of inertia for the towfish was approximated by the following equation.

$$I_o = 1/2m\left(\frac{d_b}{2}\right)^2 + ml_d^2 \tag{68}$$

where m was the mass of the towfish and d_b was the diameter of the towfish. Equation (68) was then substituted into equation (67) and rearranged to get the following quadratic equation:

$$\omega_n^2 ml_d^2 - Wl_d + 1/2\omega_n^2 m\left(\frac{d_b}{2}\right)^2 = 0 \tag{69}$$

This quadratic equation was then solved for l_d which was found to be approximately 0.36 inches. This showed the cg lies 0.36 inches below the cb. However, it should be noted that there was a slight list to starboard side when the towfish was trimmed.

6.2 Foam addition and modifications

After these calculations were done, it was determined that more foam needed to be added to the nose of the towfish. It was found that foam could be added to two places in the front of the hull. There was a pyramid shape at the front of the frame, Area 1, that only a cable had to go through so this area was used as one place to add C-Foam TP-24. This foam has a density of 24 pounds per cubic foot and is rated beyond 660 feet ($\approx$ 200 m), which was the maximum operating depth. The area outside of the frame at the nose, Area 2, had some empty space that could also be filled in with C-Foam TP-24. Figure 58 shows these two areas in red where foam could be added to the front of the hull.

There was foam in the top of the hull that had previously been poured with a density of 38.1 pounds per cubic foot known as C-Float TP-38 that could be removed and replaced with the C-Foam TP-24. These adjustments would allow the cb to move closer to the cg, in the longitudinal direction. It was also determined that the large foam block at the aft of the towfish made of C-Foam TP-24 could be removed to make the aft end of the towfish less buoyant. This redistribution of foam was done

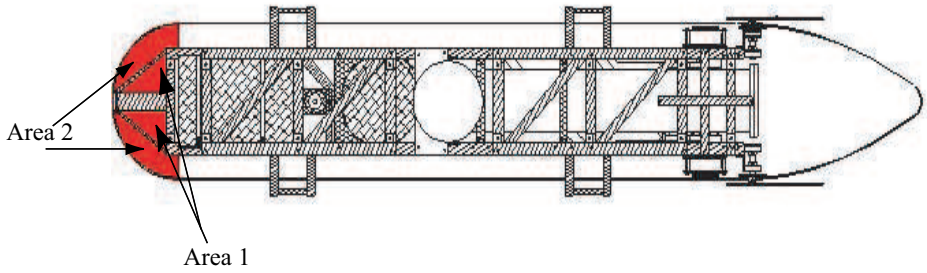

Figure 58: The area in the nose of the towfish where C-Foam TP-24 was added (adapted from [20])

so the towfish would be more equally buoyant. A Matlab program was written that calculated the new location of the cg and cb with the addition of each amount of foam. This program is included in Appendix A. After figuring out how much foam could be added and in what location, it was concluded that this addition of foam would make the distance between the cg and cb approximately 0.14 inches in the longitudinal direction which, from the simulations, allows the pitch and roll angles to remain within plus or minus a half of a degree.

Other modifications that were made included lowering the front pressure housing, adding a limit sensor mount to the frame, changing the way the VADCP was secured into the frame, extending the handles of the frame and moving the altimeter to the aft end of the towfish. The front power housing was lowered 3/4 of a inch to help make the cg as much below the cb as possible. This modification of lowering the power housing was beneficial since the power housing weighs 63 pounds dry and 22.75 pounds in water. This allowed the cg of the power housing to sit 3/4 of a inch closer to the bottom of the towfish which means the cg of the entire towfish will be lower since this put more weight towards the bottom of the towfish.

Another modification involved adding a limit sensor mount to the frame to limit the motion of the horizontal fins. This limit sensor mount is attached at the aft end of the frame. The limit sensors are connected to this mount, see Figure 59. This setup prevents the fins from moving more than plus or minus twenty degrees.

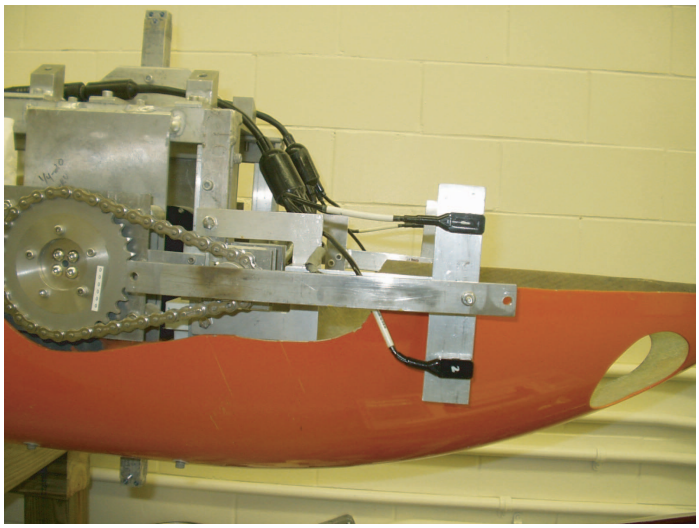

Figure 59: The limit sensor mount attached to the towfish frame

To reduce assembly time, the method of securing the VADCP to the frame was modified. The original design of securing the VADCP to the frame involved bolting two semicircular pieces of Starboard around the VADCP where the bottom Starboard piece was attached to the frame. The assemble time for this design was lengthy because there was little room in the aft end of the hull to get the bolts in the necessary places. To be more efficient aluminum bars were run through the bottom Starboard mounts, so the VADCP could be quickly secured in place by quick release hose clamps that would run around the aluminum rods and the sensor.

The last two mechanical modifications that were necessary were to extend the handles on the frame and move the altimeter to the aft end of the towfish. The handles were extended for recovery purposes. In recovering the towfish it is necessary to be able to hook one of the handles so the towfish can be pulled in, therefore by extending the handles it makes this process easier. The altimeter was moved and secured at the aft end of the towfish to allow for easier assembly. The altimeter was previously located between the computer and power housing however many cables fill up this area. By moving this to the aft end of the towfish it allows for the cables to have more room in this area and makes the assembly process quicker.

6.3 Component measurements

While doing the ballasting of the towfish, individual components were also weighed. The wet and dry weight was measured for the two pressure housings and the sensor. Tables 5 and 6 show the weights that were measured and the location of the cb and cg of these components.

Each pressure housing was weighed by two scales. Two pieces of rope were wrapped around the pressure housing. These pieces of rope fit into the two grooves of the pressure housing. The rope was used to suspend the pressure housing from the two scales to obtain the weight measurements. The wet and dry weight measurements were recorded from the scales.

Table 5: Pressure housing measurements

Item	Type	Point A	Point B	Total Weight
Power Housing	Dry	32 lbs	31 lbs	63 lbs
Power Housing	Wet	10.75 lbs	12 lbs	22.75 lbs
Computer Housing	Dry	25.5 lbs	25 lbs	50.5 lbs
Computer Housing	Wet	9.75 lbs	9.75 lbs	19.5 lbs

Through the dry and wet weights the cg and cb in the x direction were found for the power housing. The $x_{pcg} = 7.3$ inches and the $x_{pcb} = 7.0$ inches from the front of the power housing. Similar measurements were done on the computer housing however the cg and cb in the z direction were found since the computer housing sits upright in the towfish and the measurements were done when the computer housing was laying on its side. The $z_{ccg} = 5.8$ inches and the $z_{ccb} = 5.7$ inches from the top of the computer housing.

The sensor was another component that was weighed and the cg and cb were calculated. The cg was found to be 25.0325 inches back from point A and 1.4937 inches above point A. The cb was calculated as being 19.08 inches back from point A and

Table 6: Sensor measurements

Condition	Point A	Point B	Point C	Total Weight
Dry	22 lbs	31 lbs	24 lbs	77 lbs
Wet	2 lbs	2 lbs	11.5 lbs	15.5 lbs

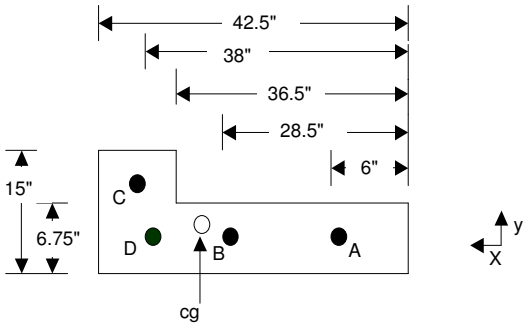

Figure 60: A side view portraying how the sensor was weighed. Points A, B, and C denote where the scales were hung above the sensor to measure the weight of the sensor.

0.8253 inches above point A. A Matlab program was written to calculate this information that is included in Appendix A. Figure 60 shows the locations of points A, B, and C which are the points where the scales were hung above the sensor to take the weight measurements of the sensor. A rope was wrapped around the sensor with a loop at each end of it to attach to the scale. This was done at each point. Note the sensor was weighed on its side, see Figure 60.

7 Conclusions and Recommendations

A two-stage towing system can effectively isolate a towed sensor platform from attitude disturbances induced by the towing vessel's motion in waves. This thesis describes modeling and fabrication of a two-stage towing system designed to carry a five-beam acoustic Doppler current profiler for measuring small-scale ocean turbulence.

The towfish is a streamlined body with cruciform fins - two fixed vertical stabilizers and two independently actuated stern planes. A numerical simulation has been developed using Matlab/Simulink which includes nonlinear rigid body dynamics and hydrodynamics. The numerical model includes an accurate representation of the actuators, including position and rate saturation as well as encoder quantization. The numerical model also includes a simple spring-damper model for the towing cable. The equivalent spring stiffness of the towing cable was determined by solving the boundary value problem describing its equilibrium configuration over the full range of expected operating speeds. Simulations using values for the actual towfish suggest that its performance will amply satisfy the specification of maintaining sensor tilt within one degree of zero.

The thesis also describes fabrication of the towfish, with particular emphasis on the forming of composite structures, such as the fiberglass hull and the syntactic foam flotation. A substantial amount of time and effort was spent trimming and balancing the towfish so that the center of gravity would precisely be below the center of buoyancy (for static stability in pitch and roll). The task was not trivial, because the towfish is densely packed with sensors, actuators, and other components. The thesis describes the trimming and balancing process and includes Matlab scripts used to plan and predict changes in weight and balance.

Remaining work includes validating the LabVIEW-based PID control routine and tuning the control gains in sea trials scheduled for July 2005.

References

[1] Just What is an AUV Anyway. International Submarine Engineering Ltd., 2001.

[2] Kurt Andress. Mechanical notes from k7nv. Taken from: Macwhyte Rope Company, July 2001.

[3] J.W. Crane and D.E. Humphreys. Modeling and Simulation of Underwater Vehicles. *SCS Summer Simulation Conference*, July 1991.

[4] W.C. Durham. AOE 5214 aircraft Dynamics & Control Lecture Notes. 2004.

[5] Bernard Etkin and Lloyd Reid. *Dynamics of Flight-Stability and Control*. John Wiley and Sons, 3rd edition, 1996.

[6] Thor I. Fossen. *Guidance and Control of Ocean Vehicles*. John Wiley and Sons, 1994.

[7] Thor I. Fossen. *Marine Control Systems: Guidance, Navigation, and Control of Ships, Rigs and Underwater Vehicles*. Marine Cybernetics, 2002.

[8] Hugh B. Freeman. Naca Report No. 432, Force Measurements on a 1/40-Scale Model of the U.S. Airship Akron. Technical report.

[9] A.E. Gargett. Observing Turbulence with a Modified Acoustic Doppler Current Profiler. *Journal of Atmospheric and Ocean Technology*, 11(6):1592–1610, 1994.

[10] S.F. Hoerner. *Practical Information on Aerodynamic Drag and Hydrodynamic Resistance*. 1965.

[11] Naomi E Leonard. Stability of a Bottom-Heavy Underwater Vehicle. *Automatica*, March 1997.

[12] Edward V. Lewis, editor. *Principles of Naval Architecture*, volume 3. The Society of Naval Architects and Marine Engineers, 1989.

[13] A R J M Lloyd. *Seakeeping*. Ellis Horwood, 1989.

[14] B. R. Munson, D.F. Young, and T. H. Okiishi. *Fundamentals of Fluid Mechanics*. John Wiley and Sons, 1990.

[15] R.C. Nelson. *Flight Stability and Automatic Control*. McGraw-Hill, 2nd edition, 1998.

[16] J.N. Newman. *Marine Hydrodynamics*. The MIT Press, 1977.

[17] Oceans 1992. *Stability of Towfish used as Sonar Platforms*, volume pp.888-893 of *Proceedings of Mastering The Oceans Through Technology*, Newport, RI, 1992. J.M. Preston.

[18] J.M. Preston. Stability of Towfish as Sonar Platforms and Benefits of the Two-part Tow. *Defense Research Establishment Pacific (DREP) Technical Memorandum*, pages 89–119, December 1989.

[19] R.R. Rodriguez. Performance Evaluation of the Control Surface Actuators for the Towed Body for Mine Countermeasures Sensor Testing. Technical Report CSS/TR-97/20, Dahlgreen Naval Surface Warfare Center, Panama City, FL, September 1997.

[20] Eric M. Schuch. Towfish Design, Simulation and Control. MS Thesis, Virginia Polytechnic Institute and State University, June 2004.

[21] Michael S. Triantafyllou and Franz S. Hover. Maneuvering and Control of Marine Vehicles, January 2002.

[22] Steven Vogel. *Life in Moving Fluids, The Physical Biology of Flow*. Princeton University Press, 1994.

[23] C.A. Woolsey and A.E. Gargett. Passive and Active Attitude Stabilization for a Tow-fish. *Conference on Decision and Control*, pages 2099–2104, December 2002.

8 Appendix A- Matlab and Mathematica code

Matlab code that calculates the cb and cg of the towfish when foam has been added to the nose of the towfish.

File Name :$CGCB.m$

```
rhosw=64;       % density of salt walter
rho24=24.1;     % density of TP-24
rho38=38;       % density of TP-38
g=32.3;         % gravity (lb*ft/s^2)

%%%%%%%%%% Flotation at Aft of Towfish %%%%%%%%%%%%%%%%

Vf=39.75*8.5*3/(12^3);    % volume in feet of the rectangular block
                          % at the back of the towfish
W1=(rhosw-rho24)*Vf;      % net weight of the rectangular block
Wd=rho24*Vf;              % dry weight of the rectangular block
xdfb=40.125;              % distance to the center of the rect.
                          % block in the longitudinal direction
                          % from point A

%%%%%%%%%%%%%%Flotation in front of power housing

b=5;                     % length of base in inches
h=7;                     % length of height in inches
t=2;                     % length of the thickness in inches
Vf1=1/2*b*h*t;           % volume of this section
b1=2.5;                  % length of the base in inches
h1=2.5;                  % length of the height in inches
w1=7;                    % length of the width in inches
Vf2=b1*h1*w1;            % volume of this section
```

```
b3=4*10;                  % area of the base in inches
h3=7;                     % height in inches
Vf3=1/3*b3*h3;            % volume of this section in inches

Vtf1=(Vf1*2+Vf2+Vf3*2)/(12^3); % total volume of area infront of
                               % the power housing

W2=(rhosw-rho24)*Vtf1;         % net weight of this area
Wd2=rho24*Vtf1;                % dry weight of this area for TP24
xdfa=-15.5;                    % approximate distance to the
                               % center of mass (assumed 1/3
                               % way back)

%%%%%%%%%%%%%%%%%%%Bottom Flotation at the Front

Vtf2a=17*6.5*3; Vtf2b=14.5*2*1.5;
Vtf2=(Vtf2a+Vtf2b*2)/(12^3);  % volume in ft of the area under
                              % the front pressure housing
W3=(rhosw-rho24)*Vtf2;        % net weight of this volume
Wd3=rho24*Vtf2;               % dry weight of this volume
xdfa1=-6;                     % distance from point A to the
                              % center of the floatation piece

%%%%%%%%%%%%%%%%%Top Flotation Replacing the TP38 Foam

Vtf3=(33*2.5*6)/(12^3);       % Volume in feet of the piece
                              % of the top hull that we can
                              % replace by TP24 foam
W4=(rhosw-rho24)*Vtf3;        % net weight of this volume with TP24
                              % foam
W5=(rhosw-rho38)*Vtf3;        % net weight of this volume with TP38
```

```
                                % foam

Wd4=W4-W5;                      % the difference in the net weight
                                % between the two foams
xdfa2=1.25;                     % the distance back from point A to the
                                % center of this piece of foam

Vtf4=(22*2.5*6)/(12^3); W6=(rhosw-rho24)*Vtf4;
W7=(rhosw-rho38)*Vtf4; Wd5=W6-W7; xdfa3=39;

Fa=160;                         % orginal weight at point A read by the
                                % scale
Fb=322;                         % orginal weight of point B read by the
                                % scale
xdb=37.5;                       % distance in inches point B is from
                                % point A

%%%%%%%%%%%%%%Finding the Towfish Dry Weight and center of Gravity

W=Fa+Fb-Wd+Wd2+Wd3-Wd4-Wd5      % Total Dry Weight after adding foam
                                % in the front and taking out foam
                                % in the back (lbs)

xcg=(Fb*(xdb)-Wd*xdfb+Wd2*xdfa+Wd3*xdfa1-Wd4*xdfa2-Wd5*xdfa3)/W
%The center of gravity in inches back from point A

Fba=18;      % The weight at point A when the towfish was
             % orginally measured in water
Fbb=19;      % The weight at point B when the towfish was
             % originally measured in water
AddedW=63;   % The amount of weight added at point B for wet
```

```
            % measurements

%%%%%%%Finding the Towfish center of buoyancy and Buoyancy

B=(W+AddedW-W1+W2+W3+Wd4+Wd5)-(Fba+Fbb) % The buoyancy of the
                                        % towfish (lbs)

xcb= (W*xcg+(AddedW-Fba)*xdb+(-W1*xdfb)+W2*xdfa+W3*xdfa1+(Wd4*xdfa2)
     +(Wd5*xdfa3))/B
% the center of buoyancy in the longitudinal direction

diffxcb_xcg=xcb-xcg
% The difference in the distance longitudinally betweeen the xcg
% and xcb in inches

diffB_W=B-W
% The difference in the weight and buoyancy (lbs)

fivepercent=W*0.05
% The amount of buoyancy needed to make the towfish 5 percent
% buoyant (lbs)

actualpercentage=diffB_W/W
% The actually percentage that the towfish is buoyant

%%%%%%%%%%%%%%%%%%%%%%%%

Vtt=Vtf1+Vtf2+Vtf3+Vtf4
% The amount of volume that needs to be added to the haul
% of foam to make the cb move forward
```

```
Wtt=Vtt*rho24
% The weight of the foam needed to move the xcb within 0.16"
% of the xcg

Vtneed=(Vtt-Vtf3)*rho24
```

Matlab code that calculates the cb and cg of the sensor and the two pressure housings.

File Name:*CGCBSensor.m*

```
%%%%%%%%%%%Sensor measurements %%%%%%%%%%%%%%%%%%%%%%%%%%%%%

%%%%%%%%Dry Weight Measurements%%%%%%%%%

WA=22; WB=31; WC=24; WT=WA+WB+WC;

xba=22.5; xca=32; xaddeda=30.5; yba=0; yca=8.5-3.74;


%%%%%%Sum of the moments at point A

xcg=(WB*xba+ WC*xca)/WT % x center of gravity
ycg=WC*yca/WT % y center of gravity

BA=2; BB=2; BC=11.5; Wadded=10.6;

B=WT+Wadded-BA-BB-BC % Buoyancy of the sensor

B-WT

xcb=(WT*xcg+Wadded*xaddeda-BB*xba-BC*xca)/B % x center of buoyancy
```

```
ycb=(WT*ycg-BC*yca)/B % y center of buoyancy

%%%%%%%%%%%%%%%Computer Housing Measurements%%%%%%%%%

WcA=25.5; WcB=25; WcT=WcA+WcB; Xabc=9.1;

zcgAc=Xabc*WcB/WcT % x center of gravity from point A

BcA= 9.75; BcB=9.75; Bc=WcT-BcA-BcB;

zcbAc=(WcT*xcgAc-BcB*Xabc)/Bc

Bc-WcT

%%%%%%%%%%%%%%%Power Housing Measurements%%%%%%%%%%

WpA=32; WpB=31; WpT=WcA+WcB; Xabp=12.25;

xcgAp=Xabp*WpB/WpT % x center of gravity from point A

BpA= 10.75; BpB=12; Bp=WpT-BpA-BpB;

xcbAp=(WpT*xcgAp-BpB*Xabp)/Bp

Bp-WpT
```

Mathematica code used to find the Force on the towfish at different velocities and the l_i distance (this is the distance from depressor to the towfish nose)

File Name: Springdisplacementnew1.nb

```
(*The following units are defined in feet*)
dbb=17/12;
lb=100.5/12;
Cf=0.004;
t=2.25/12;
c=18/12;
t90=0.75/12;
t99=0.50/12;
b= 30.5/12;
d=16.75/12;
xf=33.75/12;
 rho=64;
B=497.0849*32.2;   (*Buoyancy Force of the Towfish*)
W=473.5327*32.2;(*Weight Force of the towfish*)

Cdob=0.44*(dbb/lb)+4*Cf*(lb/dbb)+4*Cf*Sqrt[dbb/lb];

(*Coefficient of drag found from the body*) alpha=0;

Clb=0.3508*alpha;
(*Clalpha on the body found from the US Airship
Akron Data *)
Cdb=Cdob+K*Clb^2; (*Cd of the body*)
Lb=Clb*1/2*rho*V^2*Sb; (*Lift on the towfish body*)
Sb=Pi*dbb^2/4;
Db=Cdb*1/2*rho*V^2*Sb;
Clalphatheory=2*Pi+4.9*t/c;
phiTE=2*ArcTan[0.09,(1/2*(t90/c)-1/2*(t99/c))];
Chart1value=1/2*(t90/c-t99/c)/9;
K=0.915;
```

```
M=0;
Clalpha=1.05*K*Clalphatheory/Sqrt[1-M^2];
Kappa=Clalpha/(2*Pi);
AR=b/c;
gamma=ArcCos[b/2/d];
Clalpha1=2*Pi*AR/(2+Sqrt[AR^2/Kappa^2*(1+(Tan[gamma])^2)+4]);
Clf=Clalpha1*deltaE;
Cdof=0.0098;
K1=0.0128125;
Cdf=Cdof+K1*Clf^2;
Sf=b*c;
Lf=Clf*1/2*rho*V^2*Sf;
Df=Cdf*1/2*rho*V^2*Sf;

Eq1=T*Cos[theta]-Db-Df;
Eq2=T*Sin[theta]-Lf+-B+W;
Eq4=(B+Lb)*lb/2+Lf(lb/2+xf)-W*lb/2;
Solve[{Eq4\[Equal]0},{deltaE}]

deltaE=-1.63027/V^2;

T*Sin[theta]-Lf+-B+W T*Cos[theta]-Db-Df
T=304.708/Sin[theta];


Solve[{T*Cos[theta]-Db-Df\[Equal]0},{theta}]


Clear[dbb, lb, Cf, t, c, t90, t99, b, d, xf, rho, B, W,Cdob,
alpha, Clb, Cdb, \ Lb, Sb, Db, Clalphatheory, phiTE,
Chart1value,K, M, Clalpha, Kappa, AR, \ gamma, Clalpha1, Clf,
```

```
Cdof, Cdf, Sf, Lf, Df, Eq1, Eq2, Eq4, deltaE, theta, T]


Parameters={CDc->1.05, dc->0.0656167979, rhof->64,
Gamma\[Rule]0.0001};

Eq1=CDc*dc*0.5rhof*V^2*Sin[phi[h]]+Gamma/.Parameters;
Eq2=(CDc*dc*0.5*rhof*V^2*Cos[phi[h]]-Gamma*Tan[phi[h]])
/T[h]/.Parameters;
Eq3=Tan[phi[h]];


Tc1={0};
deltax={0};
deltax2={0};
deltah={0};
deltah2={0};
deltac1={0};
t=1;
y1={0};
B2={0};
V1={0};
k1={0};
qr=0.01 (*step size the program is iterating at*)
LD={164.0420};

For[y=qr,y\[LessEqual]100,y=y+qr,
  y1=Append[y1,y]] (*Setting up Initial conditions*)

  For[V=3.3 , (* initial velocity 3.3 ft/s *)
    V<10.3,   (* stop the loop when the velocity gets
```

```
               to 10.3 ft/s*)
  V=V+0.1 , (*Velocity step size *)
  t=t+1;

Thetac=ArcCot[2.0775*10^-19*((3.41457*10^17/V^2)
+1.58803*10^17*V^2)];

(* Angle the cable makes with the towfish from horizontal *)

Tc=304.708/Sin[Thetac]; (* Force on the towfish from the cable *)

(*This uses the Numerical Differential Solver to calculate
the values of Tension in the cable,phi the angle the tension
acts and the x position of the cable over a depth of 100 ft.
The depth was chosen to be larger than the depth of any of
the cables to get more data than needed and the excess is
then not used.*)

 Sol=NDSolve[{T'[h]\[Equal]Eq1,phi'[h]\[Equal]Eq2, x'[h]
     \[Equal]Eq3, T[0]\[Equal]Tc,phi[0]\[Equal]Pi/2-Thetac,
     x[0]==0},{T,phi,x},{h,0,100}];
Clear[w,tt,deltaw];
w=Sqrt[(x[0]/.Sol)^2];
(* this sets the intial diagonal distance of the cable to
zero*)
tt=2;
(*This loop sums up the lengths of the cable at a depth of
every qr amount by taking the change in x distance and change
in h distance and find the square root of the square of those
two changes. This loop breaks when the length w becomes
larger than the actual cable length. *)
```

```
 For[c1=0,c1<40  ,t2=tt-1; c2=c1-qr;
  deltaw=Sqrt[(y1[[tt]]-y1[[t2]])^2+((x[c1]/.Sol)-
  (x[c2]/.Sol))^2];
  w=w+deltaw;
  A=x[c1]/.Sol;B=y1[[tt]];tt=tt+1;
  If[w[[1]]>164.0420,
  Break[]], c1=c1+qr];

(* This loop assigns values to x and h until the length of
the cable (w) is at 50 meters, the x and h components vary
depending on the   velocity the vehicle is being towed at *)

B1=B-qr; (*This is the height of the cable (from the
towfish to the depressor) before the for loop broke*)

F=(LD[[1]]-(w-deltaw))/deltaw;

S1=x[B1]/.Sol; (* This is the x distance of the cable
(from the towfish to the depressor) before the for loop
broke *)
S2=x[B]/.Sol;
xstar=S1[[1]]+F*(S2[[1]]-S1[[1]]); (*Actual x distance
at the end of the cable *)
ystar=B1+F*(B-B1); (*Actual depth of the end of the cable*)
B2=Append[B2,ystar]; (* This is a vector of the height
values at different velocities*)

Tc1=Append[Tc1,Tc]; (*This is a vector of the force on
the towfish at different velocities *)
deltax=Append[deltax,xstar[[1]]];
```

```
  (*This is a vector of x distances for different towing
  speeds *)

  wy=w-deltaw+Sqrt[(xstar-x[B1]/.Sol)^2+(ystar-B1)^2];
  V1=Append[V1,V];
  kiv=Sqrt[B2[[2]]^2+deltax[[2]]^2];
  kcv=Sqrt[xstar^2+ystar^2];
  kc=kcv-kiv;
  k1=Append[k1,kcv[[1]]];
  Print[Tc," ",xstar,"   ",ystar, "   ", V, "  "
  , kcv, "   " wy]]

Tc1=Delete[Tc1,1]

<<NumericalMath‘PolynomialFit‘

V1=Delete[V1,1]

qq={{0,0}}

For[p=1, p<71, p=p+1, qq=Append[qq,{V1[[p]],Tc1[[p]]}]]
qq

qq=Delete[qq,1];


bab=ListPlot[qq,PlotRange\[Rule]{{3,10.5},{0,950}},
    AxesLabel\[Rule]{"V(ft/s)", "Ft (lbf*ft/s^2)"}];

q1=PolynomialFit[qq,1]; qa=Expand[q1[x]]
```

```
qbb = Plot[qa,{x,0,11},PlotStyle\[Rule]{RGBColor[1,0,0]}];

q2=PolynomialFit[qq,2]; qc=Expand[q2[x]] qcc=
Plot[qc,{x,0,11},PlotStyle\[Rule]{RGBColor[0,1,0]}];

q3=PolynomialFit[qq,3]; qd=Expand[q3[x]] qdd=
Plot[qd,{x,0,11},PlotStyle\[Rule]{RGBColor[0,0,1]}];

q4=PolynomialFit[qq,4]; qe=Expand[q4[x]] qee=
Plot[qe,{x,0,11},PlotStyle\[Rule]{RGBColor[0.2,0.2,0.2]}];

Show[{bab,qcc}]

k1=Delete[k1,1] nn={{0,0}} For[n=1,n<71,
n=n+1,nn=Append[nn,{V1[[n]],k1[[n]]}]] nn=Delete[nn,1]
bad=ListPlot[nn,PlotRange\[Rule]{{3,10.5},{160,164.043}},
AxesLabel\[Rule]{"V(ft/s)", "l (ft)"}];

n1=PolynomialFit[nn,1]; na=Expand[n1[x]] naa=
Plot[na,{x,0,11},PlotStyle\[Rule]{RGBColor[1,0,0]}];

n2=PolynomialFit[nn,2]; nb=Expand[n2[x]] nbb=
Plot[nb,{x,0,11},PlotStyle\[Rule]{RGBColor[0,1,0]}];

n3=PolynomialFit[nn,3]; nc=Expand[n3[x]] ncc=
Plot[nc,{x,0,11},PlotStyle\[Rule]{RGBColor[0,0,1]}];

n4=PolynomialFit[nn,4]; nd=Expand[n4[x]] ndd=
Plot[nd,{x,0,11},PlotStyle\[Rule]{RGBColor[0.2,0.2,0.2]}];

n5=PolynomialFit[nn,5]; ne=Expand[n5[x]] nee=
```

```
Plot[ne,{x,0,11},PlotStyle\[Rule]{RGBColor[0.2,0.2,0.2]}];

Show[{bad,ncc}]
```

9 Appendix B- Detailed Description of the Simulink Simulation

A Simulink simulation has been developed to model the towfish system and to look at how changing various parameters would affect the stability of the towfish. This Simulink simulation has been developed with a starboard and port fin command that output a tilt angle depending on the conditions input into the system. The PID controller developed through the Ziegler-Nichols method, moves the control fins in response to tilt error. Both the starboard and port command go through a zero-order hold and iterate through this loop. This simulation requires a script file that must be run first which initializes all the parameters. An S-function, a JONSWAP time series and a Depressor Fluctuation Table Generator are all script files or functions that have been written in Matlab for this simulation. The code for these different files has been included at the end of this appendix. Figure 61 shows the closed-loop system for the towfish.

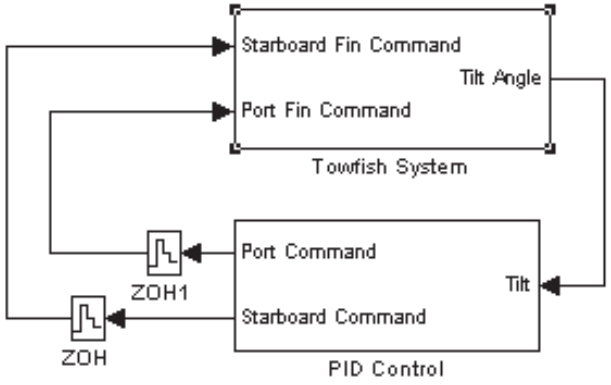

Figure 61: Closed-loop system for the towfish

The first block in the closed-loop system is the towfish system shown in Figure 62. For the towfish system a port and starboard fin command is input and the pitch angle, roll angle and the depth are output. Within this towfish system block the port and

starboard fin commands are used to develop a fin deflection. This output depends on the actuator's capabilities. This deflection is plotted on a port and starboard fin scope. Also this system determines the depressor position. From the depressor position, depressor velocity, starboard fin deflection, and port fin deflection the S-function is run. This function integrates the nonlinear towfish dynamics and outputs a tilt angle.

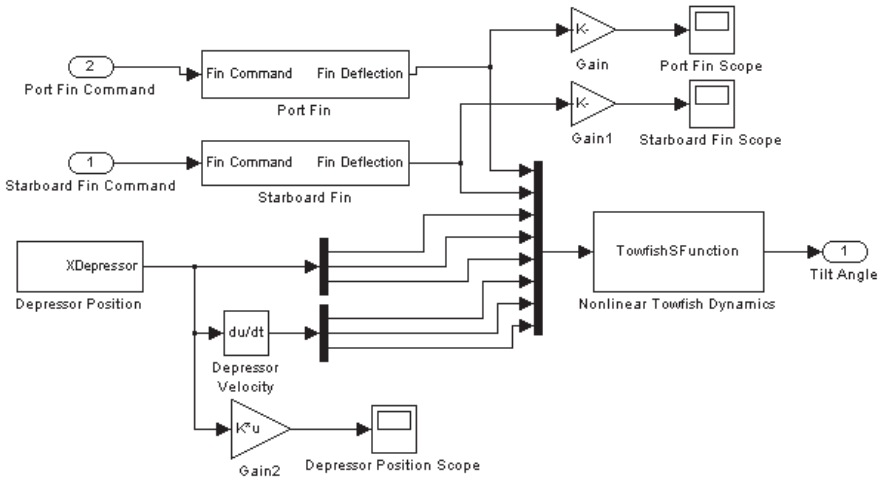

Figure 62: Simulink block that describes the towfish system

A more detailed description of how the fin deflections for the starboard and port fins are achieved follows. The port fin command is input into the port fin block. The rate limiter makes sure the input is within the fins angular-rate range capabilities. The command then travels to a saturation function that makes sure the command is within the possible upper and lower limits for the fin. This command then moves to a quantizer that discretizes input at a given interval. This interval is dependent on the encoder resolution. From this an output of the actual fin deflection is developed. This process is done for both the starboard and port fins individually. Figure 63 displays the Simulink blocks used for this process.

This command from the fin deflection goes to a gain and produces a figure that shows

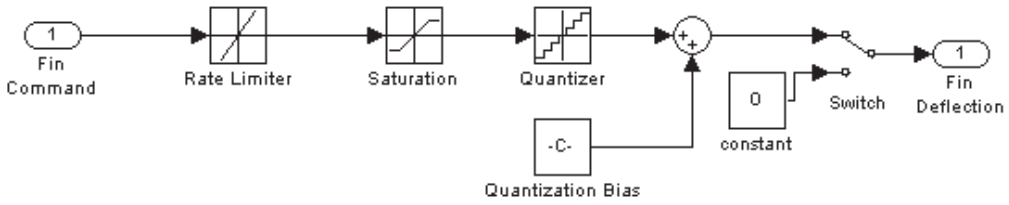

Figure 63: Simulink block that limits the fin movement

the deflection of the port and starboard fins. The command from the fin deflection is also sent to the towfish S-Function.

The other part of the towfish system involves the depressor position. This Simulink block can be seen in Figure 64.

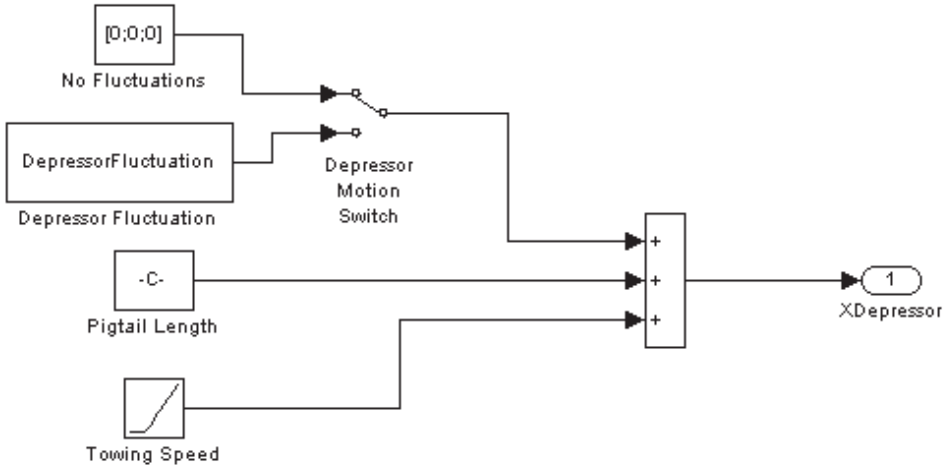

Figure 64: Simulink block that develops the depressor motion

The position of the depressor depends on the fluctuation of the depressor, the length of the pigtail and the towing speed. The depressor fluctuation is developed through the depressor fluctuation generator function which includes wave motion created from the sea state along with sinusoidal motion. This function uses a signal that has been

developed by the JONSWAP wave spectrum through summing the sinusoids at N different frequencies within the spectrum to estimate wave heights. The depressor position is then defined by sinusoidal motion and the x_{random}, y_{random} and z_{random}, where x_{random}, y_{random} and z_{random} are the signal that is generated from the JONSWAP spectrum for the x, y and z axes. This Simulink simulation also gives the option of assuming no fluctuation in the depressor and setting its position to a zero vector. The depressor position is dependent on the pigtail length and the towing speed of the vehicle also. The towing speed for this problem has been determined to be between 3.3 ft/s to 9.8 ft/s (1 to 3 m/s) and the pigtail length has initially been set at 164.04 feet (50 m). From these three inputs the position of the depressor is developed and output into the towfish system. From the depressor position the velocity of the depressor is found through taking derivative of the position. The depressor position is output to a plot that shows the depressor position versus time.

Next, the two fin deflections and the depressor position and velocity are input into the S-function. The S-function is a function that models the nonlinear dynamics of the towfish in Simulink. This function has 12 continuous states, 8 inputs, and 3 outputs. Through running this function, the depth of the towfish, pitch angle and the roll angle are output.

The second main block in the towfish closed-loop system is the PID Control block, Figure 65. The towfish pitch angle and roll angle are input into the PID controller. The roll angle is input into the PID controller that has proportional, integral and derivative parameters that have been developed to control the roll of the system. The process of developing these values is described in Section 5.1. The commanded roll moment is sent to the starboard and port command. This same process is done for the pitch angle with the PID pitch controller that was developed. Thus, a port and starboard command are produced.

The PID Control block outputs the port and starboard command to the zero-order hold blocks. These commands are output to separate zero-order hold blocks and looped back to the towfish system. This loop runs for a designated time that can be indicated in the system. It should be noted that the Simulink simulation is designed

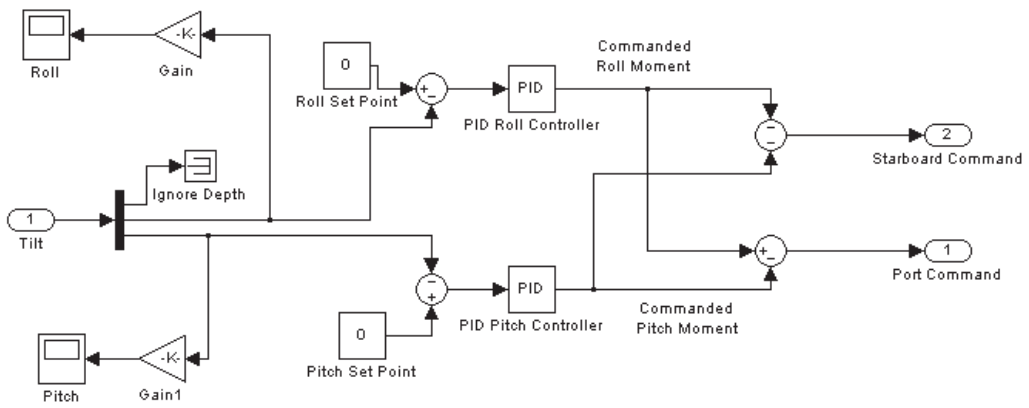

Figure 65: Simulink block that describes the PID control

to implement the port and starboard commands that are output every 0.25 seconds. This time constant of 0.25 seconds is dependent on the systems capabilities.

Simulations were run for the closed-loop system of the towfish and a parametric study was conducted. From these simulations it was noted that due to encoder quantization the roll angle fluctuated constantly. To remove this constant fluctuation a dead zone block was added to the roll PID Control block, see Figure 66. This Dead Zone block changes the modified angle to zero when the error was between plus or minus 0.1 degrees. When the error became larger than this range the PID controller was used to correct the roll angle. At this point simulations were run to see how the Dead Zone affected the roll angle variation of the towfish and how it compared to the previous results.

The parameters of the towfish system have been input into a script file named TowfishSimulinkScript. This file defines all the initial parameters and runs the Depressor Fluctuation Table Generator function. This function determines the position of the depressor over a specified period of time. The position of the depressor is based on the sea state and the sinusoidal motion. The following is the TowfishSimulinkScript file that was written along with the DepressorFlucuationTableGenerator. The JONSWAPTimeSeries is used by the DepressorFluctuationTableGenerator to develop the

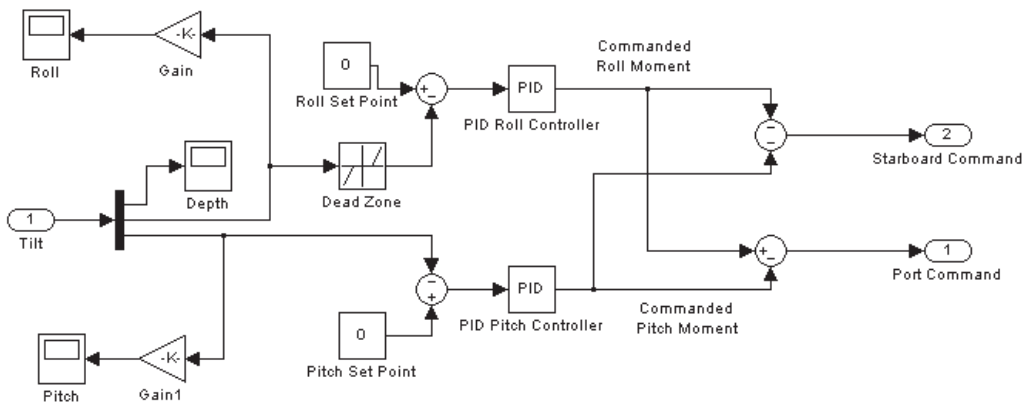

Figure 66: PID controller block with the dead zone

position of the depressor based on the sea state according to the JONSWAP wave spectrum. The code for the S-Function that is used in this simulation has also been included.

This code is the script file for the Simulink simulations called TowfishSimulinkScript. This script file needs to be initially run because it contains the parameters of the system. The script file calls the depressor fluctuation table generator to develop the position of the depressor.

File Name: TowfishSimulinkScript.m

```
clear close all

global rho g

% NOTE: All units are metric unless otherwise specified!

% Physical constants
rho = 64.0*16.018463; % Density of sea water (64.0 lbs/ft^3)
```

```
g = 9.80665;          % Acceleration due to gravity (m/s^2)
Ustar = 6.6;     % Nominal towing speed (ft/s)
% Determine significant wave height from sea state.
(Table 4.2, pg. 125 in Fossen)

SeaState =3;

WaveHeights = [0.05; 0.3; 0.875; 1.875; 3.25;
5.0;7.5; 11.5];

Hs = WaveHeights(SeaState);

% Compute random depressor motion
DepressorDepth=200;
PendulumAmplitude = Hs;

PendulumFrequency = sqrt(g/DepressorDepth);

DepressorFluctuationStartTime=0;
DepressorFluctuationSampleTime=0.1;
DepressorFluctuationEndTime=300;
T =
[DepressorFluctuationStartTime:DepressorFluctuationSampleTime:
DepressorFluctuationEndTime]';

% Define number of frequency components for random wave motion.
N = 1000;

DepressorFluctuation
=DepressorFluctuationTableGenerator(PendulumAmplitude,
PendulumFrequency,Hs,N,T);
```

```
%%%%%% Actual and Displaced Mass %%%%%%%
Weight = 471.2535*4.4482216;   % Estimated dry weight (N)
mb = Weight/g;             % Estimated mass of the body (kg)
BuoyancyFactor = 1.0548; Buoyancy = BuoyancyFactor*Weight;
mf = BuoyancyFactor*mb;   % Displaced mass (kg)

% Compute rigid body and potential flow hydrodynamic parameters
% for a 6:1 ellipsoid
FinenessRatio = 6;
%Volume = mf/rho;
%Radius = (Volume/((4/3)*pi*FinenessRatio))^(1/3);
%D = 2*Radius;
Db = 17*0.0254;          % Diameter of the body (m)
lb = FinenessRatio*Db;   % Length of the body (m)
Sb = pi*(Db/2)^2;        % Frontal area of the body (m^2)
Volume = (4/3)*Sb*lb;

% Inertia (Approximated by an ellipsoid with the body frame at
%the geometric center)%%

Ix = (mb/5)*(2*(Db/2)^2);
Iy = (mb/5)*((lb/2)^2+(Db/2)^2);
Iz =Iy;
Ixy = 0;
Ixz = 0;
Iyz = 0;

%%%%%%%%%%%%%% Tail fin parameters %%%%%%%%%%%%%%%
c = 1.31*0.3048;      % chord length (constant chord)
b = (20+2*15)*0.0254; % Tail fin span
```

```
                    % (20 inch spread and 2 15-inch fins)
AR = b/c;           % Aspect ratio
St = b*c;           % Tip-to-tip fin area
CLalpha2D = 2*pi;   % From Anderson Pg 277, Eq 4.58
CLalphat = CLalpha2D/(1+(CLalpha2D/(pi*AR)));
                    % From Anderson Pg 343, Eq 5.68
CD0 = 0;
epsilon = 0.971;    % Induced drag factor.
                    % From Anderson Pg 340, Fig 5.18
lt = (3/8)*lb;      % Approximate distance from towfish CB
                    % to tail AC
Vt = (lt*St)/(Sb*lb); % Tail volume
eta = 1;            % Tail efficiency factor (no wing downwash)
lf = lt + c/4;      % Distance from the body axis origin to fin
                    % geometric center
%%%%%%%%%%%%%%%%%%%%%%%%%%%%%%%%%%%%%%%%%%%%%%%%%%%%%%%%%%%%%%%%

%%%%%% Tail fin added mass and inertia (Newman and Lewis) %%%%%%
Yvdot = pi*rho*b*(c/2)^2;
Zwdot = Yvdot;

Nvdot = lf*Yvdot;
Mwdot = Nvdot;

Nrdot = (lf^2)*Yvdot;
Mqdot = Nrdot;
Kpdot2D = (2/pi)*rho*(b/2)^4;
Kpdot = Kpdot2D*c;

% Location of CG
```

```
xcg =0*0.0254;
ycg =0*0.0254;
zcg =1*0.0254;

Xcg = [xcg;ycg;zcg];

%%%%%% Body added mass and inertia parameters (Fossen, 1992) %%%%%%%
e = sqrt(1-(Db/lb)^2);

alphao = (2*(1-e^2)/(e^3))*((1/2)*log((1+e)/(1-e))-e);

betao =(1/(e^2))-((1-e^2)/(2*e^3))*log((1+e)/(1-e));

k1 = alphao/(2-alphao);
k2 = betao/(2-betao);

k3 = (betao-alphao)*e^4/((2-e^2)*(2*e^2-(2-e^2)*(betao-alphao)));

%%%%%% Mass and inertia matrices %%%%%%%
D = mb*hat(Xcg) + [0 0 0; 0 0 Mwdot; 0 Nvdot 0];

M = mb*(eye(3) + diag([k1; k2; k2])) + diag([0; Yvdot; Zwdot]);
% NOTE: There is a small but negligible error in the body added mass
I = diag([1; 1+k3; 1+k3])*diag([Ix; Iy; Iz]) + [0 -Ixy -Ixz; -Ixy
0 -Iyz; -Ixz -Iyz 0] + diag([Kpdot; Mqdot; Nrdot]);
% NOTE: There is a small but negligible error in the body
% added inertia
GeneralizedInertia = [M D'; D I];

InverseGeneralizedInertia = inv(GeneralizedInertia);
%%%%%%%%%%%%%%%%%%%%%%%%%%%%%%%%%%%%%%%%%%%%%%%%%%%%%%%%%%%%%%%%%%%
```

```
%%%%% State the body viscous hydrodynamic parameters %%%%%
CLalphab1 = 0.1858; % From NACA Report No. 432 Table 1 using a
                    % quadratic fit from 0 deg to 12 deg pitch
CLalphab2=0.964;    % From NACA Report No. 432 Table 1 using a
                    % quadratic fit from 0 deg to 12 deg pitch
CMalphab = 1.3076;  % From NACA Report No. 432 Table 1 using
                    % linear fit from 0 deg to 12 deg pitch
Cf = 0.004;         % From Hoerner FDD Section 3-12 for
                    % supercritical flow.
CDb0 = 0.44*(Db/lb)+4*Cf*(lb/Db)+4*Cf*sqrt(Db/lb);
                    % From Hoerner FDD Section 3-12 for
                    % supercritical flow.
%%%%%%%%%%%%%%%%%%%%%%%%%%%%%%%%%%%%%%%%%%%%%%%%%%%%%%%%%%%%%%%%

%%%%%%%% Hydrodynamic damping moment (Nelson) %%%%%%%%
Clp = -2*(CLalphat/3); % Taper ratio of 1, multiplied by 2
                       % for both horizontal and vertical
                       % sections
Cmq = -2*eta*CLalphat*Vt*(lt/lb);
Cnr = Cmq;

% Hydrodynamic center for fins
zac = (b/4);    % From Etkin and Reid table C1 pg 355
yac = (b/4);

Xac1 = [-lt; 0 ; zac];
Xac2 = [-lt; -yac; 0];

Xac3 = [-lt; 0;-zac];
Xac4 = [-lt; yac; 0];
```

```
%%%%%%%%%%%%%%%%%%%%%%%%%%%%%%%%%%%%%%%%%%%%%%%%%%%%%%%%%%%%%%%%%%%%%%%

%%%%%%%%% Tether-related parameters %%%%%%%%%

L = 50;         % Pigtail length
k1bar=-66.91692616014574+ 2*13.210490472628948*Ustar;
k2bar=3.532241835195228-2*0.39671163916258595*Ustar
+3*0.015240238304699729*Ustar^2;
% 3rd order polynomial approximation

kbar =k1bar/k2bar*0.4535923;
% This converts kbar from lb/s^2 to kg/s^2
zeta = 1;       % Assumed critically damped
omegan = sqrt(kbar/M(1,1));
% Second order system approx s^2 + (b/m)s + k/m
bbar = M(1,1)*2*zeta*omegan;

%%%%%%%%%%%%%%%%%%%%%%%%%%%%%%%%%%%%%%%%%%%%%%%%%%%%%%%%%%%%%%%%%%%%%%%

%%%%%%%%% Servo-related parameters %%%%%%%%%
ServoTimeConstant = 0.5;
GearRatio = 3;
MaxServoSpeed = 2*pi/16;
RateLimit = GearRatio*MaxServoSpeed;
MaxFinAngle = 20*(pi/180);
RadiansPerCount = (2*pi)/(640/GearRatio);
Ts = 0.25;
%%%%%%%%%%%%%%%%%%%%%%%%%%%%%%%%%%%%%%%%%%%%%%%%%%%%%%%%%%%%%%%%%%%%%%%

%%%%%%%%% Define an initial state for simulation %%%%%%%%%
U0=Ustar*0.3048; % converts the speed from ft/s to m/s
```

```
X0 = 0;
Y0 = 0;
Z0 =0;

phi0 = 0*pi/180;
theta0 = 0*pi/180;
psi0 = 0*pi/180;

alpha0 = 0*(pi/180);
beta0 = 0*(pi/180);
RWindToBody0 =
expm(hat([0;-alpha0;0]))*expm(hat([0;0;beta0]));

BodyVelocity0 = RWindToBody0*[U0;0;0];

u0 = BodyVelocity0(1);
v0 =BodyVelocity0(2);
w0 = BodyVelocity0(3);

p0 = 0;
q0 = 0;
r0 = 0;

x0 = [X0; Y0; Z0; phi0; theta0; psi0; u0; v0; w0; p0; q0; r0];

qbar0 = (1/2)*rho*U0^2;

% Initial deflection of pigtail
StaticDeflection = (0.0194*qbar0*Volume^(2/3)+CDb0*qbar0*Sb)/kbar;
```

```
% Control parameters
% Gain = UltimateGain*0.6;
% Pki = Gain/(0.5*UltimatePeriod);
% Pkd = Gain*(0.125*UltimatePeriod);
Rkp = 0.1*(18*0.6);
Rki = Rkp/(0.5*0.95);
Rkd = 2*Rkp*(0.125*0.95);
Pkp = 0.1*(10*0.6);
Pki = Pkp/(0.5*2.8);
Pkd = 2*Pkp*(0.125*2.8);
% Rkp = 0*(18*0.6);
% Rki = 0*Rkp/(0.5*0.95);
% Rkd = 0*Rkp*(0.125*0.95);
% Pkp = 0*(10*0.6);
% Pki = 0*Pkp/(0.5*2.8);
% Pkd = 0*Pkp*(0.125*2.8);
```

This is the S-function that is used in the Simulink simulation. It takes the fin deflections, depressor position and velocity and uses the towfish nonlinear dynamics to output the roll and pitch angle along with the depth of of the towfish.

File Name: TowfishSFunction.m

```
function  [sys,x0,str,ts] = sfuncont(t,x,u,flag,x0,...
    rho,U0,kbar,bbar,L,AR,b,Sb,lb,St,Volume,Xcg,M,D,I,...
    PendulumAmplitude,Xac1,Xac2,Xac3,Xac4,...
    InverseGeneralizedInertia,Weight,Buoyancy,CLalphab1,...
    CLalphab2,CMalphab,CDb0,CLalphat,Clp,Cmq,epsilon)
```

```
%   TowfishSFunction: An M-File S-function which models the
%   nonlinear towfish dynamics in Simulink.

switch flag
  case 0           % Initialization
    sys = [12,     % number of continuous states
           0,      % number of discrete states
           3,      % number of outputs
           8,      % number of inputs
           0,      % reserved must be zero
           0,      % direct feedthrough flag
           1];     % number of sample times
    x0  = x0;
    str = [];
    ts  = [-1 0];  % sample time:[period,offset]-Inherit
                   % sample time

  case 1           % Derivatives: Nonlinear spring with
                   % forcing

% STATE COMPONENTS: [X Y Z phi theta psi u v w p q r]'
% INPUTS: Port (d2) and starboard (d4) fin deflections;
% Depressor location (XDepressor) and velocity (UDepressor)
% OUTPUTS: Depth (Z), pitch angle (theta), and roll angle (phi)

% STATE COMPONENTS
X = x(1);
Y = x(2);
Z = x(3);
phi = x(4);
theta = x(5);
```

```
psi =x(6);
U = x(7);
V = x(8);
W = x(9);
P = x(10);
Q = x(11);
R = x(12);

% INPUTS
d2 = u(1);
d4 = u(2);
XDepressor = [u(3);u(4);u(5)];
UDepressor =[u(6);u(7);u(8)];

% Define hydrodynamic angles
Speed = sqrt(U^2 + V^2 + W^2);
qbar = (1/2)*rho*Speed^2;

alpha = atan(W/U);

beta = asin(V/Speed);
mu = asin(sqrt((V^2 + W^2)/Speed^2));

% Water current to body rotation matrix
RWindToBody = expm(hat([0;-alpha;0]))*expm(hat([0;0;beta]));

% Hydrodynamic force and moment on the body
CWb = -[0.3511*(mu^2)+0.0194; CLalphab1*beta+CLalphab2*beta^2;
CLalphab1*alpha+CLalphab2*alpha^2];

CBb = RWindToBody*CWb;
```

```
% Extra zero AOA drag due to skin friction
CWb2 = -[CDb0;0;0];
CBb2 = RWindToBody*CWb2;

BodyForce = CBb*qbar*Volume^(2/3) + CBb2*qbar*Sb;
% See NACA report No. 432, Table 1
BodyMoment = [0;CMalphab*alpha*qbar*Volume;
CMalphab*(-beta)*qbar*Volume];
% See NACA report No. 432, Table 1

% Hydrodynamic force and moment from control surfaces.
% +d2, +d4 gives -pitch
% +d2, -d4 gives +roll
CW1 = -[((CLalphat*beta)^2)/(pi*epsilon*AR);CLalphat*(beta);0];
CW2=-[((CLalphat*(alpha+d2))^2)/
    (pi*epsilon*AR);0;CLalphat*(alpha+d2)];
CW3= -[((CLalphat*beta)^2)/(pi*epsilon*AR);CLalphat*(beta);0];
CW4=-[((CLalphat*(alpha+d4))^2)/
    (pi*epsilon*AR);0;CLalphat*(alpha+d4)];

CB1 = RWindToBody*CW1;
CB2 = RWindToBody*CW2;
CB3 =RWindToBody*CW3;
CB4 = RWindToBody*CW4;

TailForce = (CB1 + CB2 + CB3 + CB4)*qbar*St*0.5;

TailMoment = (cross(Xac1,CB1) + cross(Xac2,CB2) + cross(Xac3,CB3)
+ cross(Xac4,CB4))*qbar*St*0.5;
```

```
% Body to Inertial rotation matrix
RBodyToInertial =
expm(hat([0;0;psi]))*expm(hat([0;theta;0]))*expm(hat([phi;0;0]));

% Towing force spring model
XNose = [X;Y;Z] + RBodyToInertial*[(lb/2);0;0];

UNose = RBodyToInertial*cross([P;Q;R],[(lb/2);0;0]) +
RBodyToInertial*[U;V;W];



DeltaX = XDepressor - XNose;
DeltaU = UDepressor - UNose;

% XDepressorNominal = XNose + RBodyToInertial*[160.834; 0; 31.86];
% This the nominal condition for the towfish being
% towed at 3.3 ft/s
% DeltaX = norm(XDepressor - XDepressorNominal);
% DeltaR = XDepressor - XNose;
% DeltaU = UDepressor - UNose;

Ftowfishdepressor =
[kbar*(norm(DeltaX)-L)+bbar*(dot(DeltaU,(DeltaX/norm(DeltaX))))
;0;0];



% Cable to inertial rotation matrix
gamma = atan(DeltaX(3)/DeltaX(1));

sigma = asin(DeltaX(2)/norm(DeltaX));
```

```
RCableToInertial = expm(hat([0;-gamma;0]))*expm(hat([0;0;sigma]));

TowingForce = RBodyToInertial'*RCableToInertial*Ftowfishdepressor;
TowingMoment = cross([(lb/2);0;0],TowingForce);

% Hydrodynamic damping moment
Lp = Clp*(qbar*St*b)*(b/(2*U0));

Mq = Cmq*(qbar*Sb*lb)*(lb/(2*U0));
Nr = Mq;

DampingMoment = [Lp*P;Mq*Q;Nr*R];

% Weight and buoyant forces
WeightForce = (RBodyToInertial')*[0;0;Weight];

BuoyantForce = (RBodyToInertial')*[0;0;-Buoyancy];

% CG offset moment
CGMoment = cross(Xcg,WeightForce);

% Hydrodynamic force and moment from body, control surfaces and
% towing cable
Force = TowingForce + BodyForce + TailForce + WeightForce +
BuoyantForce;

Moment = TowingMoment + BodyMoment + TailMoment + DampingMoment +
CGMoment;

sys =[RBodyToInertial*[U;V;W];...
     P+Q*sin(phi)*tan(theta)+R*cos(phi)*tan(theta);...
```

```
    Q*cos(phi)-R*sin(phi);...
    Q*sin(phi)/cos(theta) + R*cos(phi)/cos(theta);...
    InverseGeneralizedInertia*[cross((M*[U;V;W] +...
    (D')*[P;Q;R]),[P;Q;R]) + Force;...
    Cross((I*[P;Q;R] + D*[U;V;W]),[P;Q;R]) +...
    Cross((M*[U;V;W] + (D')*[P;Q;R]),[U;V;W]) + Moment]];

  case 2     % Discrete state update
    sys = []; % do nothing

  case 3
    sys = [x(3); x(4); x(5)];

  case 9      % Terminate
    sys = []; % do nothing

  otherwise
    error(['unhandled flag = ',num2str(flag)]);
end
```

This is the JONSWAP time series function that develops the random x position, random y position and random z position depending on the sea state. This is based off the JONSWAP wave spectrum.

File Name: JONSWAPTimeSeries.m

```
function Signal = JONSWAPTimeSeries(Hs,N,tspan)

% This file generates a random signal according to the JONSWAP wave
% spectrum, as described in Marine Control Systems by T. Fossen
% (Section 4.2, pp. 128-129)
```

```
rho = 64.0*16.018463;     % Density of sea water (64.0 lbs/ft^3)
g = 9.80665;              % Acceleration due to gravity (m/s^2)

% Define spectral range
omega_1 = 0.1;
omega_2 = 10;

% Divide spectrum into bins of random width and select center
% frequencies
OmegaBounds = sort(omega_1 + (omega_2-omega_1)*rand(N+1,1));
DeltaOmega = diff(OmegaBounds);

omega = OmegaBounds(1:N) + (1/2)*DeltaOmega;

% Compute the JONSWAP wave spectrum parameters for the given
% sea state.
gamma = 3.3;
B = 3.11*Hs^2;
T0 = 2*pi*(4*B/5)^(-0.25);

T1 = 0.834*T0;

sigma = le(omega,5.24/T1)*0.07 + gt(omega,5.24/T1)*0.09;

Y = exp(-(((0.191*T1*omega -
ones(size(omega)))./(sqrt(2)*sigma)).^2));

% Compute the JONSWAP wave spectrum for the given sea state.

S=155*(Hs^2/T1^4)*omega.^(-5).*exp((-944/T1^4)*omega.^(-4)).*
```

```
(3.33.^Y);

% Compute a time series based on the wave spectrum above.
% (Select N random center frequencies between omega_1 and omega_2.)

OmegaBounds = sort(omega_1 + (omega_2-omega_1)*rand(N+1,1));
DeltaOmega = diff(OmegaBounds);
OmegaCenters = OmegaBounds(1:N) + (1/2)*DeltaOmega;

% Generate time series as a sum of sinusoids with random phase shifts.
zeta0 = sqrt(2*S.*DeltaOmega);

Signal = cos(tspan*omega'+2*pi*ones(size(tspan))*rand(1,N))*zeta0;
```

This is the Depressor Fluctuation Table Generator that uses the JONSWAP time series and the sinusoidal position to determine the depressor position.

File Name: DepressorFluctuationTableGenerator.m

```
function DepressorFluctuation =
DepressorFluctuationTableGenerator(PendulumAmplitude,
PendulumFrequency,Hs,N,T)

% Generate depressor motion based on the wave model in
% RandomSignalGenerator.m and a spherical pendulum model
% for the main catenary.

RandomPendulumAmplitude = JONSWAPTimeSeries(Hs,N,T);
```

```
RandomXPosition = JONSWAPTimeSeries(Hs,N,T);
RandomYPosition =JONSWAPTimeSeries(Hs,N,T);
RandomZPosition =JONSWAPTimeSeries(Hs,N,T);

phi1 = PendulumFrequency*T;
phi2 = PendulumFrequency*T + 4*pi*(rand(1,1)-0.5)*ones(size(T));

XPosition = RandomXPosition +
sin(phi1).*cos(phi2).*RandomPendulumAmplitude;

YPosition = RandomYPosition + sin(phi2).*RandomPendulumAmplitude;

ZPosition = RandomZPosition +
cos(phi1).*cos(phi2).*RandomPendulumAmplitude;

DepressorFluctuation = [T, XPosition, YPosition, ZPosition];

clear DepressorDepth omega_Depressor T PendulumAmplitude
RandomXPosition RandomYPosition RandomZPosition clear
SinusoidalXPosition SinusoidalYPosition SinusoidalZPosition
XPosition YPosition ZPosition
```

10 Appendix C- Calibrating the Tilt Sensor

The towfish contains a vertical gyro, which was chosen to perform attitude measurements along with angular rate sensing. There is also a sensing unit within the VADCP that measures the pitch and roll angles with respect to the VADCP. The precision of this tilt sensor within the VADCP is much less accurate, so the vertical gyro was purchased and secured inside the computer housing. This device has the capability of determining the pitch and roll angles within a half of a degree statically. This static accuracy is relevant due to the slow dynamics and the fact that the sensor has to maintain static equilibrium attitude for accurate measurements. The vertical gyro and the tilt sensor inside the VADCP are oriented differently.

The rotation matrix that maps vectors in the frame fixed to the vertical gyro into the reference frame fixed to the body of the towfish is defined as R_{BS}. It is assumed that the VADCP is the body of the towfish and that the tilt sensor inside of it lines up with the body frame axis. The rotation matrix R_{BS} can be found through the two rotations R_{BI} and R_{SI}.

$$R_{SI} = R_{SB}R_{BI}$$

The matrix R_{BI} is parameterized by the true roll, pitch, and yaw angles (ϕ, θ, ψ) where the matrix R_{SI} is defined by the "raw" roll, pitch and yaw angles $(\tilde{\phi}, \tilde{\theta}, \tilde{\psi})$ given by the vertical gyro. The tilt sensor inside the VADCP is used to determine ϕ and θ. The dynamic measurement unit (DMU) within the vertical gyro is used to measure $\tilde{\phi}$ and $\tilde{\theta}$. It is assumed without loss of generality that ψ=0.

To determine R_{BS}, two static tests on firm ground can be performed. The first test has been defined when the body of the towfish is at rest and all of the components are aligned as they will be in the sea trials. Thus the true pitch angle and the true roll angle from the body-aligned VADCP tilt sensor can be defined as θ_1 and ϕ_1. The pitch and roll angles thus measured from the DMU can be defined as $\tilde{\theta_1}$ and $\tilde{\phi_1}$. The rotation matrices can be written in terms of column vectors.

$$R_{SI} = [\tilde{X}_1, \tilde{Y}_1, \tilde{Z}_1]$$

$$R_{BI} = [X_1, Y_1, Z_1]$$

therefore

$$[\tilde{X}_1, \tilde{Y}_1, \tilde{Z}_1] = R_{SB}[X_1, Y_1, Z_1] \tag{70}$$

where $\tilde{X}_1$, $\tilde{Y}_1$, and $\tilde{Z}_1$ are defined by the columns of the 3-2-1 rotation matrix. Thus $\tilde{X}_1$ and $\tilde{Y}_1$ depend on $\tilde{\phi}_1$, $\tilde{\theta}_1$, and $\tilde{\psi}_1$ however $\tilde{Z}_1$ only depends on $\tilde{\phi}_1$ and $\tilde{\theta}_1$ which can be measured by the DMU. Therefore

$$\tilde{Z}_1 = R_{SB} Z_1 \tag{71}$$

where

$$\mathbf{\tilde{Z}_1} = \begin{pmatrix} -\sin\tilde{\theta}_1 \\ \sin\tilde{\phi}_1 \cos\tilde{\theta}_1 \\ \cos\tilde{\phi}_1 \cos\tilde{\theta}_1 \end{pmatrix}$$

and

$$\mathbf{Z_1} = \begin{pmatrix} -\sin\theta_1 \\ \sin\phi_1 \cos\theta_1 \\ \cos\phi_1 \cos\theta_1 \end{pmatrix}$$

These values can be computed directly from the tilt sensor and the DMU. The unit vector can be defined as

$$\lambda_z = R_{SB} Z_1$$

The second static test performed involves changing the pitch angle of the body by some amount $\Delta\theta$ without changing the roll or yaw angle. This change in pitch can be measured using the body-aligned tilt sensor. This rotation can be defined as a rotation about the y axis as

$$\mathbf{R_{BI_2}} = R_{BI_1} \begin{pmatrix} \cos\Delta\theta & 0 & -\sin\Delta\theta \\ 0 & 1 & 0 \\ \sin\Delta\theta & 0 & \cos\Delta\theta \end{pmatrix}$$

for this condition it is assumed that $\psi = 0$ therefore R_{BI_1} can be defined as

$$\mathbf{R_{BI_1}} = \begin{pmatrix} \cos\theta_1 & 0 & -\sin\theta_1 \\ \sin\phi_1\sin\theta_1 & \cos\phi_1 & \sin\phi_1\cos\theta_1 \\ \cos\phi_1\sin\theta_1 & -\sin\phi_1 & \cos\phi_1\cos\theta_1 \end{pmatrix}$$

Thus

$$\tilde{Z}_2 = R_{SB} Z_2 \tag{72}$$

$$\tilde{Z}_2 = R_{SB}(-\sin\Delta\theta X_1 + \cos\Delta\theta Z_1) \tag{73}$$

The DMU can calculate the pitch and roll measurements $\tilde{\theta}_2$ and $\tilde{\phi}_2$ for this test in order for $\tilde{Z}_2$ to be found. Then $\tilde{X}_1$ can be defined as

$$\tilde{X_1} = R_{SB} X_1$$

By rearranging equation (73), $\tilde{X_1}$ can be defined as

$$\tilde{X_1} = \lambda_x = \frac{1}{\sin \Delta\theta}(\cos \Delta\theta \tilde{Z_1} - \tilde{Z_2}) \tag{74}$$

Next λ_y can be defined as $\lambda_y = R_{SB} Y_1$. However, since R_{SB} and R_{BI} are proper rotation matrices this mean λ_y can be defined by:

$$\lambda_y = \lambda_z \times \lambda_x$$

By rearranging equation (70) and substituting in, the rotation matrix R_{SB} can be defined as the following

$$R_{SB} = [\lambda_x, \lambda_y, \lambda_z] R_{BI_1}^{-1}$$

This R_{SB} rotation matrix can be used to correct the pitch and roll angles measured by the DMU. From using equation (71) and multiplying out the $\tilde{Z_1}$ column the following expression can be developed:

$$\begin{pmatrix} -\sin\theta \\ \sin\phi\cos\theta \\ \cos\phi\cos\theta \end{pmatrix} = R_{BS} \begin{pmatrix} -\sin\tilde{\theta} \\ \sin\tilde{\phi}\cos\tilde{\theta} \\ \cos\tilde{\phi}\cos\tilde{\theta} \end{pmatrix} = \begin{pmatrix} \chi_1 \\ \chi_2 \\ \chi_3 \end{pmatrix}$$

The roll and pitch angle can therefore be computed through the following two equations.

$$\phi = \arctan \frac{\chi_2}{\chi_3} \tag{75}$$

$$\theta = \arctan \frac{-\chi_1}{\frac{\chi_3}{\cos\phi}} \tag{76}$$

The angles ϕ and θ are the pitch and roll angles corrected from the DMU to the body frame. These are important measurements for keeping the towfish within the desired attitude so the sensors can make accurate measurements. Since the vertical gyro has an accuracy of a half of degree, the measured pitch and roll angles need to be within plus or minus a half of degree due to the fact that the towfish has to be held within plus or minus one degree.

A Simulink system has been developed for correcting the measurements from the DMU to the body frame. The major block of this simulation is shown in Figure 67.

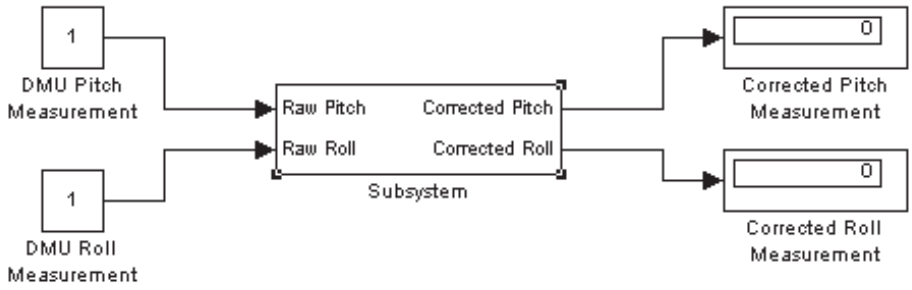

Figure 67: A system that inputs the DMU pitch and roll measurements and outputs the corrected terms with respect to the body frame

This block shows that measurements of pitch and roll are taken by the DMU unit and then input into the subsystem. This subsystem is displayed in Figure 68.

This subsystem takes the raw pitch and roll measurements made from the DMU and through the processes described previously outputs the corrected pitch and roll angle with respect to the body frame. This is done through obtaining the rotation matrix R_{BS}. A DMU correction function was written to develop the desired matrix. This

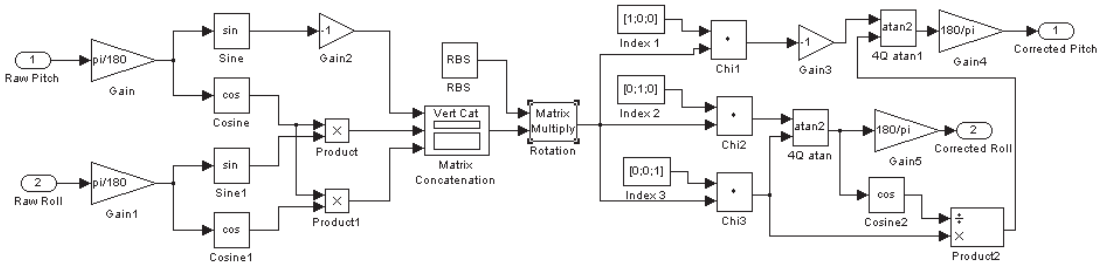

Figure 68: Simulink block that inputs the DMU pitch and roll measurements and outputs them relative to the body frame

function is included at the end of this appendix. The corrected pitch and roll angles measured by the DMU are then output from the main system.

A Matlab function, DMUcorrection was developed to transform the raw pitch and roll measurements made from the DMU to true pitch and roll measurements relative to the body frame.

File Name: DMUCorrection.m

```
function RBS =
DMUCorrection(Theta1,Phi1,Theta1Tilde,Phi1Tilde,Theta2,Phi2,
Theta2Tilde,Phi2Tilde)

% RBS = DMUCorrection(Theta1,Phi1,Theta1Tilde,Phi1Tilde,Theta2,
% Phi2,Theta2Tilde,Phi2Tilde)
% is a function that determines the matrix RBS from tilt data
% from two measurements. The matrix RBS rotates free vectors
% from the DMU frame into the body frame.  NOTE: Angles are
% to be entered in DEGREES.  The function executes the algorithm
% described in "Problem 1" in the PDF titled DMURotation.pdf
```

```
C = pi/180;
Theta1 = C*Theta1;
Phi1 = C*Phi1;

Theta1Tilde = C*Theta1Tilde;
Phi1Tilde = C*Phi1Tilde;

Theta2 = C*Theta2;
Phi2 = C*Phi2;
Theta2Tilde = C*Theta2Tilde;
Phi2Tilde = C*Phi2Tilde;

Z1Tilde = [-sin(Theta1Tilde); sin(Phi1Tilde)*cos(Theta1Tilde);
cos(Phi1Tilde)*cos(Theta1Tilde)];
Z1 = [-sin(Theta1);
sin(Phi1)*cos(Theta1); cos(Phi1)*cos(Theta1)];

lambdaz = Z1Tilde/norm(Z1Tilde);

Z2Tilde = [-sin(Theta2Tilde); sin(Phi2Tilde)*cos(Theta2Tilde);
cos(Phi2Tilde)*cos(Theta2Tilde)];

DeltaTheta = Theta2 - Theta1;

lambdax = (1/sin(DeltaTheta))*(cos(DeltaTheta)*lambdaz - Z2Tilde);

lambdax = lambdax - lambdax'*lambdaz;

lambdax = lambdax/norm(lambdax);

lambday = cross(lambdaz,lambdax);
```

```
lambday = lambday/norm(lambday);

RIB1 = [cos(Theta1), sin(Phi1)*sin(Theta1), cos(Phi1)*sin(Theta1);
    0, cos(Phi1), -sin(Phi1);
    -sin(Theta1), sin(Phi1)*cos(Theta1), cos(Phi1)*cos(Theta1)];

RSB = [lambdax, lambday, lambdaz]*RIB1;

RBS = RSB';
```

11 Vita

Amy Linklater was born April 24, 1981 in Dayton, Ohio. She received her Bachelor of Science degree in Aerospace Engineering in May, 2003 from Virginia Tech and continued to pursue a Master of Science degree in the area of dynamics and control. For the past two years, Ms. Linklater has been involved with several research projects. She has developed graphical animations of vehicle motions using Matlab and Virtual Reality Modeling Language (VRML) and has studied the problem of nonlinear path following for an autonomous underwater vehicle. The primary focus of Ms. Linklater's research has been the design and simulation of the towed sensor platform described in this thesis. After completing her Master of Science degree, Ms. Linklater will begin working in the simulator laboratory at Wright Patterson Air Force Base in Dayton, Ohio.